MAGNETIC HYDROGEL COMPOSITES FOR PULSATILE DRUG RELEASE

INJECTABLE, MAGNETIC PLUM PUDDING HYDROGEL COMPOSITES FOR CONTROLLED PULSATILE DRUG RELEASE

By DANIELLE MAITLAND, B.Eng & Biosciences

A Thesis Submitted to the School of Graduate Studies in Partial Fulfilment of the Requirements for the Degree of Master of Applied Science

McMaster University

MASTER OF APPLIED SCIENCE (2014) McMaster University

(Chemical Engineering) Hamilton, Ontario

TITLE: Injectable, magnetic plum pudding hydrogel composites for controlled pulsatile drug release.

AUTHOR: Danielle Maitland, B.Eng & Biosciences (McMaster University)

SUPERVISOR: Professor Todd R. Hoare

NUMBER OF PAGES: xix, 142

Abstract

Microgels, also called hydrogel nanoparticles, have many potential biomedical applications because they are easily injected and can be designed to exhibit specific, rapid, and repeatable responses to certain environmental stimuli. The release of loaded drugs from microgels can be activated under specific conditions by varying the chemical (i.e. pH) or physical (i.e. temperature) environment around the microgels, offering the potential for "on-demand" drug release. Microgels based on poly(N-isopropylacrylamide) (pNIPAM) and poly(N-isopropylmethacrylamide) (pNIPMAM) are of particular interest because they can be designed to undergo a deswelling phase transition when the temperature around them is raised above ~37°C (their volume phase transition temperature, or VPTT), inducing triggered release of drug. A main issue with using microgels as controlled delivery vehicles is that they are very mobile within the body and can diffuse away from the target tissue, losing the advantage of local drug delivery. By physically entrapping drug-loaded microgels within a hydrogel network by co-injection, the microgels are immobilized at the desired site of action while still being able to swell or deswell largely independently of the bulk hydrogel, allowing for the formation of a macroporous hydrogel upon thermal collapse of the microgels which promotes enhanced diffusion of drug from the gel for as long as the increased temperature is sustained. By physically entrapping magnetic nanoparticles along with microgels in the hydrogel matrix, remote composite heating can be triggered with exposure to an oscillating magnetic field.

Injectable, in-situ gelling magnetic plum pudding hydrogel composites were fabricated by entrapping superparamagnetic iron oxide nanoparticles (SPIONs) and thermosensitive N-isopropylacrylamide (NIPAM)-co–N-isopropylmethacrylamide (NIPMAM) microgels in a pNIPAM-hydrazide/carbohydrate-aldehyde hydrogel matrix. The resulting composites exhibited

significant, repeatable pulsatile release of 4 kDa FITC-dextran upon exposure to an alternating magnetic field. The pulsatile release from the composites could be controlled by altering the volume phase transition temperatures of the microgel particles (with VPTTs over 37°C corresponding to improved pulsatile release) and changing the microgel content of the composite (with higher microgel content corresponding to higher pulsatile release). By changing the ratio of dextran-aldehyde (which deswells at physiological temperature) to CMC-aldehyde (which swells at physiological temperature) in the composites, bulk hydrogel swelling and thus pulsatile release could be controlled; specifically, lower CMC-aldehyde contents resulted in little to no composite swelling, improving pulsatile release. *In vitro* cytotoxicity testing demonstrated that the composite precursors exhibit little to no cytotoxicity up to concentration of 2000 µg/mL. Together, these results suggest that this injectable hydrogel-microgel composite hydrogel may be a viable vehicle for *in vivo*, pulsatile drug delivery.

Acknowledgements

First and foremost I would like to thank Dr. Todd Hoare for his help, guidance and support over the past five years. I have learned innumerable skills over three summers as an undergraduate research assistant and for the past two years as a Masters student and I am grateful that he has hired me on for one more summer so I can have the satisfaction of finishing off a certain long-standing project that has miraculously been knocking around our lab for longer than I have.

I would like to give special thanks to Daryl Sivakumaran who was my first grad student supervisor when I came to the Hoare lab and who has trained me in anything and everything I've needed to know over the years.

Thank you to Scott for starting this project, passing it on to me, and putting up with my frequent questions and requests for previous data.

To Mat, Rabia, and Emilia (in chronological order, not order of importance) thank you for all of your help and for providing much needed breaks and entertainment through many impromptu hallway parties. Hopefully, with the completion of this thesis, you will be able to come to accept the fact that I am, in fact, a graduate student, and no longer a summer student.

Finally I would like to thank my parents for their endless love and support, for allowing me to take over their living room for ten days to write my thesis and for purchasing me the Keurig that has gotten me through my last few weeks.

Table of Contents

List of Figures

List of Tables

Nomenclature

AA	Acrylic Acid
AAm	Acrylamide
ADH	Adipic Acid Dihydrazide
AIBME	2,2-azobisisobutyric acid dimethyl ester
AMF	Alternating Magnetic Field
APS	Ammonium Persulfate
CMC	Carboxymethylcellulose
CMC-B	Aldehyde-functionalized carboxymethylcellulose
CNC	Cellulose nanocrystals
Dex-B	Aldehyde-functionalized dextran
DLS	Dynamic Light Scattering
DLVO	Derjaguin-Landau-Verwey-Overbeek
DMEM	Dulbecco's Modigied Eagle medium-high glucose
DMSO	Dimethyl sulfoxide
DIW	De-ionized water
EDC	N'-ethyl-N-(3-dimethylaminopropyl)-carbodiimide
EG	Ethylene Glycol
EPR	Enhanced Permeation and Retention
FBS	Fetal Bovine Serum
FF	Ferrofluid
FITC	Fluorescein isothiocyanate
FITC-Dex	Fluorescein isothiocyanate-labelled Dextran

GPC	Gel permeation chromatography
HCl	Hydrochloric Acid
Hzd-SPION	SPIONs peptized with Hydrazide-functionalized Poly(NIPAM)
LCST	Lower critical solution temperature
MBA	N,N'-methylene bisacrylamide
MNP	Magnetic Nanoparticle
MRI	Magnetic resonance imaging
MWCO	Molecular weight cut off
MTT	Thiazolyl blue tetrazolium bromide
NaCl	Sodium Chloride
NaOH	Sodium Hydroxide
NHS	N-Hydroxysuccinimide
NIPAM	N-Isopropylacrylamide
NIPMAM	N-Isoprolymethacrylamide
Nip-A	Hydrazide-functionalized Poly(NIPAM)
NIR	Near-infrared
PBS	Phosphate-buffered saline
PEG	Polyethylene glycol
PEG-SPION	SPIONs peptized with polyethylene glycol
PEO	Poly(ethylene oxide)
pNIPAM	Poly(NIPAM)
RES	Reticuloendothelial system
RPE	Retinal pigmented epithelial

SPION	Super paramagnetic iron oxide nanoparticle
TEM	Trasmission Electron Microscopy
TGA	Thiaglycolic Acid
VPTT	Volume Phase Transition Temperature
3T3	*Mus musculus* mouse cells

Declaration of Achievement

I declare that the research contribution that follows represents original work, completed and written by myself.

Colleagues or other contributors to the contents of this thesis include:

- Scott Campbell, who began this research project, is responsible for completing the hzd-SPION and PEG-SPION synthesis protocols and MTT assays and the SPION TEMs.
- Many of the figures found in the Literature Review section of this thesis were modified from figures made originally by Daryl Sivakumaran or Mathew Patenaude. Daryl also provided some editorial insight into the Literature Review section of this thesis.
- Mathew Patenaude completed the GPC analysis of pNIPAM-hydrazide shown in the appendices.
- Dr. Todd Hoare provided editorial insight into all sections of the thesis.

Chapter 1: Introduction

Effective drug therapy requires a drug to be delivered to the target tissue, cell or receptor of interest at a sufficient concentration to exert its desired effect for an adequate amount of time before the drug is diluted, deactivated and/or eliminated by the body. Drug therapy is most commonly accomplished through pills or injections, which result in systemic delivery of the drug throughout the body. Controlled, local drug delivery is an attractive alternative because it allows for effective treatment while avoiding the unpleasant side effects and risk of toxicity associated with systemic drug delivery. Biocompatible polymer systems have received wide-spread research attention for their potential use in localizing and controlling drug delivery.

Hydrogels are three-dimensional networks of water-soluble polymers created through chemical or physical crosslinking of different polymer precursors (Hoare and Kohane 2008). They have considerable potential as controlled drug delivery systems because they can be implanted adjacent to the target tissue and designed to release drug slowly over a long period of time. Because of their high water content and our ability to engineer networks with similar chemical and mechanical properties to native body tissues, hydrogel networks can also be made to illicit a minimal immune response (Hoffman 2012). However, the medical application of hydrogels is limited by their highly elastic mechanical properties which make them difficult to implant in a minimally invasive fashion (i.e. via injection), so their use generally necessitates surgical implantation (Patenaude, Smeets, and Hoare 2014). By co-injecting reactive polymers that spontaneously form a macroscopic hydrogel when mixed, surgical intervention can be avoided.

Despite the ability of hydrogels to alone provide slowed release, improved control over drug release from hydrogel matrices can be accomplished by co-incorporation of nano-scale particles

with variable physical or chemical characteristics (Hoare and Kohane 2008). Microgels, also called hydrogel nanoparticles, have many potential biomedical applications because they are easily injected and can be designed to exhibit specific, rapid, and repeatable responses to certain environmental stimuli. The release of loaded drugs from microgels can be activated under specific conditions by varying the chemical (i.e. pH) or physical (i.e. temperature) environment around the microgels, offering the potential for "on-demand" drug release. Microgels based on poly(N-isopropylacrylamide) (pNIPAM) and poly(N-isopropylmethacrylamide) (pNIPMAM) are of particular interest because they can be designed to undergo a deswelling phase transition when the temperature around them is raised above their volume phase transition temperature (VPTT), inducing triggered release of drug (Satarkar and Hilt 2008). These microgels can be made more biologically relevant by increasing their VPTT above 37°C (normal body temperature) but below 43°C (the temperature at which normal cells begin to die), such that triggered release is not induced immediately upon injection into the body and the act of triggering does not require temperatures high enough to run the risk of tissue damage.

A main issue with using microgels as controlled delivery vehicles is that they are highly mobile within the body and can diffuse away from the target tissue before delivering adequate quantities of drug. By physically entrapping drug-loaded microgels within a hydrogel network by co-injection, the microgels are immobilized at the desired site of action while still being able to swell or deswell largely independently of the bulk hydrogel. This allows for the formation of a macroporous hydrogel upon thermal collapse of the microgels. A macroporous hydrogel network would promote enhanced diffusion of drug from the gel for as long as the increased temperature was sustained.

Unfortunately, triggering thermal transitions inside the body is challenging, limiting the application of these release vehicles *in vivo*. One approach to addressing this challenge is to physically entrap magnetic nanoparticles along with microgels in the hydrogel matrix. When the composite is exposed to an oscillating magnetic field, the magnetic nanoparticles generate heat via hysteresis heating (Jackson et al. 1997), raising the composite temperature, causing microgel collapse and driving on-demand drug release using a highly penetrative but non-invasive signal (Hoare et al. 2009). Removing the magnetic field would permit convective cooling, returning the composite to its initial state and slowing drug release (Hoare et al. 2009).

The objective of this project is to determine how pulsatile release from this type of hydrogel-microgel-magnetic nanoparticle composite could be optimized and controlled.

Chapter 2: Literature Review

2.1 Drug Delivery:

There are three main factors that determine whether drug therapy will be effective: (1) the drug must be delivered to the target tissue, cell or receptor of interest; (2) the drug concentration at the tissue must be sufficient to exert the desired effect; and (3) this concentration must be maintained for an adequate amount of time before the drug is diluted, deactivated and/or eliminated by the body.

Whether a drug reaches its target tissue within the body is highly dependent on the nature of the drug and its route of administration (Saltzman 2001). The drug's chemical and physical properties determine its mobility within the body and into which tissues it will preferentially diffuse (Saltzman 2001), (Klaassen 2013). For example, substances injected into the blood stream (intravenous injection) with a hydrodynamic diameter below 10nm will be filtered by the kidney and will accumulate in the renal system or bladder until voided (Laurent et al. 2008). This characteristic is useful if the purpose of the administered drug is to treat a urinary tract infection, but would be quite dangerous if the drug caused renal toxicity or damage. Use of an improper delivery technique could result in ineffective treatment and/or toxicity to the body, making the method of drug administration pivotal in determining drug efficacy (Saltzman 2001).

The most common method of drug administration is oral ingestion, either in the form of a pill or solution. It is beneficial because of its ease of use and convenience; however, the caustic nature of the digestive tract can deactivate or denature drugs. Drugs that are absorbed intact along the digestive tract subsequently pass through the liver which can further deactivate, degrade and/or eliminate (through bile) the drugs, limiting the likelihood of the drug reaching its target tissues in sufficient concentrations (Saltzman 2001). Other methods of administration such

as intravenous injection or rectal or sublingual administration avoid first pass metabolism by the liver, increasing the bioavailability of the drug. However, they also result in systemic delivery throughout the circulatory system, which can result in significant risks of overdose or other toxic effects (Saltzman 2001).

Due to the limitations of systemic approaches, local methods of drug delivery such as topical ointments or, more recently, controlled-release devices implanted adjacent to the desired site of drug action have been developed (Saltzman 2001),(Uhrich et al. 1999). When administering medication, it is imperative that the local drug concentration be high enough to act on the desired tissue but does not exceed a maximum concentration above which the risk of toxic damage to the tissue outweighs the potential benefits of the drug. A common term used to describe this concentration range is the 'therapeutic window', which is illustrated in Figure 2.1.

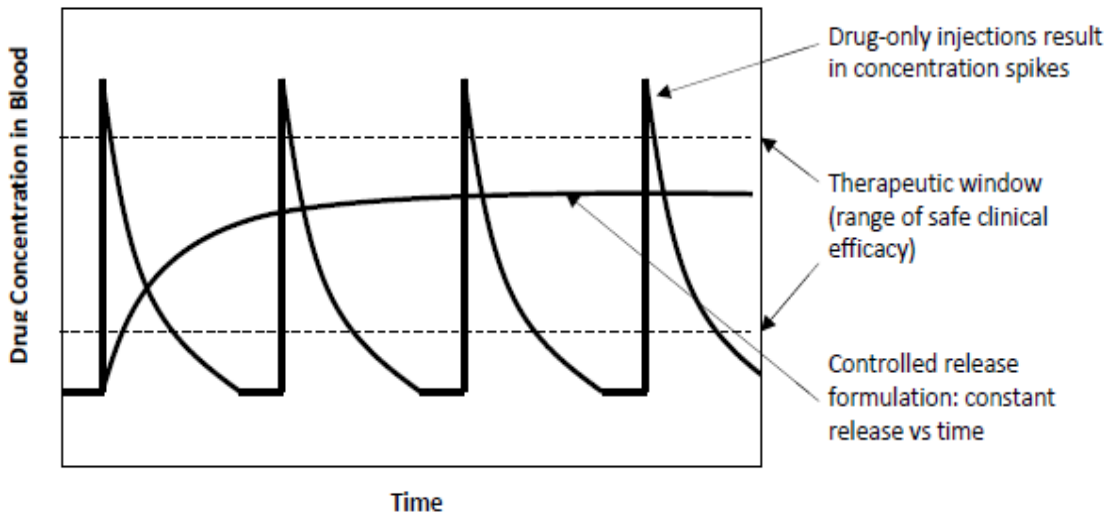

Figure 2.1 Therapeutic window for drug delivered via intravenous injection compared to using a controlled release vehicle (Reproduced with permission of Dr. Todd Hoare, McMaster University).

Most drug delivery methods, for example injections, result in a sudden spike in concentration of the drug in the blood stream, but the concentration decreases rapidly as the drug is absorbed into tissues, deactivated by chemical metabolism in the liver, or physically eliminated through the renal or digestive systems. Meanwhile, controlled drug release platforms offer the ability to stay within the therapeutic window for a longer period of time without the risk of tissue toxicity (Uhrich et al. 1999). Furthermore, systemic toxicity can be minimized by implanting the device adjacent to the site of action. This allows for the drug concentration at the site of action to be within the therapeutic window but diluted within systemic circulation to minimize adverse side effects. This type of delivery is particularly useful for highly toxic drugs with painful side-effects, such as chemotherapeutics for the treatment of cancer (Uhrich et al. 1999).

Many of the implantable, controlled release devices available and being developed are based on polymer systems because they can deliver drugs with widely varied physical and chemical characteristics while being non-toxic and eliciting a minimal immune response. Furthermore, although some polymer systems require surgical removal once their drug payload has been delivered, many systems can be designed to degrade *in vivo* in a controlled, non-toxic fashion, negating the need for surgical removal and allowing for better patient comfort (Uhrich et al. 1999).

A main consideration in the design of these types of systems is the activation of the reticuloendothelial system (RES). This system is responsible for the process by which blood-contacting foreign materials are recognized, tagged, and removed from the body or walled-off from other tissues. Recognition occurs when circulating proteins called opsonins interact with non-native surfaces, generally due to their hydrophobic or charged nature (Smeets and Hoare

2013). The proteins then 'tag' the material for removal by attaching to its surface (called opsonisation) (Jokerst et al. 2011). If small enough, the material is removed from circulation when it is engulfed by immune cells, which are subsequently filtered from the blood by the liver or spleen after which the material is degraded or eliminated (Jokerst et al. 2011). If the material is too large to be engulfed, this initiates a foreign body reaction which begins with the large-scale recruitment of immune cells to the material surface (acute inflammatory response) and results in the formation of a fibrous capsule around the biomaterial (chronic inflammatory response). The presence of a fibrous capsule is particularly detrimental in the case of devices for long-term drug release because the fibrous capsule represents an additional obstacle to drug absorption by the target tissue. Activation of the RES system can be limited by ensuring that all blood contacting surfaces of the implanted material are hydrophilic and uncharged (Jokerst et al. 2011).

Drug release from the polymer systems is commonly controlled in three different ways. A drug loaded polymer can control the release of drug by only releasing it as the polymer slowly degrades or dissolves into the biological media in which it is inserted. A semi-permeable polymer can surround a reservoir of drug that is released as water diffuses into the reservoir due to osmotic pressure and then carries dissolved drug out of the reservoir through pores in the polymer. Finally, drug can be entrapped or dissolved into a polymer and the drug is slowly released over time because the polymer phase slows diffusion of the drug (Uhrich et al. 1999). The latter mechanism is the most applicable to the research discussed in this thesis.

Not only can polymer systems release drugs in a controlled manner, but they can be designed to respond to biological stimuli which can result in triggered drug release. For example, Hoare & Pelton designed glucose-sensitive polymer particles that exhibited a 200 percent increase in volumetric swelling when exposed to glucose-containing solutions,

facilitating glucose-dependent release of insulin from the particles (Hoare and Pelton 2008),(Hoare and Pelton 2007b). Polymer systems can also be made that respond to changes in pH (Asmarandei et al. 2013), temperature (Hoare, Young, et al. 2012), (Fundueanu et al. 2013) and light (Campardelli et al. 2014). The ability to remotely trigger release from an implanted polymer device allows for even better controlled drug treatment through what is termed pulsatile drug delivery.

2.1.1 Pulsatile Drug Delivery:

While a controlled release vehicle allows for prolonged release within the therapeutic window, pulsatile release allows for repeated triggering of the polymer device to re-enter the therapeutic window without having to insert a new device. Figure 2.2 illustrates this process.

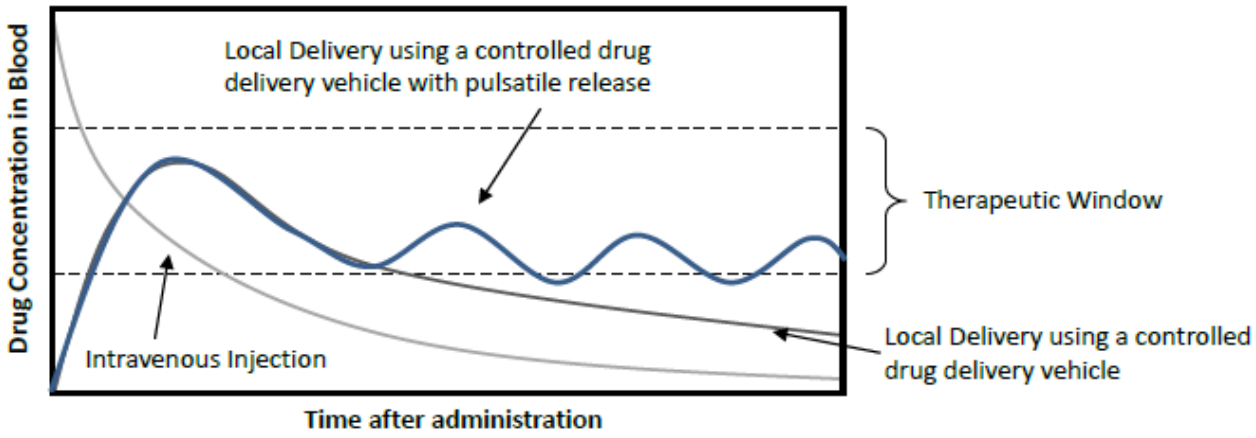

Figure 2.2: Therapeutic window for drug delivered via intravenous injection, using a controlled release vehicle and using a controlled release vehicle capable of pulsatile release (Reproduced with permission of Dr. Todd Hoare, McMaster University).

Polymer-based pulsatile release has been achieved using several different actuators. Demirel and von Klitzing achieved reversible, pulsatile release of Rhodamine B from

temperature and pH-sensitive, drug-loaded poly(vinylcaprolactam-co-2-dimethylaminoethyl methacrylate) nanoparticles with diameters between 81 and 368nm through the application of low-frequency ultrasound (Demirel and von Klitzing 2013). Nano-scale gold rods, hollow gold nanoparticles or particles with a gold nanoshell become optically excited and heat up when exposed to near-infrared (NIR) light (Campardelli et al. 2014). This characteristic has been exploited by Timko et al. who created a drug-reservoir device capped with a composite membrane containing gold nanoparticles and temperature-sensitive nanoparticles. When the membrane was exposed to NIR light, release from the drug reservoir increased up to 30-fold and the device could provide on/off pulsatile release over at least 10 cycles(Timko et al. 2014). Recently, Campardelli et al co-encapsulated hollow gold nanoshells with rhodamine in 200 nm diameter biodegradable poly(lactic acid) particles. Complete release of rhodamine from the particles could be achieved in 10 hours under NIR irradiation, compared to 12 days required for complete release in the absence of irradiation. The particles were also capable of repeatable, pulsatile release, with a maximum 2-3 times increase in release rate, when exposed to a NIR light source (Campardelli et al. 2014).

Alternating magnetic fields (AMFs) can also be used to excite and remotely heat magnetic nanoparticles (MNPs) that exhibit superparamagnetic characteristics (Laurent et al. 2008). For example, Satarkar & Hilt incorporated superparamagnetic iron oxide nanoparticles (SPIONs) into drug-loaded thermosensitive poly(N-isopropylacrylamide) (pNIPAM) nanoparticles and were able to achieve repeatable, pulsatile release of Vitamin B12 and methylene blue (Satarkar and Hilt 2008). The use of MNPs will be thoroughly discussed in later sections.

2.2 Hydrogels:

Hydrogels are three-dimensional networks of water-soluble polymers created through chemical or physical crosslinking of different polymer precursors (Hoare and Kohane 2008). Although the networks are capable of absorbing more than a thousand times their dry weight in water (Hoffman 2012), they do not dissolve in water (Saltzman 2001). Due to their high water content, coupled with our ability to engineer networks with similar chemical and mechanical properties to native body tissues, hydrogel networks can be made to illicit minimal immune responses. This makes them highly attractive for use in biomedical applications including cell encapsulation, tissue engineering, wound healing, and controlled drug release (Hoffman 2012), (Patenaude, Smeets, and Hoare 2014). However, the medical application of hydrogels is limited by the fact that their highly elastic mechanical properties make them difficult to implant in a minimally invasive fashion (i.e. via injection), such that surgical implantation is often required (Patenaude, Smeets, and Hoare 2014). Surgical implantation should ideally be avoided as it is more costly, more time-consuming for doctors, can decrease patient convenience and comfort, and also carries a significant risk of infection. Injectable hydrogel systems, consisting of polymer solutions that are liquid before insertion into the body but rapidly form hydrogels upon injection, allow for avoidance of surgery and for better conformation of the hydrogels to the space into which they are injected (Li, Rodrigues, and Tomas 2012). In these systems, a fast gelation time (less than a minute) is imperative because it prevents the polymer precursors from diffusing away from the injection site; if diffusion were to occur, a weaker gel with undesirable mechanical and/or functional characteristics (i.e. too much burst release, poor cell encapsulation) would likely result (Patenaude, Smeets, and Hoare 2014).

Injectable hydrogel networks can be formed by two primary mechanisms. With physical crosslinking of polymer chains, gelation is generally triggered by a specific characteristic, such as pH or temperature, of the body environment. For example, chitosan polymers phase separate at pH>6 to form a physically crosslinked hydrogel (Crompton et al. 2005). In contrast, chemical crosslinking of a pair of polymers possessing complementary chemistries results in spontaneous gelation and the formation of a crosslinked covalent bond network upon mixing. Figure 2.3 illustrates examples of these two processes.

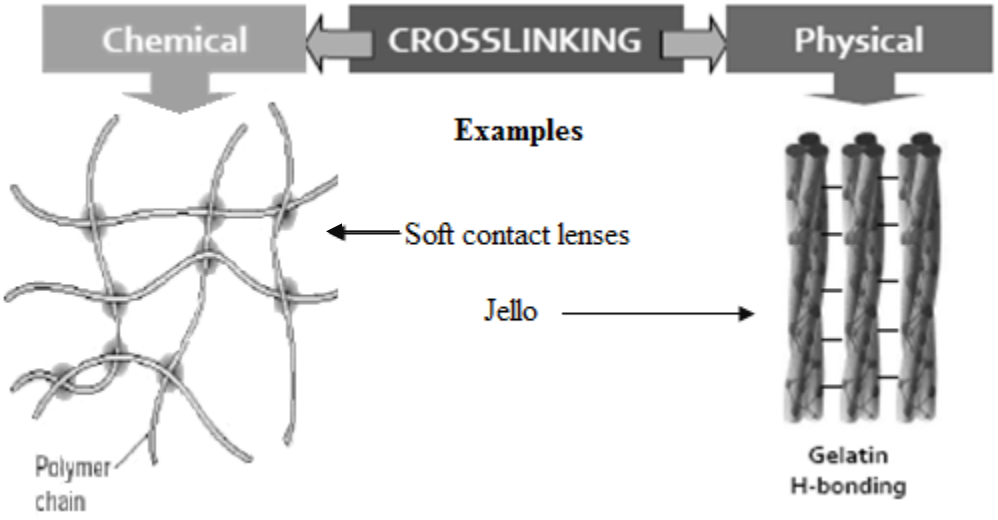

Figure 2.3: Examples of the formation of hydrogels through physical and chemical crosslinking polymers (Reproduced with permission of Dr. Todd Hoare, McMaster University).

One main benefit of using physically crosslinked hydrogels is that hydrogel formation can be achieved without the use of any reactive chemistries which can cause tissue damage or illicit immune activation in biomedical applications Unfortunately, because physically crosslinked hydrogels typically have low mechanical strength and the degradation and clearance of these hydrogels is difficult to control, this type of hydrogel is not ideal for long-term use in the body (Patenaude, Smeets, and Hoare 2014).

A main issue with the use of chemically crosslinked hydrogels is that the potential for the gel to contain unreacted, biologically active chemical residues. This risk can be mitigated by using orthogonal chemistries that do not react, or react minimally, with biological molecules. Risk can also be reduced by ensuring there is an excess of the less reactive residue of the covalent bond-forming pair, thus limiting the presence of the potentially damaging residue (Tao et al. 2013). Aside from having easily designed and controlled mechanical properties and rates of degradation, chemically crosslinked gels can be designed to gel faster and in a wider range of physiological conditions than physically crosslinked gels, making them generally better suited for a wider range of applications (Patenaude, Smeets, and Hoare 2014).

Several different chemistries are currently employed to create chemically crosslinked hydrogels. 1,-4 –addition (Michael-type addition) between a nucleophile (commonly thiol groups) and a carbonyl compound (such as ketone or an aldehyde) creates a stable hydrogel network under physiological conditions, but gel formation tends to proceed slowly (Li, Rodrigues, and Tomas 2012), decreasing the likelihood of forming a quality hydrogel after injection. Disulfide bond chemistry can be used to create a hydrogel network, but gelation rates are slow under physiological conditions, especially in the absence of an oxidizing agent (Patenaude, Smeets, and Hoare 2014). Ossipov et al created a hydrogel with oxime bonds (bonds between a hydroxylamine and an aldehyde) that gelled quickly (within 30 seconds of mixing), was stable for a period of 20 days in PBS, and showed no toxic effect when incubated with cells (Ossipov et al. 2010). Unfortunately, oxime hydrogels require an acid catalyst to gel at a high rate, making them only suitable for acidic environments within the body in the context of an injectable hydrogel formulation (Patenaude, Smeets, and Hoare 2014).

Hydrazone bonding occurs via the nucleophilic addition of a hydrazine or hydrazide's nitrogen to a carbonyl group (i.e. a ketone or an aldehyde), eliminating a water molecule. This reaction is shown in Figure 2.4 (a). For biomedical applications, a hydrazide group is preferred over a hydrazine group because it is less toxic (Patenaude, Smeets, and Hoare 2014). Hydrazone bonding between a hydrazide-functionalized polymer and an aldehyde-functionalized polymer has been shown to create mechanically robust, hydrolytically degradable hydrogels which form in a matter of seconds, have a long body residence time, and illicit minimal immune response *in vivo*, although it is advisable to ensure there is an excess of hydrazide groups to prevent undesirable aldehyde-protein interactions (Patenaude, Smeets, and Hoare 2014). Figure 2.4 (b) shows an illustration of the formation of a hydrazone-bonded hydrogel network by combining aldehyde and hydrazide functionalized precursors.

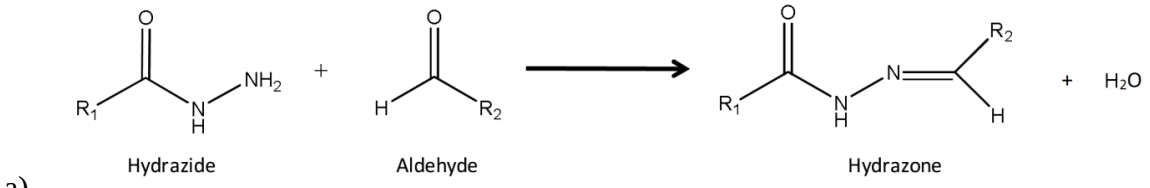

a)

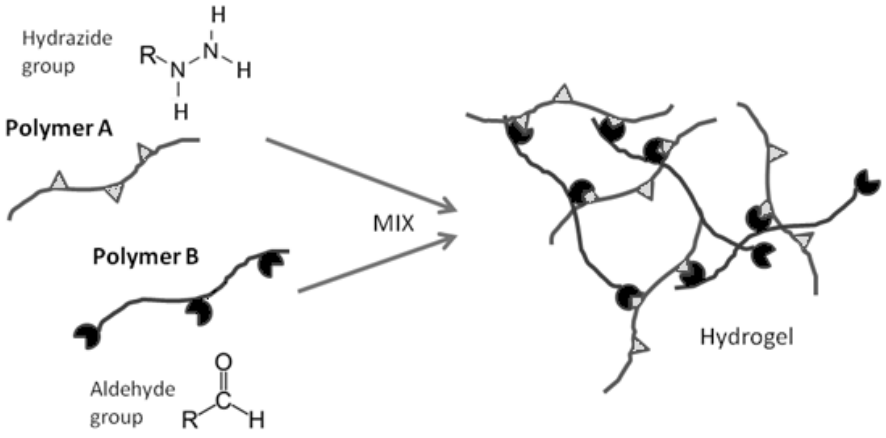

b)

Figure 2.4: (a) Hydrazone bond formation. **(b)** Hydrazone-bonded hydrogel network formation. Reproduced with permission from Dr. Todd Hoare, McMaster University.

Patenaude & Hoare created thermosensitive hydrogels by combining aldehyde and hydrazide functionalized pNIPAM polymers. The resulting hydrogel demonstrated favourable biological interactions via *in vitro* cell studies, with neither the gels nor their precursors significantly decreasing cell viability over a large concentration range (up to 2000 µg/mL) and *in vivo* subcutaneous injection using a mouse model showing a minimal inflammatory response even several months after injection (Patenaude and Hoare 2012a).

Patenaude & Hoare further demonstrated that mechanical and swelling characteristics could be easily controlled by combining hydrazide-functionalized pNIPAM with different ratios of dextran-aldehyde (which deswells at physiological temperature) to CMC-aldehyde (which swells at physiological temperature) (Patenaude and Hoare 2012b). By varying the ratio of dextran-aldehyde to CMC-aldehyde, these mixed natural-synthetic hydrogels could be tuned to have a wide range of swelling characteristics, mechanical properties and degradation times, with higher dextran-aldehyde contents corresponding to stronger, slower degrading gels (Patenaude and Hoare 2012b).

Hydrogels have shown the capacity for prolonged release of small molecule drugs (Zhang et al. 2014) as well as a wide range of macromolecular therapeutics including proteins (Ashley et al. 2013) and DNA(Wee and Gombotz 1998). Despite the demonstrated ability of hydrogels to provide slowed, sensitive release, improved control from hydrogel matrices can be accomplished by co-incorporation of nano-scale particles with variable physical or chemical characteristics (Hoare and Kohane 2008). These hydrogel nano-composites have tremendous potential for controlled release applications and will be discussed in the coming sections.

2.3 Microgels:

Microgels, also called hydrogel nanoparticles, are spherical, colloidal particles generally within the 50nm to 50µm size range composed of a micro-scale crosslinked polymer network (Pelton 2000). Figure 2.5 illustrates the structure of a typical microgel particle.

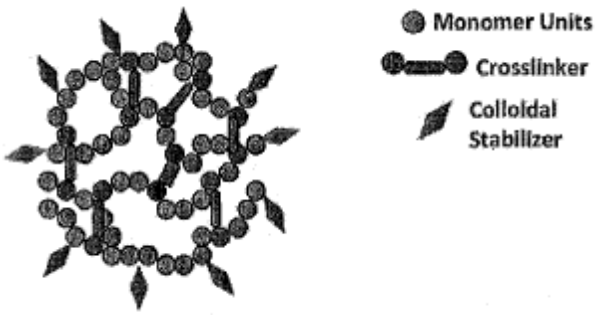

Figure 2.5: Structure of a typical microgel particle (Reproduced with permission of Dr. Todd Hoare, McMaster University).

Microgels represent an attractive and active area of research because they can be relatively easily synthesized in a way that allows for control of particle size and functionality. Size and functionality can impact the particle`s stability, biocompatibility, degradation kinetics, and viability as a long-term or controlled drug release vehicle (Smeets and Hoare 2013). Microgels are generally characterized by their diameter, swelling characteristics (degree of swelling and swelling kinetics) as well as their crosslink density, which can be determined by techniques including dynamic light scattering (DLS), electrophoresis, electron microscopy and rheology (Pelton 2000).

In order for injected microgel particles to be active in the body, they need to be in active circulation long enough to reach the desired site of action. The first characteristic of microgels that determines its bioavailability is size. Small microgels, generally with a diameter below 10

nm, are quickly cleared from circulation by renal filtration (Smeets and Hoare 2013) while larger particles, generally over 500nm, are filtered from the blood by the liver or spleen or are removed from active circulation after being phagocytosed by immune cells (Rejman et al. 2004). Size not only determines whether a particle remains in circulation, but also if it reaches its site of action. For example, because of the increased permeability of vasculature present in cancerous tumours, particles within the range of 200 nm to 1.2 μm preferentially filter into and accumulate in some cancerous tissues in a mechanism called the enhanced permeation and retention effect (EPR) (Matsumura and Maeda 1986) (Hobbs et al. 1998). Particle size is also critical in determining whether a microgel particle will be internalized by a cell or transported across the blood-brain barrier (Smeets and Hoare 2013). The physical characteristics of a microgel particle, specifically its hydrophobicity and its surface charge density, determine the degree to which it activates the RES system, with hydrophilic, charge-free particles attracting less immune system attention than hydrophobic, charged particles (Smeets and Hoare 2013).

Aside from designing particles with specific sizes and surface characteristics in mind, microgels can also be designed to react to certain stimuli. Of particular interest are temperature-sensitive microgels based on N-isopropylacrylamide (NIPAM). NIPAM contains both a hydrophobic isopropyl group and a hydrophilic amide bond, as illustrated in the monomer structure shown in Figure 2.6.

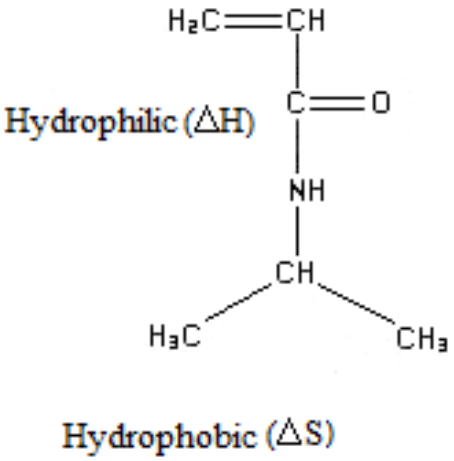

Figure 2.6: N-isopropylacrylamide monomer (Reproduced with permission of Dr. Todd Hoare, McMaster University).

pNIPAM exhibits an entropically-driven lower critical solution temperature (LCST) of around 32°C, below which the polymer is soluble and above which the polymer precipitates from solution (Pelton 2000). Rather than an LCST, pNIPAM microgels exhibit a volume-phase transition temperature (VPTT), the temperature at which the microgel volume drops suddenly as the particles expel water and deswell because of their hydrophilic to hydrophobic transition.

The LCST behaviour of NIPAM allows microgels to be fabricated by precipitation polymerization; the reaction takes place at a temperature much higher than the polymer LCST, so as linear polymer chains grow, they precipitate out of solution form precursor particles that grow through aggregation with other precursor particles to form microgels (Smeets and Hoare 2013). Pelton & Chibante first fabricated pNIPAM microgels using this procedure in 1986 (Pelton and Chibante 1986), and much research since has focused on how to best utilize, modify and target this thermosensitive “smart” polymer material.

NIPAM can be copolymerized with many different monomers to modify or improve its properties. For example, the VPTT of NIPAM-based microgels can be controlled by the co-

incorporation of hydrophilic comonomers, which result in a microgel with a higher VPTT, or the co-incorporation of hydrophobic comonomers, which result in a lower VPTT (Hoare and Pelton 2007a). Copolymerization can also be used to modify drug affinity for pNIPAM microgels. For example, by copolymerizing NIPAM with acidic functional groups, Hoare et al. were able to create anionic pNIPAM particles that were capable of binding and slowly releasing the cationic local anaesthetic bupivacaine (Hoare, Sivakumaran, et al. 2012).

For other applications, like remotely triggered pulsatile release or cancer treatment, it is desirable to increase the VPTT of the microgel to above 37°C so that microgel collapse and modulated release behaviours are not automatically activated upon injection but can be triggered by a desired stimulus, such as the increase of temperature caused by an applied alternating magnetic field or the increased temperature of approximately 39°C experienced when the microgels enter a thermogenic tumour. One way of creating a pNIPAM microgel with a higher VPTT is to copolymerize NIPAM with N-isopropylmethacrylamide (NIPMAM), which has an LCST of approximately 43°C. Copolymers of NIPAM and NIPMAM with a variety of VPTT behaviours, in which microgels with higher proportions of NIPMAM exhibited a higher VPTT, were fabricated by Hoare et al to be used to control the pulsatile, magnetically actuated temperature-sensitive release through a nanocomposite film (Hoare et al. 2011).

2.4 Superparamagnetic Iron Oxide Nanoparticles (SPIONs):

Superparamagnetic iron oxide nanoparticles (SPIONs) have been an area of great research interest in recent decades due to their varied biomedical and scientific applications including imaging (Saraswathy et al. 2014), bioseparation (Lui et al. 2013), cancer treatment

(Todd et al. 2014) and controlled, pulsatile drug release (Campbell, Patenaude, and Hoare 2013), among others.

SPIONs are generally in the size range of 4-18 nm, but the size and size distribution of the particles can be controlled by using different fabrication methods with varying control parameters (Laurent et al. 2008).

2.4.1 SPION Fabrication

SPIONs have been fabricated using emulsion techniques, in which the SPIONs are formed in uniform, aqueous-phase nanodroplets that allow for very precise control over particle size distribution (Laurent et al. 2008),(Chin and Yaacob 2007), and sol-gel systems, in which precursors are dissolved in solution to make a sol of magnetic nanoparticles formed through hydrolysis and condensation which is then heat-treated and dried to obtain SPIONs (Liu, Tao, and Shen 1997),(del Monte et al. 1997). Hydrothermal techniques, which use high pressure and temperature to form SPIONs from ferric salts dissolved in aqueous media through hydrolysis and oxidation (Laurent et al. 2008),(Wan et al. 2005), and electrochemical methods, which use an applied current to control of the size of SPIONs formed from electrolysis of an iron electrode in an aqueous solution (Pascal, Pascal, and Favier 1999), have also been reported. However, the most common method of SPION synthesis is by co-precipitation of iron salts; although control over the size distribution is limited via a precipitation-based synthesis route, it allows for the facile generation of a large quantity of nanoparticles. $\mathbf{Fe2}^{++}\ \mathbf{2Fe^{3+}} + \mathbf{8OH^-} \xrightarrow{\textbf{yields}} \mathbf{Fe_3O_4} + \mathbf{4H_2O}$ (1) describes the main chemical reaction of SPION formation (Laurent et al. 2008):

$$\mathbf{Fe^{2+}} + \mathbf{2Fe^{3+}} + \mathbf{8OH^-} \xrightarrow{\textbf{yields}} \mathbf{Fe_3O_4} + \mathbf{4H_2O} \qquad \mathbf{(1)}$$

It is believed that SPION generation follows two main steps: (1) nucleation, which forms the seeds (nuclei) for SPION creation, happens at a critical supersaturation of the species and ends quickly as the solution concentration of salts decreases and (2) particle growth, which occurs slowly as iron diffuses onto the surface of the nuclei (Laurent et al. 2008),(Boistelle and Astier 1988).

Massart et al. were the first to create SPIONs in a controlled manner by co-precipitating $FeCl_2$ and $FeCl_3$ in an alkaline solution (Massart 1981). They investigated the effect of the Fe^{2+}/ Fe^{3+} ratio and the type of base used on the SPION polydispersity and particle diameter. Further studies have suggested that to decrease the particle size distribution, the optimal Fe^{2+}/ Fe^{3+} ratio is 0.5 and the optimal iron concentration is between 39 and 78 mM, with the pH and ionic strength of the media tunable to control both the particle size and polydispersity (Babes et al. 1999), (Gribanov et al. 1990).

2.4.2 SPION Stabilization and Functionalization

Surface stabilization of SPIONs is generally used to prevent the SPIONs from aggregating when exposed to a magnetic field or when dissolved in aqueous or biological media. According to the Derjaguin-Landau-Verwey-Overbeek (DLVO) theory, a combination of van der Waals attractive forces and electrostatic repulsive forces determine whether particles will aggregate in a particular solvent (Derjaguin and Landau 1941),(Verwey and Overbeek 1948). In SPION systems, magnetic dipole forces represent an additional force of attraction between the particles. SPIONs can be stabilized by modifying their surfaces to be either more electrostatically repulsive or by adding molecules that provide steric repulsion (Laurent et al. 2008),(Vincent et al. 1986).

Monomers containing charged functional groups such as phosphates and carboxylates, can be attached to the surface of the SPIONs to increase electrostatic repulsion between the particles by imparting charge to their surface, decreasing aggregation while still maintaining a very small particle size (<10nm) (Sahoo et al. 2001) ,(Wagner et al. 2002). The addition of inorganics such as silica (Zhang et al. 2007) or gold (Lin et al. 2001) to SPION surfaces will shield the dipolar magnetic attractive forces and increase the electrostatic repulsive forces (particularly when coating with the negatively charged silica) while providing a highly functionalizable surface on which to bind biologically-relevant ligands (Laurent et al. 2008).

Coating SPIONs with polymers stabilizes the particles by increasing the steric and (sometimes) electrostatic repulsion between the particles. For example, coating SPIONs with hydrophilic polymers such as dextran (Saraswathy et al. 2014) or chitosan (Patil et al. 2014) that are well-tolerated by the immune system improves colloidal stability as well as the biocompatibility of the particles. Polymers can also improve the biological characteristics of the SPIONs; for example, SPIONs coated with poly(ethylene glycol) (PEG)-based polymers have decreased immune system activation (Aqil et al. 2008) and enhanced drug delivery capability (Andhariya et al. 2011). Particles coated with pNIPAM-containing polymers are not only colloidally stable but also thermoresponsive (Du et al. 2009) . Furthermore, particles coated with hydrazide-functionalized pNIPAM are not only thermosensitive but also capable of forming thermoresponsive, magnetic hydrogel matrices (Campbell, Patenaude, and Hoare 2013).

In addition to being functionalized with monomers, inorganics or polymers, an active area of research involves attaching biological molecules to SPIONs to give them bioactive properties. For example Bachelet-Violette et al functionalized SPION surfaces with fucoidan, a ligand for a receptor expressed on the surface of activated platelets. Activated platelets play an

important role in the hardening/ blocking of arteries, and giving the SPIONs an affinity for activated platelets has the potential to allow for better imaging of cardiovascular disease (Bachelet-Violette et al. 2014). Licciardi et al demonstrated that tumour cells could be made to selectively uptake SPIONs by functionalizing their surface with folate derivatives, providing the potential for targeted drug delivery to cancer cells as well as the potential for better imaging and better targeted hyperthermia treatment of the cancer (Licciardi et al. 2013).

2.4.3 SPION Paramagnetism and Remote Heating

Magnetic materials contain regions of uniform magnetization which are called magnetic domains. Due to the very small size of SPIONs, they contain only a single magnetic domain (called a monodomain), meaning that the entire particle is magnetized with a uniform, mono-directional magnetization (Laurent et al. 2008). The direction of a particle's magnetization vector with relation to its crystalline structure is what determines the magnetic energy of a particle at any given time. Certain orientations called easy directions (generally located opposite to each other on the particle) minimize the magnetic energy of the particle; magnetic energy increases as the angle between the magnetization vector and the easy directions increase (Crangle 1991). The act of a particle reorienting to switch its magnetization from one easy direction to another is called a relaxation. The average time between two switches or the time to return to an equilibrium after agitation is called the Néel relaxation time (Laurent et al. 2008). In magnetic fluids, two types of relaxations dictate the relaxation rate of a particle: Néel relaxation and Brownian relaxation. Brownian relaxation is the viscous rotation of the entire particle in solution (Laurent et al. 2008),(Rosenweig 1985). When the magnetic relaxation of a particle is fast enough (or the time between magnetic measurements is long enough) the system appears to be always in equilibrium (i.e. have zero average magnetization) even though it is magnetic and can

be easily and dramatically magnetized by an externally applied field. This is called 'superparamagnetism' (Bean and Livingston 1959).

The magnetic properties of the SPIONs provide three very important ways in which they can be manipulated and used. First, their magnetic properties make them very useful contrast agents for magnetic resonance imaging (MRI) (Pouliquen et al. 1991). Second, the particles can be oriented, directed, and moved by magnetic fields, allowing for particle localization (Todd et al. 2014) and flow control (Pouponneau, Leroux, and Martel 2009). Third, when exposed to an alternating magnetic field, the reorientation of the magnetic domains results in power dissipation (hysteresis heating) and to a lesser extent, the particles can physically move (frictional or mechanical heating) to facilitate remote heating of SPIONs and their surrounding environment by a highly penetrative but non-invasive magnetic field (Jackson et al. 1997). Combined, these characteristics have resulted in a wide variety of technological applications.

2.4.4 SPION Technological Applications

Many biomedical and scientific applications of SPIONs are currently being investigated. As a result of their magnetic properties, SPIONs are very effective contrast agents for MRI (Wagner et al. 2002). They have been used to visualize activated platelets (Bachelet-Violette et al. 2014), monitor the movement of SPION-labelled stem cells during wound healing (Chen et al. 2014), and have been modified to selectively aggregate in tumours which would allow for improved imaging in addition to possible hyperthermia treatment (Licciardi et al. 2013). Due to their remote heating capabilities and the fact that cancer cells are more easily killed by high temperatures compared to native tissues, SPIONs can be used to thermally ablate tumours using hyperthermia treatments (Laurent et al. 2008),(Patil et al. 2014), (Aqil et al. 2008). Several such systems have been approved for clinical trials for cancer treatment and have shown promising

results (Laurent et al. 2011). SPIONs have also been used to deliver gene vectors into cells (called magnetofection) (Huang et al. 2013), as non-toxic tracers in bioassays (Lak et al. 2013), and by modifying the surface with cell-specific ligands, as magnetic carriers for specifically harvested cells (Lui et al. 2013), (Pavlov et al. 2013).

Of specific interest is the use of SPIONs for controlled or pulsatile drug release. As mentioned above, after injection, SPIONs can be directed to their desired site of action by biological interactions (such as ligands or antibodies attached to their surface) and/or magnetic steering. Todd et al. used a magnet to attract and trap SPIONs at the tumour site, facilitating slow desorption of drug into the tumour from the SPION-functionalized diatoms (Todd et al. 2014). In some systems, heating and controlled drug release are synergistic, but not connected. For example, in the system developed by Meenach et al, magnetic nanoparticles were coated with a slowly-degrading polymer that released drug as it degraded. In this system, the SPIONs could be used to help localize the particles in the tumour and heated to damage the cancer cells to increase the efficacy of the drug being released, but magnetic activation was not used to control drug release (Meenach et al. 2012). Other systems attach drug-loaded, thermosensitive polymers to the SPION surface so that magnetically heating the particles results in increased, potentially pulsatile release either due to the collapse of the polymer attached to the particle surface (Milošević et al. 2014), or by the increased degradation of a heat sensitive polymer (Hawkins, Satarkar, and Hilt 2009).

As free particles injected into the body, SPIONs must be smaller than 200 nm to prevent immune cell phagocytosis and sequestration in the spleen and larger than 10 nm to avoid renal clearance (Laurent et al. 2008). By incorporating the particles into biocompatible, bulk matrices,

their remote heating characteristics can be exploited in interesting ways while eliciting less immune activation. Several such composites are described in the Section 2.5.

2.5 Hydrogel Composites:

Incorporating nanoparticles with different characteristics into hydrogel networks creates hydrogel composites, also called hydrogel nanocomposites. These composites help address the limitations of both the nanoparticle and hydrogel systems. By physically entrapping nanoparticles within a hydrogel network by co-injection, they are immobilized at the desired site of action, are able to react to their environment largely independently of the bulk hydrogel, and retain their unique physical or chemical properties all while avoiding immune activation by 'hiding' in a biocompatible hydrogel network. Nanoparticle incorporation into hydrogel networks also addresses some limitations of hydrogel systems, providing (for example) better controlled release or improved mechanical properties. For example, by reinforcing a hydrogel network made of crosslinked aldehyde-functionalized dextran and hydrazide-functionalized CMC with rod-like cellulose nanocrystals (CNCs), Yang et al were able to better control and improve the mechanical properties of the resulting composites (Yang et al. 2013). Sivakumaran et al entrapped anionic pNIPAM microgels into a dextran-aldehyde, CMC-hydrazide system creating so called 'plum-pudding' hydrogel composites, illustrated in Figure 2.7. The hydrogel composites had improved drug release properties, with localized release of cationic bupivacaine occurring for up to 60 days compared to the less than one week of release observed from the hydrogels or microgels alone (Sivakumaran, Maitland, and Hoare 2011).

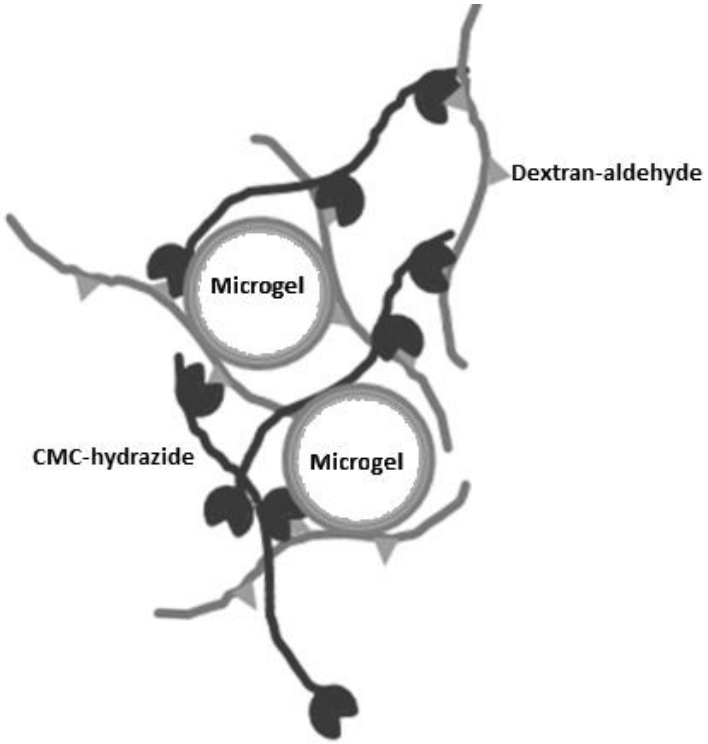

Figure 2.7: Microgels imbedded in a hydrogel network to make a 'plum-pudding' nanocomposite (Reproduced with permission of Dr. Todd Hoare, McMaster University).

Hydrogels can also be imbued with magnetic properties through the co-incorporation of SPIONs into the composite. For example, Satarkar et al created a thermosensitive pNIPAM-SPION hydrogel valve and were able to successfully use it to control the flow through a microfluidic device. Through the application of AMF, the SPIONs heated the composites above the VPTT of the pNIPAM hydrogel, resulting in composite shrinkage and opening of the fluid channel (Satarkar et al. 2009).

For controlled drug release applications, Rovers et al created a surgically implantable cylindrical poly(methyl methacrylate)–SPION composite and coated it with a 0.3 mm layer of thermoresponsive poly(butyl methacrylate-stat-methyl methacrylate) polymer loaded with ibuprofen. Reversible increases in ibuprofen release from the composite by up to 25 times were

achieved in a pulsatile manor through AMF activation (Rovers 2012). Campbell et al (2013) created injectable magnetic hydrogel composites by functionalizing the surface of iron oxide nanoparticles with hydrazide-functionalized pNIPAM (hzd-SPIONs) and gelling them with aldehyde-functionalized dextran. The resulting gels were highly elastic and demonstrated repeated pulsatile release of the cationic, local anaesthetic bupivacaine upon application of an oscillating magnetic field (Campbell, Patenaude, and Hoare 2013).

Functional polymer composites can be made by co-incorporating both SPIONs and thermosensitive microgels into a polymer matrix. Hoare et al created composite ethyl cellulose membranes containing magnetic nanoparticles and p(NIPAM-NIPMAM) microgels (VPTT approximately 40°C) that were affixed to implantable reservoirs containing sodium fluorescein. When an oscillating magnetic field was applied to the membrane at 37°C, the composite temperature increased above the microgel VPTT, the microgels collapsed, and a 10 to 20 fold increase in differential flux from the reservoir was observed (Hoare et al. 2009). No significant increase in drug flux was noted when the composite did not contain the thermosensitive microgels or when pNIPAM microgels with an VPTT of 32°C were used (Hoare et al. 2009). Hoare et al further demonstrated that pulsatile drug release from such a device could be controlled by modifying the VPTT of the microgel, changing the membrane thickness and increasing the loading density of the microgels in the membrane. Drug dose could be modified from 0.1-10 μg/hr and the release could be reproduced between different pulse cycles and across different membranes (Hoare et al. 2011).

2.6 Research Objectives

The objectives of this research project are to create an injectable, biocompatible pNIPAM/carbohydrate magnetic nanocomposite with embedded thermosensitive microgel particles for controlled, localized pulsatile drug release. The goal is to optimize pulsatile release from this system by determining the effect of using different types of SPIONs, the effect of incorporating microgel particles into the composite, the effect of incubating the composites at different temperatures, the role of microgel VPTT on pulsatile release, the effect of microgel content on pulsatile release, and the effect of bulk hydrogel swelling on pulsatile release.

2.7 Materials Used:

2.7.1 Hydrogel Components:

The composite's bulk hydrogel was formed via hydrazone crosslinking between aldehyde-functionalized dextran and/or CMC and hydrazide functionalized pNIPAM, analogous to the hydrogels previously described by Patenaude and Hoare (Patenaude and Hoare 2012b).

2.7.1.1 Aldehyde-functionalized Dextran

Dextrans are generally synthesised by the enzymatic action of dextransucrase enzymes (secreted by the microbial species *Leuconostoc, Lactobacillus and Streptococcus*) on sucrose and are defined as homopolysaccharides containing a significant amount (generally more than 50%) of consecutive α(1,6)-linkages in their major chains. Side-chains also occur, mostly at the α(1,3) sites and less frequently from the α(1,2) and α(1,4) linkages, with the specific structure depending on which microbial strain was used for dextran production (Naessens et al. 2005). The structure of dextran is illustrated below in Figure 2.8.

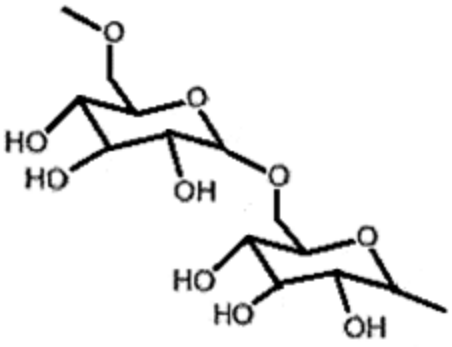

Figure 2.8: A dextran molecule.

In terms of biomedical uses, dextran or dextran polymer derivatives have been utilized as blood plasma substitutes and blood thinners (Naessens et al. 2005). Dextran is an attractive material for use in hydrogels because it demonstrates low tissue toxicity and can be enzymatically degraded under physiological conditions (Chiu et al. 1999).

In order to be able to form a hydrazone-bond-based hydrogel, dextran can be aldehyde-functionalized via the chemistry illustrated in Figure 2.9 (Patenaude and Hoare 2012b) .

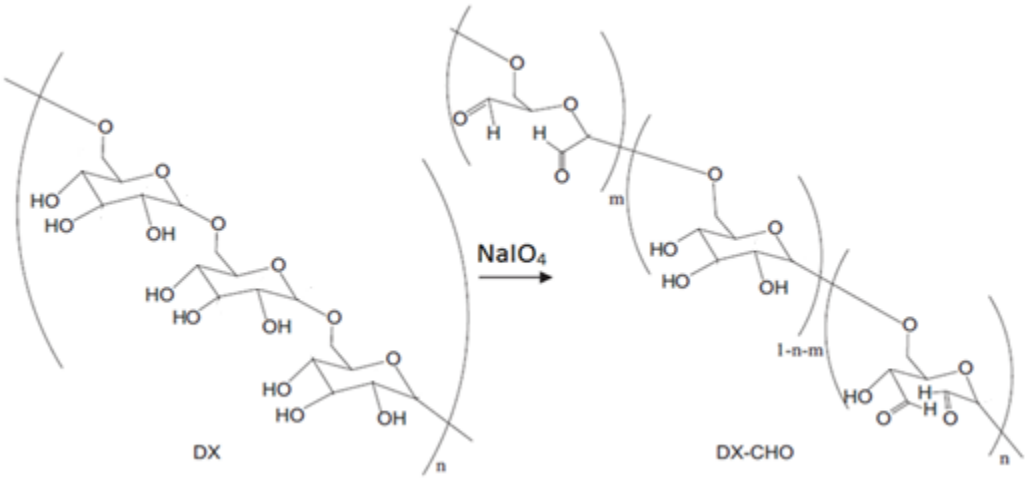

Figure 2.9: Aldehyde functionalization of dextran (Reproduced with permission of Dr. Todd Hoare, McMaster University).

Aldehyde-functionalized dextran has been utilized extensively in the formation of injectable hydrogel matrices by the Hoare lab in the formation of mixed natural-synthetic hydrogels (Patenaude and Hoare 2012b), slow releasing microgel/hydrogel plum-pudding nanocomposites (Sivakumaran, Maitland, and Hoare 2011), and highly elastic, SPION-hydrogel composites for pulsatile drug delivery (Campbell, Patenaude, and Hoare 2013). The polymer has shown to be non-cytotoxic even at high concentrations (2000 µg/mL) (Sivakumaran, Maitland, and Hoare 2011), and hydrogel composites made with aldehyde-functionalized dextran have been well tolerated by tissues *in vitro* and *in vivo* (Patenaude and Hoare, unpublished).

2.7.1.2 Aldehyde-functionalized Carboxymethyl Cellulose

Carboxymethylcellulose (CMC) is an ionic ether cellulose derivative where 25% to 75% (per disaccharide unit) of the cellulose's hydroxymethyl ($-CH_2OH$) groups are substituted with carboxymethyl ($-CH_2COOH$) groups (Barbucci, Magnani, and Consumi 2000). In terms of biomedical uses, CMC is commonly used to reduce epidural scarring and prevent postoperative adhesions (Barbucci, Magnani, and Consumi 2000).

Both hydrazide and aldehyde functionalized CMC have been used to form a hydrazone-bond-based hydrogel (Sivakumaran, Maitland, and Hoare 2011), (Patenaude and Hoare 2012b). The aldehyde-functionalization of CMC is illustrated in Figure 2.10. Use of aldehyde functionalized CMC has been shown to create hydrogels which swell significantly in solution at physiological temperature (Sivakumaran, Maitland, and Hoare 2011), (Patenaude and Hoare 2012b). This swelling can be contributed to the anionic functional groups on CMC, which create an osmotic pressure gradient across the gel/solvent interface, driving solvent into the gel and significantly increasing gel swelling due to Donnan equilibrium effects (Ricka and Tanaka 1984).

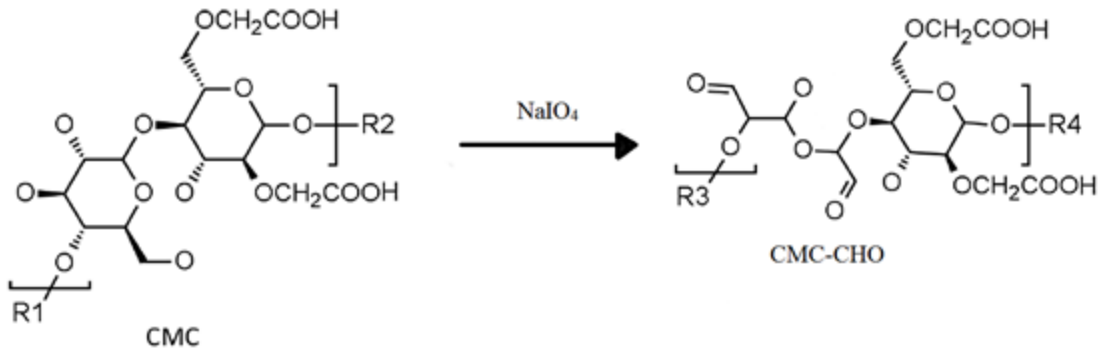

Figure 2.10: Aldehyde functionalization of carboxymethylcellulose (Reproduced from Patenaude & Hoare, 2012a with permission).

Aldehyde-functionalized CMC has been shown to be non-cytotoxic, even at high concentrations (2000 µg/mL) (Sivakumaran, Maitland, and Hoare 2011), and hydrogel composites made with aldehyde-functionalized dextran have been well tolerated by tissues *in vitro* and *in vivo* (Patenaude and Hoare, unpublished).

2.6.1.3 Hydrazide-functionalized pNIPAM

NIPAM (Figure 2.6) can be copolymerized with acrylic acid and subsequently hydrazide functionalized via carbodiimide coupling of a large excess of adipic acid dihydrazide for use in forming hydrazone-bonded hydrogels (Patenaude and Hoare 2012a). The synthesis process is illustrated in Figure 2.11.

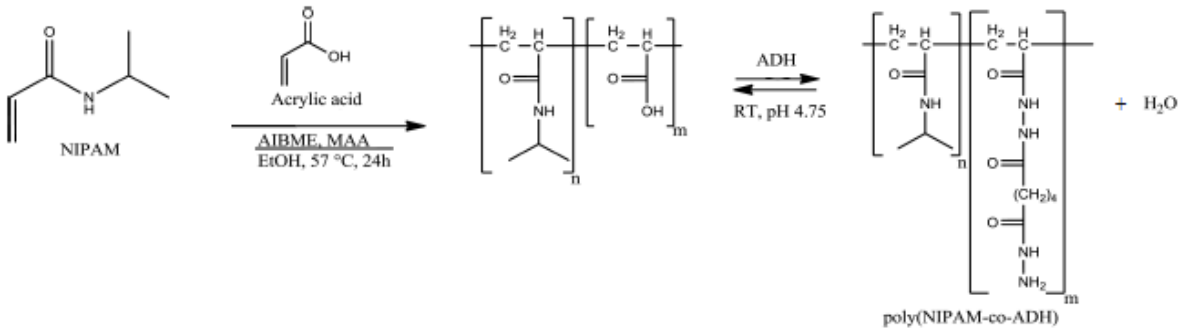

Figure 2.11: Hydrazide functionalization of pNIPAM (Reproduced with permission of Dr. Todd Hoare, McMaster University).

Use of chain-transfer agents during the polymerization process makes it possible to limit the polymer molecular weight to less than 22 kDa, ensuring that polymer size will be below the renal clearance cut-off of 40 kDa such that hydrogel degradation products would not bioaccumulate (Patenaude and Hoare 2012a).

pNIPAM-hydrazide and hydrogels formed using the polymer retained their LCST behaviour and were non-cytotoxic to 3T3 mouse fibroblast cells up to a concentration of 400 µg/mL and to retinal pigmented epithelial (RPE) cells over all concentrations tested (up to 2000 µg/mL)(Patenaude and Hoare 2012a). *In vivo* tests demonstrated that pNIPAM-hydrazide and its hydrogels induce a very limited, acute inflammatory response (similar to what is seen for a control injection of phosphate-buffered saline) 48 hours after injection. At 5 months post-injection, the gel was still present at the injection site and there was no sign of a chronic inflammatory response to the hydrogel (Patenaude and Hoare 2012a).

2.7.2 Poly (NIPAM-NIPMAM) Microgels

Microgels fabricated by copolymerization of NIPAM, NIPMAM and acrylamide (AAm) for use in pulsatile drug delivery have been reported previously by Hoare et al. (Hoare et al. 2011). NIPMAM, illustrated in Figure 2.12, has a higher LCST (~43°C) than NIPAM (~32°C) because the presence of an additional methyl group on the polymer backbone that increases the polymer stiffness, limits the formation of intramolecular interactions, and inhibits the collapse of the polymer (Hertle and Hellweg 2013).

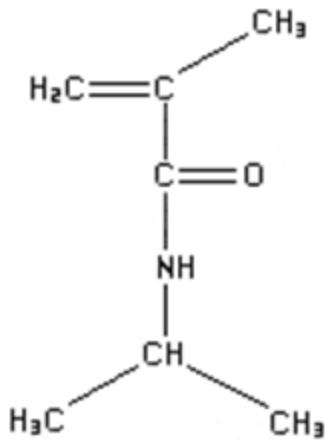

Figure 2.12: N-isopropylmethacrylamide structure.

In vitro testing of these microgels has demonstrated that they are non-cytotoxic even at high concentrations (2000 µg/mL) and that their VPTT behaviour can be varied from approximately 35°C to 40°C by changing the NIPAM:NIPMAM ratio (Campbell & Hoare, unpublished).

2.7.3 Iron Oxide Nanoparticles:

Two different surface coatings were applied to the SPIONs used in this project: polyethylene glycol (PEG-SPIONs) and pNIPAM-hydrazide (hzd-SPIONs).

2.7.3.1 PEG-functionalized SPIONs

Polyethylene glycol (PEG), also known as polyethylene oxide (PEO), is a hydrophilic, uncharged, non-immunogenic polymer that is often referred to as a ‘stealth’ polymer due to its ability to circulate in the blood stream without being recognized as a foreign body by the immune system (Smeets and Hoare 2013). It can be used to decrease nanoparticle aggregation by lowering the particles’ surface energy and reducing the force of van der Waals attraction between particles (Jokerst et al. 2011). The structure of PEG is illustrated in Figure 2.13. Due to its

'stealth' properties, nanoparticle systems (including SPIONs) frequently incorporate PEG on their surface to improve their potential for biomedical application (Jokerst et al. 2011).

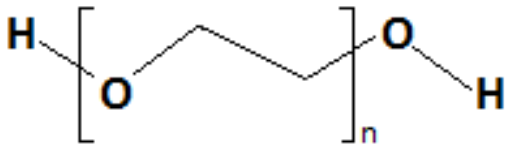

Figure 2.13: Polyethylene glycol (PEG) molecule.

2.7.3.2 pNIPAM-Hydrazide Functionalized SPIONs

Campbell & Hoare fabricated SPION particles coated with hydrazide functionalized pNIPAM in order to create a magnetic hydrogel composite with magnetic nanoparticles that could be covalently crosslinked into the hydrogel network instead of being physically entrapped (Campbell, Patenaude, and Hoare 2013). The resulting particles were superparamagnetic and non-cytotoxic up to high concentrations (2000 µg/mL), with subcutaneous injections of hzd-SPION / dextran-aldehyde hydrogels *in vivo* indicating minimal chronic immune response with no fibrous capsule formation around the composite (Campbell, Patenaude, and Hoare 2013).

2.7.4 Fluorescein isothiocyanate-Dextran (FITC-Dex)

Fluorescein isothiocyanate (FITC) is a fluorescein derivative that has been widely used as a fluorescent tag to allow for easy tracking, visualization and quantification of larger molecules. It was first utilized beginning in 1958 when A.H. Coons first attached it to antibodies to allow for antigen localization and identification (Coons 1958), (Borek 1961). FITC is an attractive fluorescent tag because it can be easily attached to a wide range or molecules while remaining stable and maintaining a high degree of fluorescence (Marshall, Eveland, and Smith 1958). The chemical structure of FITC is illustrated in Figure 2.14a.

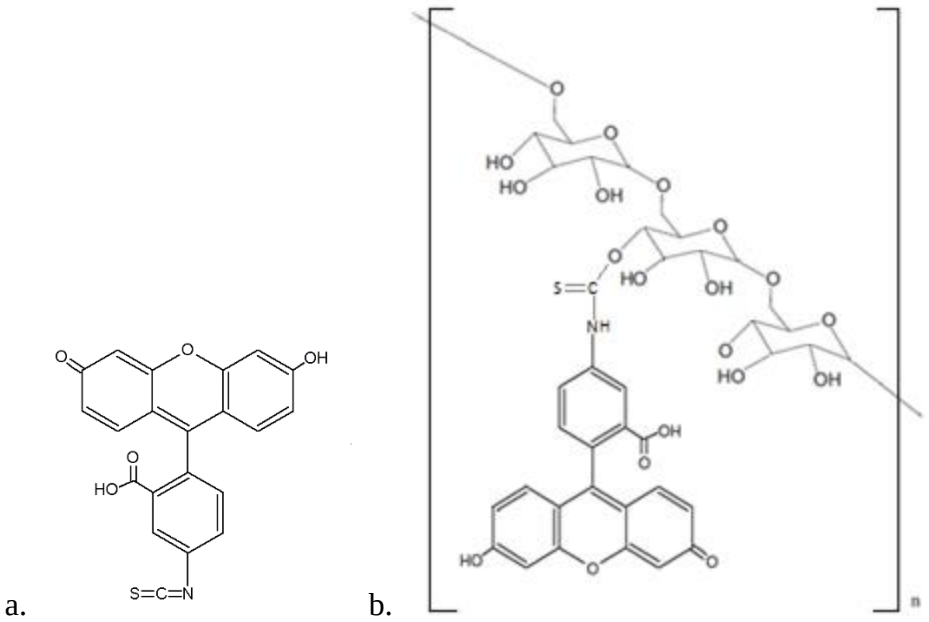

Figure 2.14: a. Fluorescein isothiocyanate chemical structure b. Illustration of fluorescein isothiocyanate -labelled dextran.

Dextran molecules are frequently labelled with FITC (as illustrated in Figure 2.14b) for use as model proteins or model macromolecules because they can be selected for size (between 4000-150000), are non-toxic, and their concentration can be easily quantified (Stock, Cilento, and McCuskey 1989). Similar to fluorescein and FITC, the concentration of FITC-Dex in solution can be determined using a spectrofluorometer and the molecules (independent of molecular weight) have a maximum excitation (absorption) wavelength of 495 nm and an emission maximum at 512 nm (Ohtani et al. 1991).

Chapter 3: Materials and Methods

3.1 Reagents:

Aldehyde Functionalized Dextran and Carboxymethyl Cellulose:

Dextran from *Leuconstroc spp* (MW ≈500,000), sodium carboxymethyl cellulose (CMC, MW ≈ 700,000), sodium periodate (>99.8%) and ethylene glycol (99.8%) were purchased from Sigma Aldrich (Oakville, Ontario).

Acrylic Acid Functionalized P(NIPAM) (P(NIPAM-co-AA))

NIPAM monomer (99%) was purchased from Thermo Fisher Scientific (New Jersey, NJ). 2,2-azobisisobutyric acid dimethyl ester (AIBME; 98.5%) was purchased from Wako Chemicals. Thioglycolic acid (≥ 98.1%) and acrylic acid (AA; 99%) were purchased from Sigma Aldrich (Oakville, Ontario).

Hydrazide Functionalized P(NIPAM-co-AA)

Adipic acid dihydrazide (ADH; 98%) was purchased from Alfa Aesar (Ward Hill, MA). N'-ethyl-N-(3-dimethylaminopropyl)-carbodiimide (EDC; commercial grade) was purchased from Sigma Aldrich (Oakville, Ontario). Hydrochloric acid was purchased from LabChem Inc. (Pittsburgh, PA).

Poly (NIPAM-Acrylamide-NIPMAM)

NIPAM monomer (99%) was purchased from Thermo Fisher Scientific (New Jersey, NJ). NIPMAM monomer (97%), N-N'-methylene bisacrylamide (MBA; 99%), Acrylamide

(AAm; ≥ 99%) and ammonium persulfate (APS; 98%) were purchased from Sigma Aldrich (Oakville, Ontario).

Superparamagnetic Iron Oxide Nanoparticles (SPIONs):

Iron (II) chloride tetrahydrate (98%) and iron (III) chloride hexahydrate (97%), ammonium hydroxide (28-30% NH_3 content) and poly(ethylene glycol) (PEG; 8kDa) were purchased from Sigma Aldrich (Oakville, Ontario).

Drug Release Studies

Fluorescein isothiocyanate-labelled dextran (FITC-Dex) (MW≈ 4 kDa and 70kDa) was purchased from Sigma Aldrich (Oakville, Ontario). Phosphate buffered saline was prepared using sodium chloride, sodium phosphate, potassium chloride and potassium phosphate purchased from Sigma Aldrich (Oakville, Ontario).

Cell Culture:

3T3 *Mus musculus* mouse fibroblast cells were obtained from Cedarlane Laboratories Ltd. (Burlington, ON) and were cultured in media containing Dulecco's Modified Eagle Medium-high glucose (DMEM), fetal bovine serum (FBS) and penicillin streptomycin (PS) acquired from Invitrogen Canada (Burlington, ON). Trypsin-EDTA was also acquired from Invitrogen Canada (Burlington, ON). Dimethyl sulfoxide (DMSO) and thiazolyl blue tetrazolium bromide (MTT) were purchased from Caledon Laboratory Chemicals (Georgetown, ON) and Sigma Aldrich (Oakville, ON), respectively.

All water used was purified using a Barnstead Nanopure ultrapure water system and was Milli-Q grade.

Appendix A (Table A.1) contains further information about the reagents used.

3.2 Purification of NIPAM and NIPMAM Monomers:

NIPAM or NIPMAM monomers (30 g) were mixed with toluene (300 mL) and hexane (20 mL). The mixture was heated in an oil bath to 60°C until the monomer dissolved, after which it was transferred to an ice bath for 1-2 hours to allow for recrystallization. The solution was filtered and rinsed with hexane, with the isolated, recrystallized NIPAM or NIPMAM dried under nitrogen for 12 hours before being stored in a 4°C refrigerator.

3.3 Synthesis of NIPAM-co-AA:

Synthesis of NIPAM-co-acrylic acid was based on methods described by Patenaude and Hoare (Patenaude and Hoare 2012b) . N-Isopropylacrylamide monomer, purified to 99.9% using a 60:40 toluene:hexane mixture (4.0 g), acrylic acid (0.952 mL), 2,2-azobisisobutyric acid dimethyl ester (AIBME) initiator (0.056 g), and thioglycolic acid (87µL) were dissolved in 20 mL absolute ethanol. Polymerization was allowed to proceed overnight in a three-necked flask with an attached condenser at 56°C under nitrogen purge and magnetic stirring at 200 rpm. Solvent was removed at reduced pressure at 50°C using a rotary evaporator. The viscous product was redissolved in 200 mL of deionized water and dialyzed with Spectrum Labs membrane tubing with a MWCO of 12-14,000 Da. A minimum of six, six hour dialysis cycles were completed against deionized water before the solutions were lyophilized and stored in their dried form for later use.

3.4 Hydrazide Functionalization of NIPAM-co-AA to produce NIPAM-co-ADH:

Hydrazide functionalization of NIPAM-co-AA was based on methods described by Patenaude and Hoare (Patenaude and Hoare 2012a). NIPAM-co-AA (3.0 g) and a 5x molar excess of adipic dihydrazide (ADH, 7.25 g) were dissolved in 600 mL deionized water in a 1 L round bottom flask. The pH was adjusted to 4.75 using 1.0 M HCl. A 2.5x molar excess of N'-ethyl-N-(3-dimethylaminopropyl)-carbodiimide (EDC, 3.99 g) dissolved in 5 mL of deionized water was added to the solution, and dropwise addition of 0.1 M hydrochloric acid was used to maintain the pH at 4.75 for the duration of the reaction. The reaction was allowed to proceed for 4 hours until it was stopped by increasing the pH to 7 through the addition of 0.1 M sodium hydroxide. The polymer solution was dialyzed with Spectrum Labs membrane tubing with a MWCO of 12-14,000 Da. A minimum of six, six hour dialysis cycles were completed against deionized water before the solutions were lyophilized and stored in their dried form for later use.

3.5 Aldehyde Functionalization of Dextran and Carboxymethyl Cellulose:

Dextran or CMC (500 kDa or 700 kDa, 3.0 g) were dissolved in 300 mL of deionized water in a 500 mL round bottom flask under magnetic stirring at 400 rpm. Sodium periodate ($NaIO_4$, 1.6 g) was dissolved in 15 mL of deionized water and added dropwise to the polymer solution, after which the solution was left to stir for 2 hours. Ethylene glycol (0.8 mL) was then quickly added to the solution and left to react for 1 hour. The resulting solution was dialyzed with Spectrum Labs membrane tubing with a molecular weight cut-off (MWCO) of 12-14,000 Da. A minimum of six 6 hour dialysis cycles were completed against deionized water before the solutions were lyophilized and stored in their dried form in a 4°C refrigerator for later use.

3.6 Poly (NIPAM- NIPMAM) Microgel Polymerization:

Poly(NIPAM-NIPMAM) microgels were produced using methods described by Hoare et al (2011) (Hoare et al. 2011). Recipes utilizing different amounts of NIPAM and NIPMAM monomers, chosen to achieve different temperature behaviours, can be found in Table 3.1. As an example of one of these formulations, acrylamide (0.05 g), methylene bisacrylamide (0.08 g), and purified NIPAM and NIPMAM monomers (combined mass of 1.4 g) were dissolved in 150 mL of deionized water in a three-necked, 250 mL round bottom flask with 200 rpm of magnetic stirring and attached condenser. After purging with nitrogen for 25 minutes and heating to 70°C, ammonium persulfate (0.10 g) initiator dissolved in 5 mL of deionized water was added to the solution. The reaction was allowed to proceed overnight under nitrogen at 70°C and dialyzed with Spectrum Labs membrane tubing with a MWCO of 12-14,0000 Da for a minimum of six, 6 hour dialysis cycles against deionized water before the solutions were lyophilized and stored in their dried form for later use.

Table 3.1: Recipes for p(NIPAM-NIPMAM) microgels. Note that the sample codes represent the NIPMAM:NIPAM mass ratio used to prepare the microgel.

Polymer Code	NIPMAM:NIPAM Ratio	NIPAM Monomer (g)	NIPMAM Monomer (g)	AAm (g)	MBA (g)
$M_{1.8}$ (High)	1.8:1	0.9	0.5	0.05	0.08
$M_{1.3}$ (Med-High)	1.33:1	0.8	0.6	0.05	0.08
M_{1} (Med)	1:1	0.7	0.7	0.05	0.08
$M_{0.56}$ (Med-Low)	0.56:1	0.5	0.9	0.05	0.08
$M_{0.27}$ (Low)	0.27:1	0.3	1.1	0.05	0.08

3.7 PEG-Functionalized SPIONs:

Iron (III) chloride hexahydrate (3.04 g) and iron (II) chloride tetrahydrate (1.98 g) were dissolved in a 2:1 molar ration in 12.5 mL of deionized water in a 50 mL round bottom flask.

Ammonium hydroxide (6.5 mL) was added dropwise under magnetic mixing at 500 rpm for 10 minutes. After an additional 10 minutes of mixing, PEG (MW= 8 kDa, 1.0 g) was dissolved in 10 mL of deionized water and added to the iron mixture. The mixture was heated to 70°C for 2 hours to peptize the iron particle surface with PEG. After two hours, the ferrofluid was cooled and washed using magnetic separation against 0.15 M saline for a minimum of 5 cycles and concentrated using a permanent magnet. Concentration was determined gravimetrically after the ferrofluid had been stored overnight in a 140°F oven to remove water. The solution was concentrated to between 15-and 20 wt% solids, which was subsequently diluted to make the 5 wt% composites.

3.8 pNIPAM-Hydrazide Functionalized SPIONs

pNIPAM-hydrazide functionalized SPIONS were produced using the method described by Campbell and Hoare (Campbell, Patenaude, and Hoare 2013). Iron (III) chloride hexahydrate (3.04 g) and iron (II) chloride tetrahydrate (1.98 g) were dissolved in a 2:1 molar ration in 12.5 mL of deionized water in a 50 mL round bottom flask. Ammonium hydroxide (6.5 mL) was added dropwise under magnetic mixing at 500 rpm for 10 minutes. After an additional 10 minutes of mixing, pNIPAM-hydrazide (2.0 g) dissolved in 15 mL of deionized water was added to the iron mixture. The mixture was heated to 70°C for 2 hours to peptize the iron particle surface with pNIPAM-hydrazide. After two hours, the ferrofluid was cooled and washed using magnetic separation against 10 mM phosphate buffered saline (PBS) for a minimum of 5 cycles and concentrated using a permanent magnet to create a solution with 8 wt% pNIPAM-hydrazide (polymer attached to the SPION surface) and 10 wt% SPIONs.

3.9 Double Barrel Syringe Apparatus:

All components of the double barrel syringe apparatus were purchased from Medmix Systems (Switzerland). The components of the double-barrel apparatus (1-4) can be seen in Figure 3.1. The hydrazide-functionalized ('A') polymer is loaded into one side of the double barrel (3) and the aldehyde-functionalized ('B') polymer is loaded into the other side. The A and B solutions contact mix and begin to form a hydrogel inside of the static mixer (4) which is screwed onto one end of the double barrel. The mixed solution passes through a 20-gauge needle (5) and into cylindrical moulds. The ends of the double barrel are sealed with O-rings (2) and the solution is advanced through the mixer by compression of the plunger (1).

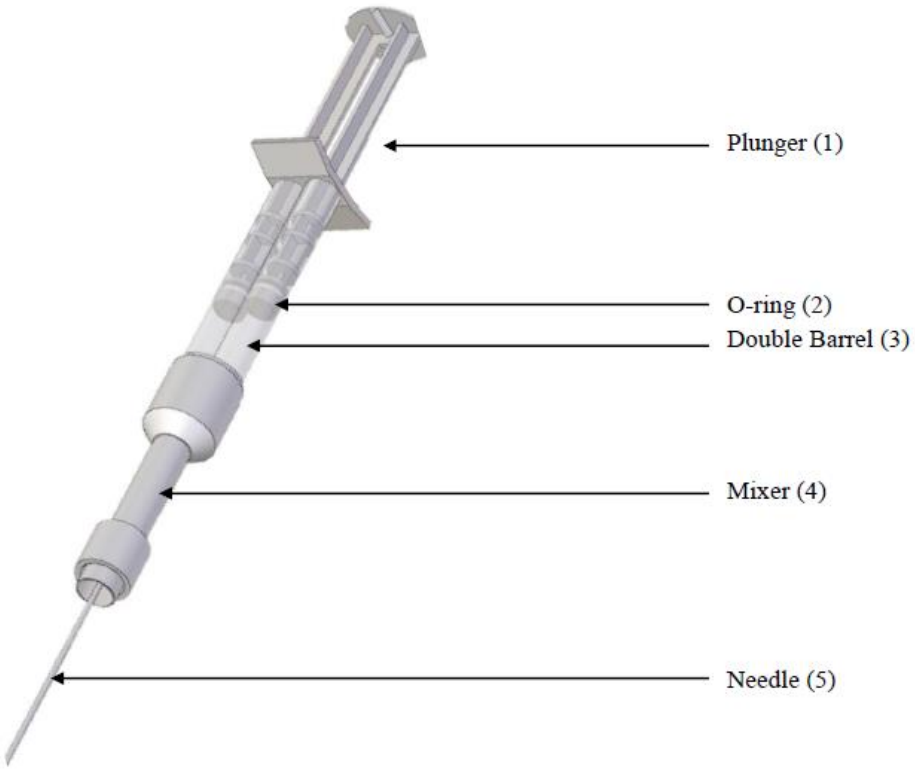

Figure 3.1: Double barrel apparatus for creation of hydrogel composites.

3.10 Hydrogel-Microgel-SPION Composite:

For drug release studies, 0.15 M saline, concentrated SPION solution, and 4 kDa FITC-Dex were combined with reactive hydrogel precursors and mixed in proportions to create a final composite with 1 wt% 4 kDa FITC-Dex (~50 mg total) and 5 wt% SPIONS. For swelling studies, 4 kDa FITC-Dex was excluded. This solution was spread evenly amongst 4 x 2 mL micro-centrifuge tubes. In the first two tubes (A-tubes), pNIPAM-hydrazide polymer (~95 mg per tube) was dissolved at a concentration of 8 wt%. In the second set of tubes (B-tubes), dextran-aldehyde (~95 mg per tube) was dissolved at a concentration of 8 wt%. Varying concentrations of microgel (from 4 wt% to 10 wt%, corresponding to 180 mg to 500 mg) were then dissolved in varying proportions in each of the four tubes to equalize the viscosity of each solution. Solutions were left on a desktop shaker for 2-3 days and pushed through a 20 gauge needle 2-3 times to ensure adequate mixing and dissolution prior to using them for gel formation.

For the tests investigating the effect of hydrogel swelling on pulsatile release, 6 wt% hydrogel (pNIPAM-hydrazide and dextran-aldehyde and/or CMC-aldehyde, ~70 mg per tube) and 6 wt% microgel (276 mg total between all the tubes) were used.

The hydrogel-microgel-SPION composites were created using the double barrel syringes described in section 3.9 by loading the contents of the A-tubes and the B-tubes into the separate barrels. The composite was injected into cylindrical, silicone rubber moulds (rubber obtained from McMaster Carr (Illinois, USA)). Due to the size constraints of the drug release set-up, smaller moulds with a diameter of 0.6 cm and a height of 0.32 cm were used for drug release studies while moulds with a diameter of 0.95 cm and a height of 0.32 cm were used for the swelling kinetics studies.

For the pNIPAM-hydrazide-SPION composites, the B-tubes were prepared in a similar manner but without the addition of the SPION solution (to avoid gelation prior to co-extrusion) and with 2 wt% 4 kDa FITC-Dex (no 4 kDa FITC-Dex was dissolved in the hzd-SPION solution). The A-tube included only the 10 wt% SPIONs coated with 8 wt% pNIPAM-hydrazide. Upon mixing these two precursor solutions, a composite with an overall composition of 8 wt% hydrogel, 5 wt% SPIONs and 1 wt% drug (analogous to those produced with non-functionalized SPIONS) was produced.

Control composites were made using the identical procedure, with one component being excluded from the formulation. Table 3.2 shows a summary of all the composites tested. Tests were name using the following convention: uM_v-w FF- xH y Carb-Tz, where u is the weight percent microgel in the composite, v is the NIPMAM: NIPAM ratio of the microgel, w is the type of SPION used (PEG-FF or hzd-FF), x is the weight percent hydrogel in the final composite, y is the mass percentage of each aldehyde-carbohydrate of interest used, Carb (Dex or CMC) indicates whether dextran-aldehyde or CMC-aldehyde was used as the aldehyde component of the hydrogel, and z = baseline incubation temperature of the composites. A complete summary of all the components used for each test can be found in Appendix A (Table A.2).

Table 3.2: Composition of tested composites.

Polymer Code	Hydrogel: wt% (CMC-B fraction)	Microgel: wt% (recipe)	SPIONs: wt% (type)	Incubation Temp
8$M_{0.56a}$- PEG FF-8H 100 Dex-T37	8 wt% (0)	8 wt% ($M_{0.56}$)	5 wt% (PEG-SPIONs)	37°C
0M- PEG FF-8H 100 Dex-T37	8 wt% (0)	**0 wt%**	5 wt% (PEG-SPIONs)	37°C
8$M_{0.56a}$-**0 FF**-8H 100 Dex-T37	8 wt% (0)	8 wt% ($M_{0.56}$)	**0wt%**	37°C
0M-Hzd FF-8H 100 Dex-T37	8 wt% (0)	**0 wt%**	**5 wt%, (hzd-SPIONs)**	37°C
8$M_{0.56a}$-**Hzd FF**-8H 100 Dex-T37	8 wt% (0)	8 wt% ($M_{0.56}$)	**5 wt%, (hzd-SPIONs)**	37°C
8$M_{0.56a}$-PEG FF-8H 100 Dex-T**22**	8 wt% (0)	8 wt% ($M_{0.56}$)	5 wt% (PEG-SPIONs)	**22°C**
8$M_{0.56a}$-PEG FF-8H 100 Dex-T**43**	8 wt% (0)	8 wt% ($M_{0.56}$)	5 wt% (PEG-SPIONs)	**43°C**
8**$M_{0.27}$**-PEG FF-8H 100 Dex-T37	8 wt% (0)	8 wt% (**$M_{0.27}$**)	5 wt% (PEG-SPIONs)	37°C
8**$M_{0.56b}$**-PEG FF-8H 100 Dex-T37	8 wt% (0)	8 wt% (**$M_{0.56b}$**)*	5 wt% (PEG-SPIONs)	37°C
8**M_1** -PEG FF-8H 100 Dex-T37	8 wt% (0)	8 wt% (**M_1**)	5 wt% (PEG-SPIONs)	37°C
8$M_{1.8}$-PEG FF-8H 100 Dex-T37	8 wt% (0)	8 wt% (**$M_{1.8}$**)	5 wt% (PEG-SPIONs)	37°C
4$M_{1.8}$-PEG FF-8H 100 Dex-T37	8 wt% (0)	**4 wt%** ($M_{1.8}$)	5 wt% (PEG-SPIONs)	37°C
6$M_{1.8}$-PEG FF-8H 100 Dex-T37	8 wt% (0)	**6 wt%** ($M_{1.8}$)	5 wt% (PEG-SPIONs)	37°C
10$M_{1.8}$-PEG FF-8H 100 Dex-T37	8 wt% (0)	**10 wt%** ($M_{1.8}$)	5 wt% (PEG-SPIONs)	37°C
6$M_{1.8}$-PEG FF-6H **100 CMC**-T37	6 wt% (**1**)	6 wt% ($M_{1.8}$)	5 wt% (PEG-SPIONs)	37°C
6$M_{1.8}$-PEG FF-6H **75 CMC**-T37	6 wt% (**0.75**)	6 wt% ($M_{1.8}$)	5 wt% (PEG-SPIONs)	37°C
6$M_{1.8}$-PEG FF-6H **50 CMC**-T37	6 wt% (**0.5**)	6 wt% ($M_{1.8}$)	5 wt% (PEG-SPIONs)	37°C
6$M_{1.8}$-PEG FF-6H **25 CMC**-T37	6 wt% (**0.25**)	6 wt% ($M_{1.8}$)	5 wt% (PEG-SPIONs)	37°C
6$M_{1.8}$-PEG FF-6H **0 CMC**-T37	**6** wt% (**0**)	6 wt% ($M_{1.8}$)	5 wt% (PEG-SPIONs)	37°C

*A microgel made with the same NIPMAM:NIPAM ratio but with slightly different VPTT properties was used for the VPTT comparison tests. Microgel from the same batch was used for all other $M_{0.56}$ tests.

3.11 Hydrogel Characterization:

3.11.1 Conductometric and Potentiometric Titrations of NIPAM-co-AA and Hydrazide Functionalized NIPAM-co-AA

The percentage of the carboxylic acid residues present on NIPAM-co-AA that were functionalized with hydrazide groups was determined by comparing the potentiometric titrations of pNIPAM-co-AA and pNIPAM-hydrazide using the method previously described (Hoare and Pelton 2004). Titrations were completed using a Mandel PC Titrator with PC-titrate software (Version 3.0). 50 mg of dried polymer was dissolved in 50 mL of 10^{-3} M NaCl in a clean, 100 mL beaker fitted with an overhead mixer, thermometer and pH and conductivity electrodes from ManTech associates. Temperature was maintained at 25°C. 0.1 M HCl and 0.1 M NaOH (Acculate Standards) were used to control the pH of the solution. The solution pH was decreased to 2.0 prior to titration. Data was acquired using a base-into-acid titration with an endpoint pH of 11.5. By comparing the volume of titrant required to titrate the carboxylic acid groups present on NIPAM-co-AA versus the volume required to titrate the remaining carboxylic acid groups present on pNIPAM-hydrazide, the degree of hydrazide functionalization was determined.

3.11.2 Conductometric and Potentiometric Titrations of Silver(I) Oxide Oxidized Aldehyde Functionalized Dextran and CMC

The degree of aldehyde functionalization of dextran and CMC after periodate oxidation was determined using the method describe by Patenaude et al. (Patenaude et al. 2014). DIW (10mL) was used to dissolve oxidized dextran (0.1 g) and sodium hydroxide (0.248 g). Silver(I) oxide (0.386 g) was added to the solution to oxidize the aldehyde groups to carboxylic acid groups. The solution was left to stir overnight, after which 5 mL was removed and added to 45 mL of DIW. This solution was then titrated as described in section 3.10.1, detecting the total

concentration of carboxylic acid groups resulting from the oxidation. For CMC-aldehyde, a comparative titration was also completed on 50 mg of un-oxidized polymer, with the number of carboxyl groups present on the CMC-backbone subtracted from the total signal to determine the aldehyde content.

3.12 Microgel Characterization:

The temperature behaviour of the p(NIPAM -NIPMAM) microgels was determined by dynamic light scattering a Brookhaven 90Plus Particle Analyser running Particle Solutions Software (Version 2.6). Detection was done using a 659 nm laser at a 90° angle. Lyophilized microgels were reconstituted in 0.15 M saline at a concentration of 1.5 mg/mL. Reading time for each measurement was 2 minutes per sample (4 readings were taken at each temperature), with 5 minute temperature stabilization at each temperature point at 1°C intervals from 25°C to 50°C. The experimental uncertainties represent the standard deviation of repeated measurements (n=4).

3.13 SPION Characterization:

The size of both PEG- and hzd- SPIONS was determined at room temperature by TEM using Image J software. Successful functionalization of pNIPAM-hydrazide was determined by gel-testing the SPIONs: a solution of hzd-SPIONs was mixed with a 4 wt% dextran-aldehyde solution and observed to ensure adequate hydrogel formation occurred.

3.14 Composite Swelling:

Composites were injected into moulds with a diameter of 0.95 cm and a height of 0.32 cm. The composites were placed in pre-weighed cell culture inserts (2.5 cm in diameter with 8

μm pore size), with the membrane perforated 20 times with a 20 gauge needle to facilitate the flow of PBS into and out of the inserts. The composites were weighed immediately after gelation and at pre-determined time intervals after incubation in 5 mL of 10 mM PBS at 37°C inside 12-well cell culture plates. At each time interval, the cell inserts were removed, dabbed dry with a Kimwipe to remove excess water, and their mass was recorded. Percent mass change was calculated using the equation:

$$\textbf{\textit{Percent Weight Change}} = \frac{\textbf{\textit{Mass}}_{time} - \textbf{\textit{Mass}}_{initial}}{\textbf{\textit{Mass}}_{initial}} \textbf{\textit{x}}\ \mathbf{100}\% \qquad (2)$$

A minimum of 5 composites were tested for each sample, and error bars represent the standard deviation of the percent weight change of these replicates.

3.15 Composite Degradation:

Composites made using moulds with a diameter of 0.95 cm and a height of 0.32 cm were placed in the same cell inserts used for swelling tests. Composites (n=6) were placed in 5 mL of 10 mM PBS (pH=7.4) or pH= 3 or pH = 1 hydrochloric acid. Composite weight was recorded over time until the bulk material had completely degraded. Error bars represent the standard deviation of the percent weight change of replicate composites.

3.16 Pulsatile Drug Release Experimental Set-Up:

A magnetic drug release apparatus was assembled, as shown in Figure 3.2 and Figure 3.3, is to allow for multiple (n=4) composites to be in equivalent positions within the magnetic field while maintaining a constant temperature of 37°C around the composites. As shown in Figure 3.2, constant temperature was maintained by placing the samples in a jacketed flask (6) which is

connected to a water bath (1,2) that pumps water through the jacket at a temperature of 37°C. The composites (7) were placed on holders (3) which keep them at equivalent heights within the test tubes (4) and make them easy to remove. Each composite was immersed in 4mL of 10mM PBS. The test tubes were kept in place by a Styrofoam platform (seen in Figure 3.3), which is equipped with a thermometer to allow for monitoring of the temperature inside the jacketed flask and has the added benefit of improving the system's insulation. The jacketed flask is in turn placed inside a twice coiled, 8 cm diameter solenoid operated at 200 kHz, 30 A, and 1.3 kW to facilitate the application of an oscillating magnetic field of equal strength to each sample for pre-determined time points, facilitating pulsatile drug release measurements.

Upon testing, the temperature around the composites during an extended AMF pulse increased rapidly from 37°C (incubation temperature) to approximately 43°C, typically considered a good upper limit temperature for avoiding cytotoxicity upon short-term exposure (Jordan et al. 1999).

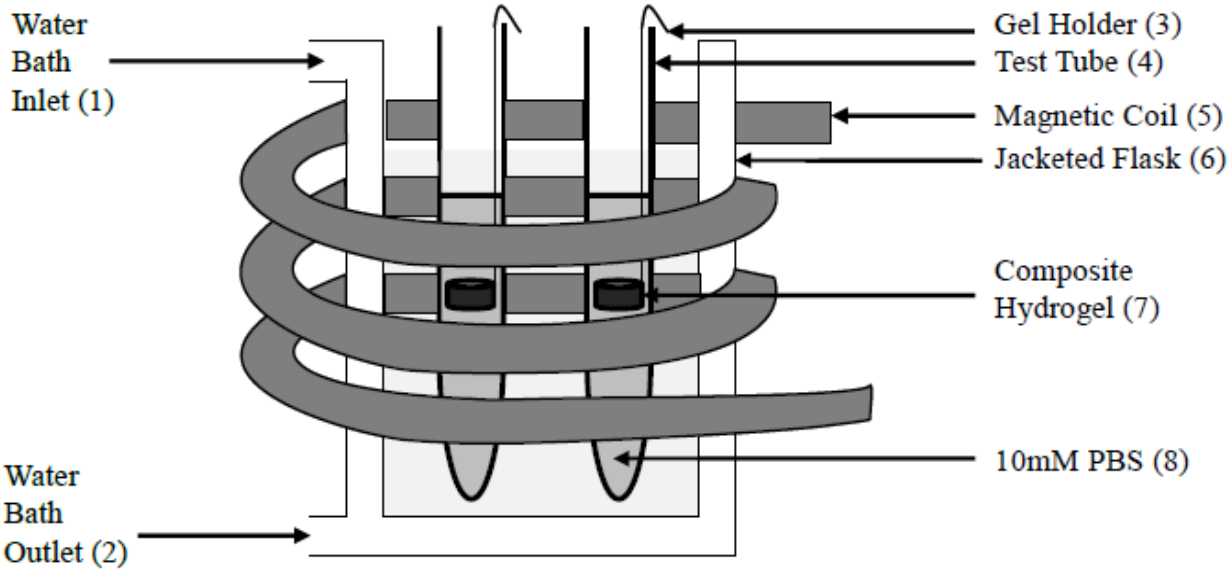

Figure 3.2: Diagram of set-up for pulsatile drug release experiments.

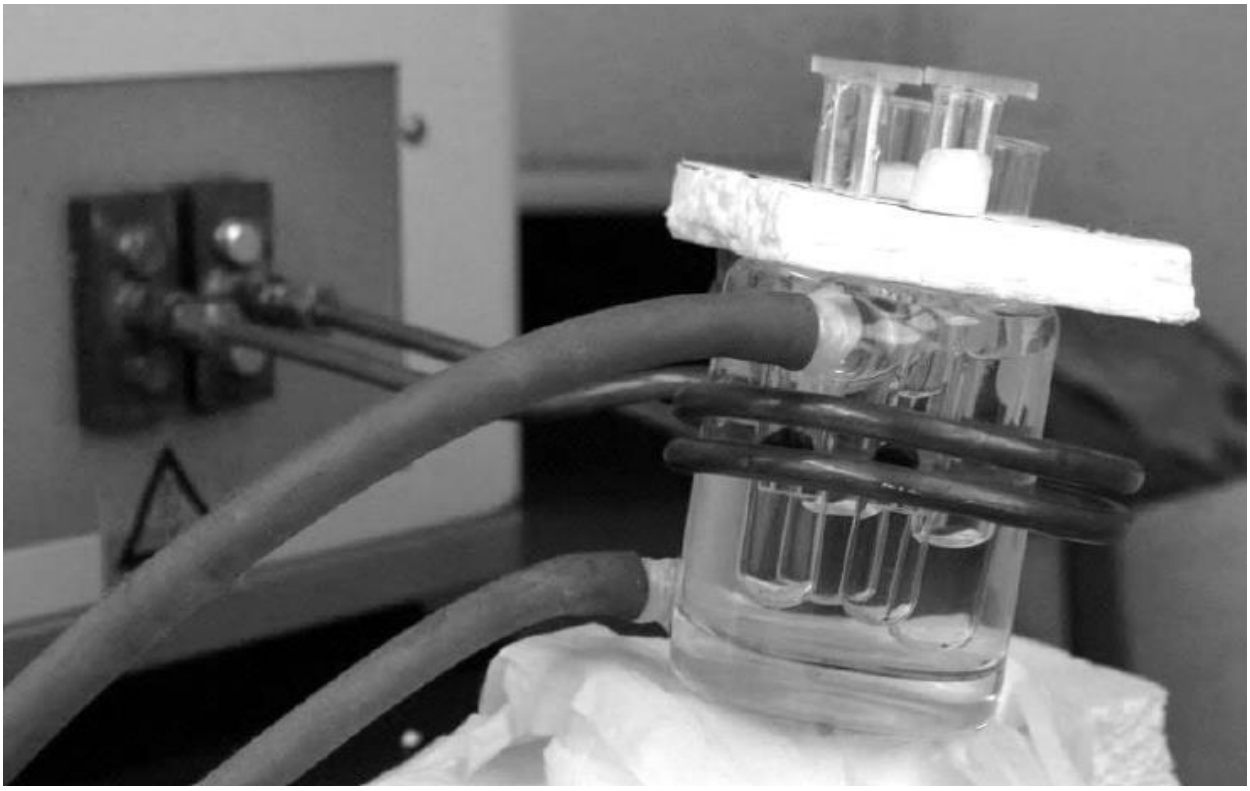

Figure 3.3: Photograph of the set-up for pulsatile drug release experiments.

3.17 Pulsatile Drug Release Experiments:

Samples were collected at 10 minute intervals from the test-tubes for 30 minutes before and after a 10 minute pulse (1.3 kW, 200 Hz, 30 A). Magnetic induction was only applied between the 3rd and 4th sample points. Concurrent with the pulsatile release tests, a set of control gels (n=4) was kept in identical test tubes in a water bath at 37°C and were sampled at the same time intervals (but never exposed to magnetic induction). 3 x 200 µL samples were removed from each test-tube at each test time point into 96-well plates. 600 µL of fresh, pre-heated PBS was added back into the test-tube to ensure the composites remained fully immersed and maintain infinite sink conditions during the release process. This process was repeated on days one, two, three and five to evaluate the composites' ability to facilitate repeated magnetically

induced pulsatile release. The composites were exposed to 4 pulses on days one, two and three and 3 pulses on day five. The concentration of released 4kDa FITC-Dex was measured using the fluorescein protocol on a Perkin Elmer Victor 3V 1420 Multi Label Counter using Wallac 1420 Manager Software (Version 3.00.0.52). The calibration curves can be found in Appendix B (Figure B.1).

The effect of the magnetic pulse on release was calculated as the percent increase in release rate. The predicted release rate was determined based on interpolating between the rates observed at the two time points prior and two time points after pulsatile induction. The percent increase in predicted release rate was calculated using the following equations:

$$\textit{Predicted Release Rate} = \frac{Rate_{P-20min} + Rate_{P-10min} + Rate_{P+10min} + Rate_{P+20min}}{4} \quad (3)$$

$$\textit{Percent Increase in Release Rate} = \frac{\boldsymbol{Rate_{P-0min} - Predicted\ Release\ Rate}}{\boldsymbol{Predicted\ Release\ Rate}} \quad \textbf{(4)}$$

An exponential function was fitted to the 10, 20, 30, 50 and 60 minute data points and used to predict the release rate for the first pulsatile time point (at 40 minutes), because this time point fell within the range over which the composite was still exhibiting burst release of drug and Equation 3 did not provide an adequate estimate.

The percent increase in release rate was calculated for both the pulsatile and control composites. Error bars represent the standard deviation in the readings for multiple composites (n=4). The percent increase in release rate values reported in the results section are equal to the pulsatile percentage increase in release rate minus the control percentage increase in release rate; the rationale behind this calculation is that because the pulsatile and control tests were completed in the same apparatus at the same time, any environmental factors (i.e. a change in room

temperature or a fluctuation of water bath temperature) that resulted in 'pulse' behaviour of the control composite at that time point would inflate the observed composite percent increase in release rates of the pulse composites by the same amount. Significant pulsatile response was considered to be present if the difference between the pulsatile and control composite percent increase in release rates was greater than 0, within error.

3.18 Cell Viability:

3T3 *Mus musculus* mouse fibroblast cells were used to test cell viability. The cells were grown using a proliferation media composed of 500 mL DMEM, 50 mL FBS and 5 mL PS. Procedures for polymer sterilization, cell splitting, culturing, and freezing for the MTT assay used to determine cell viability are described below.

3.18.1 Polymer Sterilization:

Polymers were sterilized prior to cell viability testing by exposure to UV radiation inside a laminar flow cabinet. Polymers were weighed and spread out in a single layer in a petri dish and exposed to 2 hours of UV radiation before being flipped over and irradiated for an additional 2 hours to ensure complete sterilization.

3.18.2 Cell Thawing:

Cell containing cryovials were submerged in a 37°C water bath with gentle agitation until the contents thawed. The vial contents were then transferred to a 15 mL centrifuge tube, and 10 mL of fresh, FBS-containing media was added before the sample was centrifuged at 1000 rpm for 5 minutes. The supernatant was aspirated and replaced with 15 mL of fresh, warmed media. Cells were dispersed with gentle pipetting, and the cell suspension was transferred to a 75 cm^3

flask and incubated at 37°C and 5% CO_2. Media was aspirated and replaced with fresh media every 3 days and cells were passaged every 4-6 days.

3.18.3 Cell Splitting and Counting

After the old media was aspirated off, 5 mL of trypsin-EDTA was added to the flask. The flask was rocked gently for 5-10 minutes to detach the cells. 6 mL of media was then added to the flask to deactivate the trypsin, with the full solution transferred to a 15 mL centrifuge tube and centrifuged at 1000 rpm for 5 minutes. The supernatant was aspirated and replaced with 15 mL of fresh, warmed media. Cells were dispersed with gentle pipetting. To passage the cells, 100 µL of the suspension was removed to 75 cm^3 flasks with 15 mL of fresh media and incubated at 37°C and 5% CO_2. To count the cells, 100 µL of the suspension was removed and placed onto a haemocytometer. The cells in the outer quadrants (1 quadrant = area of 0.1 mm^3) were counted under magnification to determine the number of cells per quadrant. The cell concentration and number of cells present was calculated using the following equations:

$$\boldsymbol{Cell\ Concentration = Cell\ per\ quadrant \frac{\text{cells}}{0.1\ mm^3}\ x\ 10000\ \frac{0.1\ mm^3}{mL}\ [=]\ \frac{cells}{mL}} \quad (5)$$

$$\boldsymbol{Number\ of\ Cells = Cell\ Concentration\ \frac{cells}{mL}\ x\ 15mL} \quad (6)$$

3.18.4 MTT Assay

After cell splitting and counting, 25,000 3T3 cells and 1 mL of media were added to each well of a 24 well polystyrene plate. After the cells were incubated at 37°C and 5% CO_2 for 24 hours, the media was aspirated and cells were exposed to 1mL of media containing dissolved, sterilized polymers at concentrations of 100 µg/mL to 2000 µg/mL. The cells were incubated in the polymer solutions for 24 hours. A positive control containing cells and no polymer and a negative control containing no cells and no polymer were also completed. Four repeats were

performed for each polymer concentration and control, with error bars representing the standard deviation of these multiple measurements.

The thiazolyl blue tetraxolium bromide (MTT) stock solution was reconstituted with 10mM PBS to create a solution with a concentration of 4 mg/mL MTT. The solution was sterile filtered, after which the MTT stock solution was diluted to 0.4 mg/mL with cell media. The polymer solution covering the cells was aspirated and each well was rinsed with 0.5mL of media which was then removed. 150 µL of 0.4 mg/mL MTT solution was added to each well, and the cells were incubated in the MTT solution for 4 hours. After the incubation period, 250 µL of DMSO was added to each well to dissolve the insoluble formazan precipitate. Plates were placed on a shaker for 20 minutes or until the purple formazan was completely dissolved. 2 x 200 µL was removed from each well, transferred to a 96 well polystyrene plate, and read in a microplate reader (Biorad, Model 550). Cell viability was determined by comparing the degree of formazan absorption at 540 nm for all wells containing polymer to the absorption of the positive control wells (cells not exposed to any polymer). The percent cell viability was calculated using the equation:

$$\boldsymbol{Cell\ Viability}\ (\%) = \frac{\boldsymbol{Absorbance}_{\boldsymbol{cells\ exposed\ to\ polymer}}}{\boldsymbol{Absorbance}_{\boldsymbol{positive\ control}}} \quad (7)$$

3.19 Error and Statistical Significance:

In all cases, error bars represent the standard deviation in measurements based on multiple samples ($n \geq 4$). Statistically significant differences between any pair of samples were determined using a two-tailed t-test with $p<0.05$ assuming unequal variances.

Chapter 4: Material Characteristics

4.1 Hydrazide Functionalized pNIPAM:

Hydrazide functionalized pNIPAM was highly soluble in 0.15 M saline at all weight percent solutions investigated, resulting in a solution with a viscosity very similar to water. For this reason, for composite formation, most of the microgel was dissolved with the pNIPAM-hydrazide to equalize the viscosity between the 'A' and 'B' solutions prior to loading into the double barrel device.

4.1.1 Degree of Functionalization

The reaction of adipic acid dihydrazide with pNIPAM-co-AA via EDC/NHS chemistry results in the consumption of one carboxylic acid group for every hydrazide group that is conjugated to the pNIPAM-co-AA polymer. By determining the number of carboxyl groups present before and after the EDC/NHS reaction through conductometric titration, the number of hydrazides present per polymer chain can be calculated. Figure 4.1 shows that fewer titratable carboxylic acid groups are present after hydrazide functionalization. Based on the conductometric data, it is possible to calculate the mol% of acrylic acid present on the pNIPAM-co-AA polymer, how many of the pNIPAM-co-AA carboxyl groups were converted to hydrazides on pNIPAM-hydrazide, and the final mol% functionalization with hydrazide. The acrylic acid mol% of the pNIPAM-co-AA molecule was 9.4 ± 0.5%. Comparing the two titrations showed that 88 ± 4% of the carboxylic acid residues were converted to hydrazide residues, resulting in a functionalization of 8.2 ± 0.6% of monomers including hydrazide groups on the pNIPAM-hydrazide polymer.

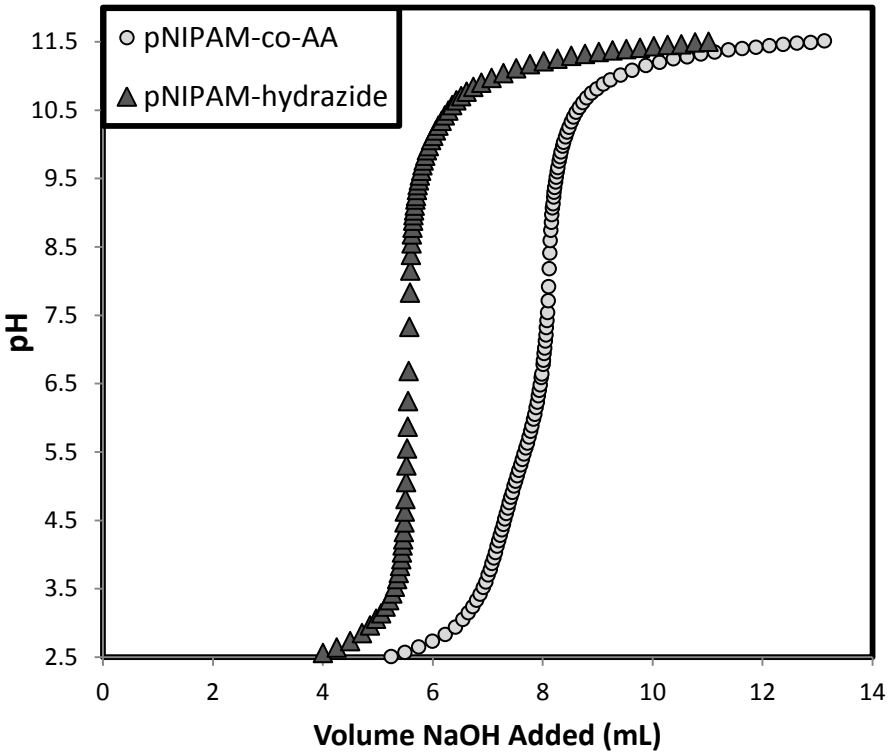

Figure 4.1: Conductometric titration of pNIPAM-co-AA and pNIPAM-hydrazide polymers.

Gel permeation chromatography showed that polymers made using this synthesis procedure had a molecular weight of 21.6 kDa (below the renal cut-off) (Patenaude and Hoare 2012a). This data can be found in Appendix C, Figure C.1.

4.2 Aldehyde Functionalized Dextran and CMC:

Aldehyde functionalized CMC and dextran were both soluble in 0.15 M saline at lower weight percents (6 wt% or below) but higher weight percent solutions (8 wt% and over) required up to 3 days of constant shaking before dissolution occurred, likely due to the high viscosity of the higher concentration samples. CMC-aldehyde dissolved faster and produced a slightly less viscous solution than dextran-aldehyde.

4.2.1 Degree of Functionalization:

Exposure to sodium hydroxide and silver(I)oxide oxidizes the aldehyde groups present on dextran or CMC to carboxylic acid groups in a 1:1 ratio (Patenaude et al. 2014). By determining the number of carboxylic acid groups on the oxidized dextran or CMC through conductometric titration, the number of aldehyde groups present per polymer chain can be calculated. Figure 4.2 shows the titration results for CMC-aldehyde and unoxidized CMC.

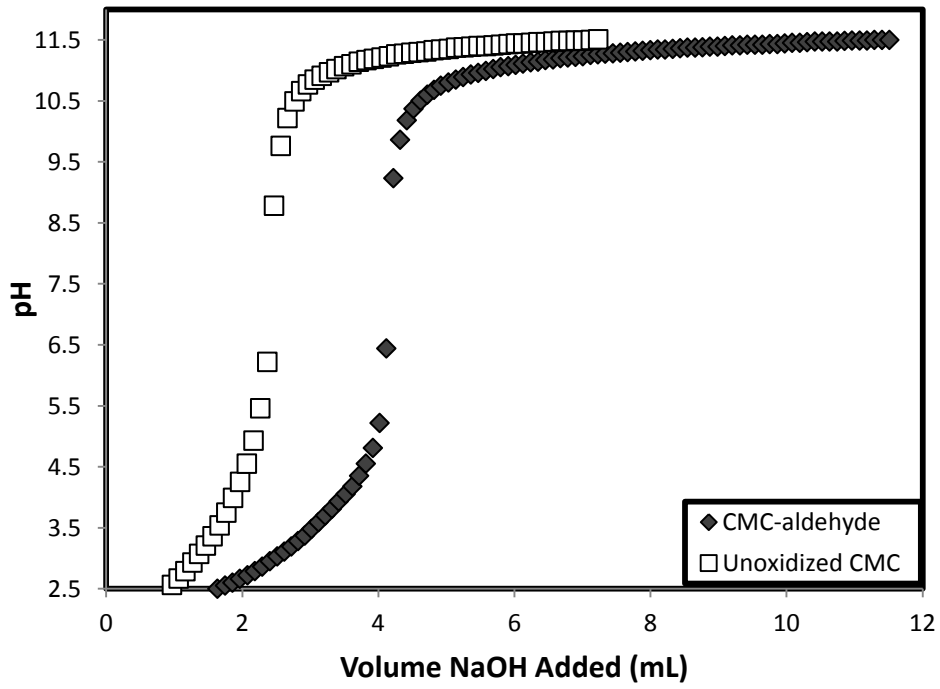

Figure 4.2: Conductometric titration of unoxidized CMC and CMC-aldehyde polymers.

Based on the conductometric results, oxidative cleavage occurred on 17.4 % of dextran residues and 13.2% of CMC residues.

4.3 Poly (NIPAM-NIPMAM) Microgels:

Microgel fabrication occurred at a temperature well above the polymer LCST (70°C) and microgel formation happened very quickly after the initiator was added to the heated monomer solution. Microgel formation could be observed as the reaction solution changed from transparent to white. After synthesis, the microgel solution was dialysed and lyophilised. Dried microgels were readily re-dispersed in 0.15 M saline, producing a slightly opaque solution at concentrations as low as 1 mg/mL. Microgels were added to the pNIPAM-hydrazide solution to increase its viscosity to equal the relatively viscous dextran and/or CMC-aldehyde solutions, important to promote thorough mixing via the double barrel syringe.

4.3.1 Temperature Dependence of Particle Size – Dynamic Light Scattering

Dynamic light scattering results for the p(NIPAM-NIPMAM) microgels fabricated using various recipes are shown in Table 4.1. The particle sizes of interest are listed in Table 4.1: 25°C (when the composite is formed), 37°C (the baseline-temperature at which the composite is tested) and 43°C (the temperature the composite reaches during magnetic heating). The particle sizes of the microgels over the entire 25°C to 50°C temperature range can be found in Figure 4.3. Microgel $M_{1.33}$ (NIPMAM: NIPAM mass ratio of 1.33) resulted in very polydisperse microgels which were not used for composite testing and, as such, were excluded from Table 4.1. The particle sizes of this microgel over the entire 25°C to 50°C temperature range can be found in Appendix C (Figure C.2). $M_{0.56a}$ was used for the tests comparing composites made with different SPION-types (with and without microgel) and incubated at different temperatures. It was statistically ($p<0.05$) larger than the $M_{0.56b}$ recipe at 37°C, but was indistinguishable from $M_{0.56b}$ at 25°C or 43°C. The $M_{0.56a}$ microgels also have a slightly higher VPTT than $M_{0.56b}$

microgels (36.5°C vs 36.2°C). Because $M_{0.56b}$ was used when comparing composites made with different VPTT behaviours, $M_{0.56b}$ is discussed in detail below and shown in Figure 4.3.

Table 4.1: Temperature dependence of the effective diameter for various p(NIPAM-NIPMAM) microgel formulations.

NIPMAM:NIPAM Ratio	NIPAM Monomer (g)	NIPMAM Monomer (g)	Effective Diameter at 25°C (nm)	Effective Diameter at 37°C	Effective Diameter at 43°C ^
$M_{1.8}$ (High)	0.9	0.5	1509 ± 89	888 ± 32	297 ± 13
M_1 (Med)	0.7	0.7	1004 ± 42	575 ± 16	327 ± 3^^
$M_{0.56a}$ (Med-Low)	0.5	0.9	1459 ± 106	595 ± 43	225 ± 9^^^
$M_{0.56b}$ (Med-Low)	0.5	0.9	1423 ± 68	508 ± 31	236 ± 14
$M_{0.27}$ (Low)	0.3	1.1	1364 ± 17	363 ± 14	229 ± 12 ^^^^

^ microgels occasionally aggregated before reaching 43°C. The smallest size reached up to this point was reported.
^^ size at 40°C
^^^ size at 42°C^^^^size at 39°C

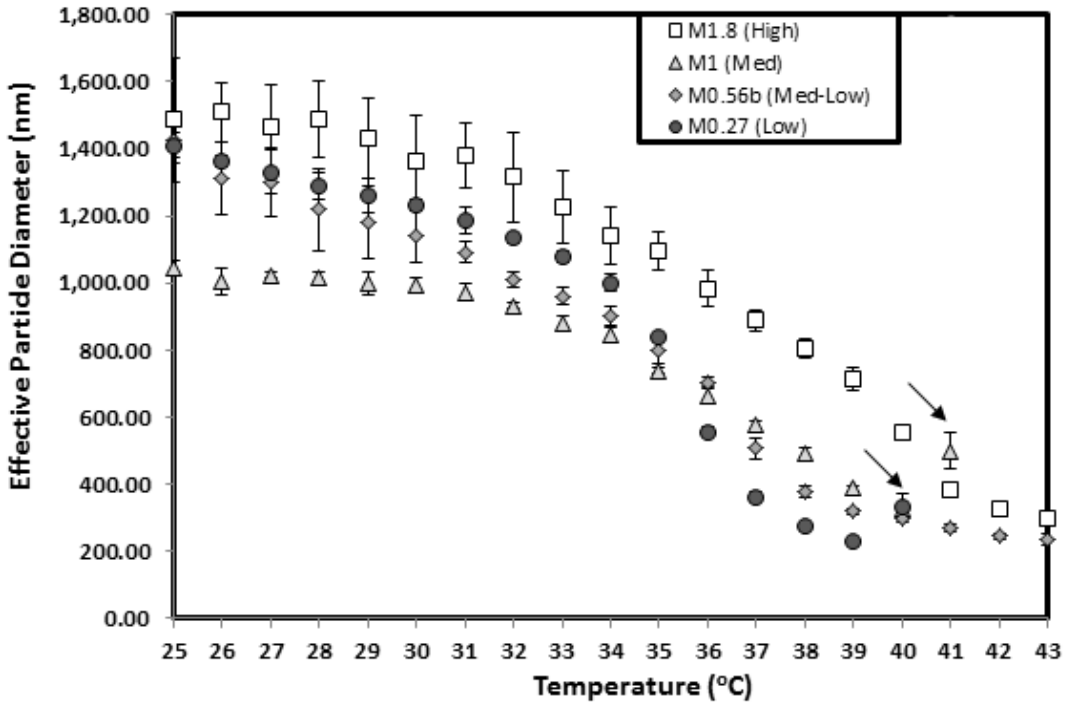

Figure 4.3: VPTT behaviour of microgels made with different NIPMAM:NIPAM ratios. Arrows indicate aggregation points of $M_{0.27}$ and M_1 microgels.

The $M_{1.8}$, $M_{0.56b}$ and $M_{0.27}$ recipes result in microgels that are the same size within error at 25°C. At 37°C, the difference in microgel sizes is statistically significant among all the microgels ($p<0.05$), with higher NIPMAM: NIPAM ratio corresponding to a larger size at 37°C. At 43°C, the $M_{0.56b}$ and $M_{0.27}$ microgels sizes are statistically the same size while the $M_{1.8}$ microgel is slightly larger.

The M_1 microgel recipe results in a particle that is significantly smaller at 25°C compared to other recipes. At 37°C, it is intermediate in size between the $M_{1.8}$ and $M_{0.56b}$ recipe microgels, and the size difference between these microgels is statistically significant ($p<0.05$). The M_1 recipe microgel particles aggregated during DLS earlier than the other microgels, resulting in an inability to assess its particle diameter at 43°C. The size of 327 ± 3 nm listed in Table 4.1 corresponds to its size at 40°C, which is not statistically significantly different from the particles sizes of $M_{0.56b}$ (321 ± 13) and $M_{0.27}$ (334 ± 37) at that temperature ($p<0.05$). The size of microgels made with the $M_{1.8}$ recipe at 40°C (491 ± 15) is significantly higher than the medium recipe microgels ($p<0.05$).

NIPMAM, illustrated in Figure 2.12, has a higher LCST (43°C) than NIPAM (32°C) because the presence of an additional methyl group on the polymer backbone increases the polymer stiffness, limits the formation of intramolecular interactions and inhibits the collapse of the polymer (Hertle and Hellweg 2013). It would therefore be expected that by incorporating more NIPMAM into the microgel structure, the microgel collapse would be delayed and the VPTT could be increased. This is the trend that our microgel sizing results demonstrated. Note that the aggregation observed at 43°C would not be expected to occur once microgels are entrapped inside hydrogels, effectively immobilizing the microgels and preventing self-associations that lead to microgel aggregation.

4.4 SPION Characterization

SPION fabrication occurred at room temperature while peptization of the SPION surface with either PEG or pNIPAM-hydrazide occurred at 70°C. After synthesis, the SPION solutions were rinsed and concentrated under magnetic separation and stored in their concentrated liquid form. PEG-SPIONs formed a stable solution in 0.15 M saline at a concentration of between 15 and 20 wt% (depending on batch) that was slightly more viscous than water. The hzd-SPION solution had a more gel-like consistency once concentrated to 10 wt% SPION solution (which also contains 8 wt% of pNIPAM-hydrazide), although the solution could still very easily be pushed through a 20-gauge needle.

4.4.1 Transmission Electron Microscope (TEM) Images

The size of SPIONs was determined using TEM. Figure 4.4 shows the results for hzd-SPIONs (a), and PEG-functionalized SPIONs (b). The hzd- SPIONs formed clusters of between 30 and 200nm, while individual particle diameters were generally between 10 and 20nm. The PEG-SPIONs formed clusters of approximately 100nm, while individual particle diameters were generally between 10 and 20nm.

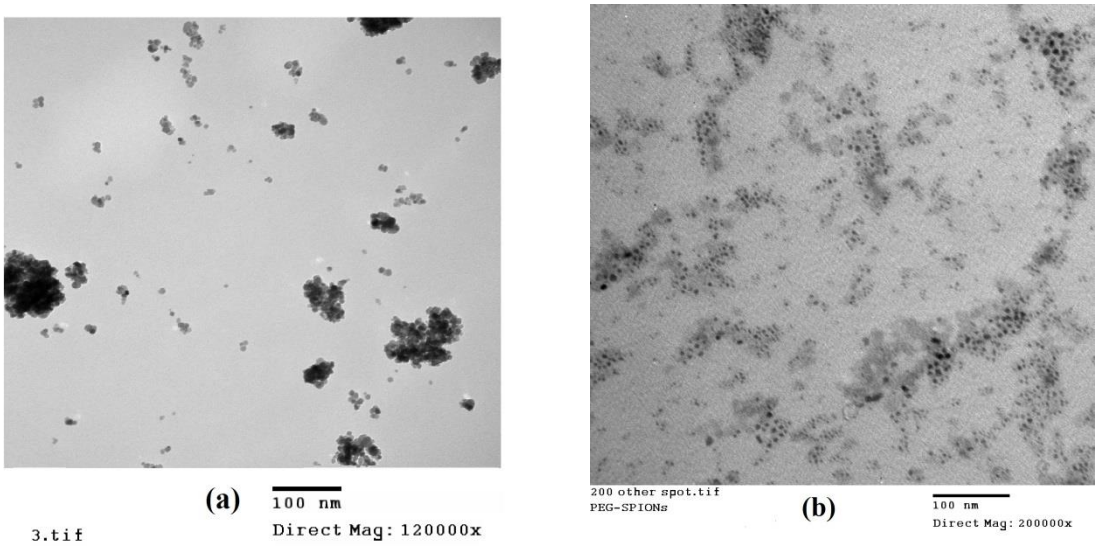

Figure 4.4: TEM image of (a) pNIPAM-hydrazide functionalized SPIONs and (b) PEG-functionalized SPIONS.

4.5 Hydrogel Composite Characteristics

The precursor solutions were extruded through a 20-gauge needle into the double barrel syringe to ensure adequate precursor mixing. While some of the solutions were difficult to extrude through the double barrel syringe due to their high viscosity (especially the 10wt% microgel composite), a consistent rate of flow was achieved for each composite tested. Gelation took between 10 seconds and 1 minute, with composites with higher microgel contents or lower hydrogel precursor contents taking longer to gel. All composites were left in their moulds for 10 minutes before testing began to ensure more than adequate time for gelation to finish. The resulting composites were elastic when touched, would bounce if dropped and could be easily removed from the moulds with little damage. Any composites containing SPIONs were black as shown in Figure 4.14 in the next section. Control composites made without SPIONs were optically clear upon formation and cloudy/ opaque when incubated in PBS at 37°C.

4.6 Swelling Measurements

The LCST of pNIPAM imparts interesting VPTT characteristics to hydrogel composites made with pNIPAM-hydrazide. In general, at temperatures of 37°C and above, the hydrogels would deswell over time, while incubation at room temperature resulted in gel swelling. Incorporation of microgels into the composite resulted in initial swelling followed by slow collapse of the gel. Incorporation of CMC-aldehyde into the hydrogel (in place of dextran-aldehyde) resulted in significant gel swelling at all temperatures tested. These results are shown in detail below.

4.6.1 Swelling of Composite Controls

The swelling of several control composites was investigated. These included: the baseline composite $8M_{0.56a}$- PEG FF-8H 100 Dex-T37 (8 wt% $M_{0.56a}$ microgel, PEG-SPIONs, 8 wt% hydrogel using Dextran B and incubated at 37°C) as well as 0M- PEG FF-8H 100 Dex-T37 (baseline made without microgel) and $8M_{0.56a}$-0 FF-8H 100 Dex-T37 (baseline made without SPIONs Figure 4.5 and Figure 4.6) as well as $8M_{0.56a}$-Hzd FF-8H 100 Dex-T37 and 0M-Hzd FF-8H 100 Dex-T37 (composites made using hzd-SPIONs with and without microgel, Figure 4.7 and

Figure 4.8). All composites contained 8 wt% hydrogel. Those composites containing microgel contained 8 wt% $M_{0.56a}$ microgels and those composites containing SPIONs contained 5 wt%. Figure 4.5 and Figure 4.7 show the initial swelling observed over the first few hours of the swelling test, while Figure 4.6 and

Figure 4.8 summarize swelling over several days of incubation at 37°C. A complete set of swelling results can be found in Appendix C (Figures C.3 and C.4).

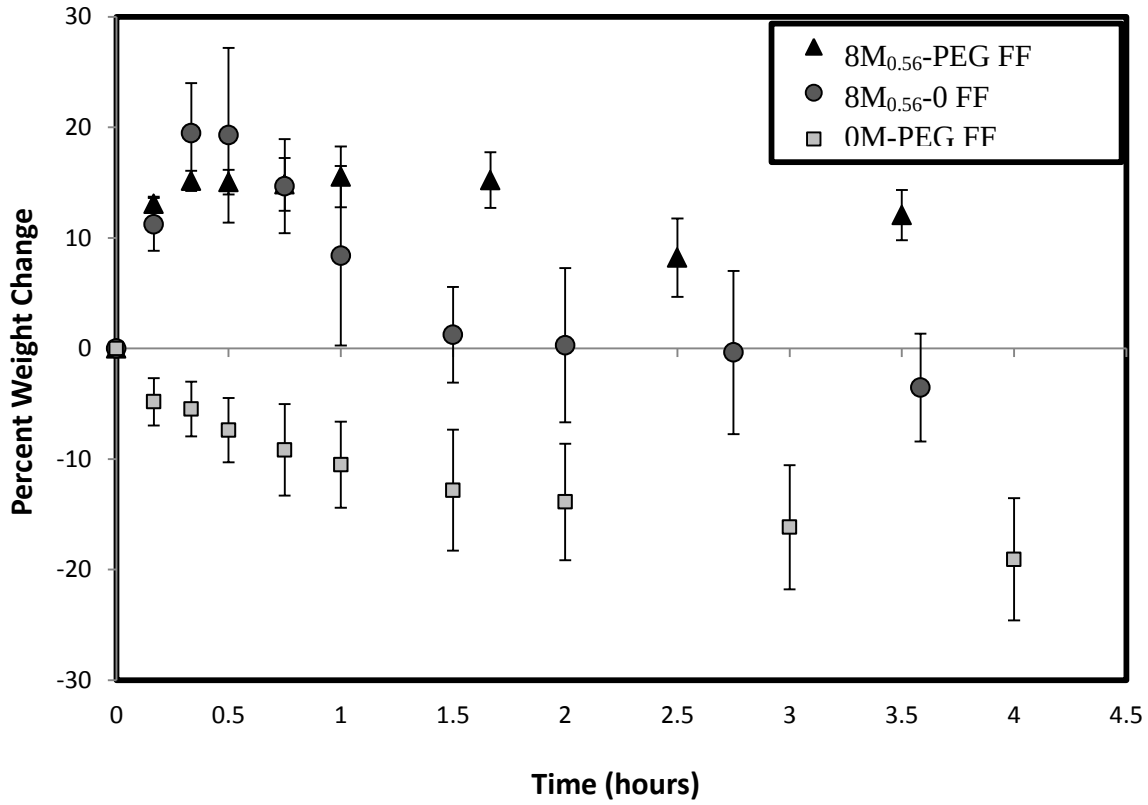

Figure 4.5: Initial swelling behaviour of composites controls made with and without microgel and/or ferrofluid.

Figure 4.5 shows that microgel incorporation ($8M_{0.56a}$-PEG FF) results in initial swelling of the composites while composites not containing microgel deswell immediately upon incubation in 37°C PBS. The $8M_{0.56a}$-0 FF composite appears to deswell slightly faster than the composite made with ferrofluid and microgel, but the difference in deswelling is not statistically significant between these two composites past the first day of testing, as shown in Figure 4.6.

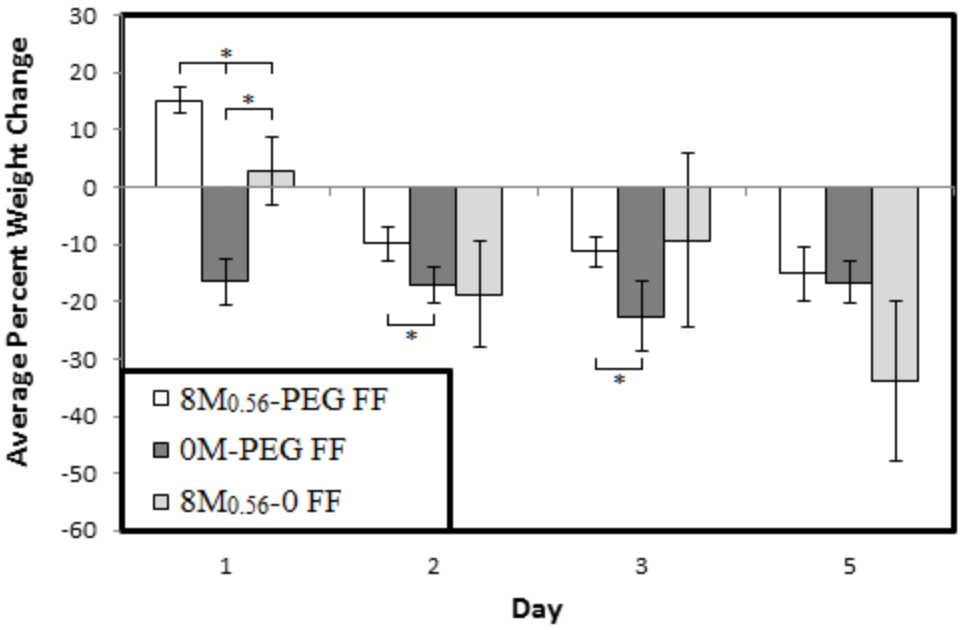

Figure 4.6: 5-day swelling behaviour of composites controls made with and without microgel and/or ferrofluid. * indicates statistical significance ($p<0.05$).

Figure 4.5 showed that the composites containing microgels, $8M_{0.56a}$-PEG FF and $8M_{0.56a}$-0 FF swell initially on day one while 0M-PEG FF composites deswell. Figure 4.6 shows that on subsequent days there is no statistically significant difference ($p<0.05$) between the deswelling of $8M_{0.56a}$-PEG FF and the $8M_{0.56a}$-0 FF control or between the $8M_{0.56a}$-0 FF and 0M-PEG FF. $8M_{0.56a}$-PEG FF composites exhibit statistically less swelling than the 0M-PEG FF control on days one, two and three, but there is no significant difference on day five, indicating that microgels may slow the rate of swelling but do not ultimately affect the equilibrium degree of swelling.

Figure 4.7 shows that swelling initially occurs with the microgel containing composites as well as the 0M-hzd-SPION composite. The swelling of the $8M_{0.56a}$- hzd-SPION composite is statistically higher than the 0M-hzd SPION control, and the 0M-hzd SPION control also deswells significantly faster than the microgel containing hzd-SPION composite ($p<0.05$).

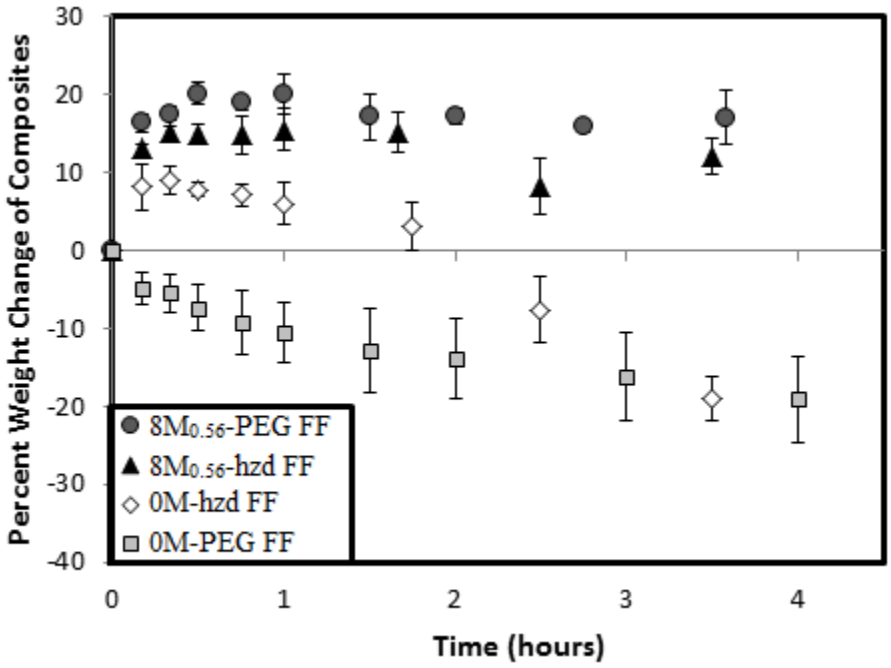

Figure 4.7: Initial swelling behaviour of composites controls made with and without microgel and PEG or pNIPAM-hydrazide ferrofluid.

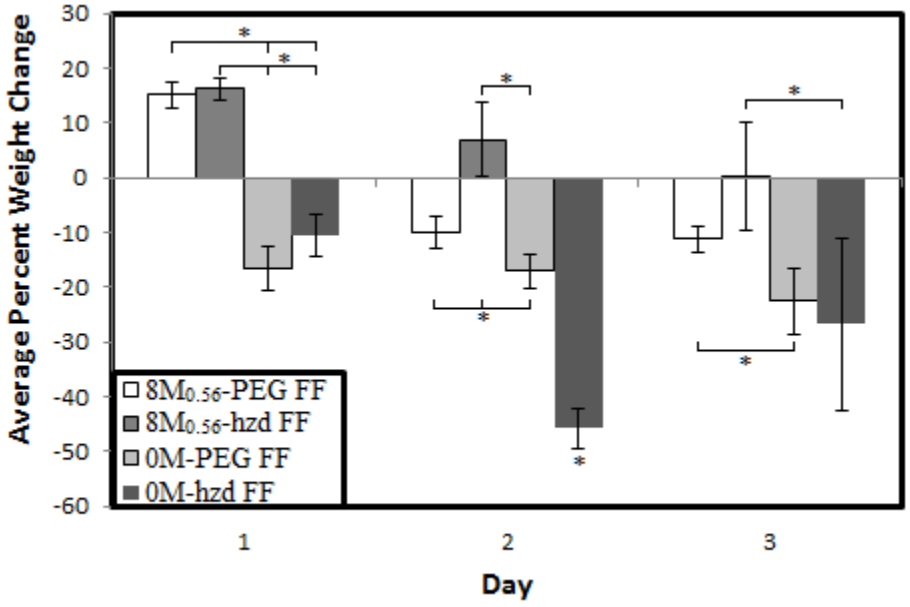

Figure 4.8: 3-day swelling behaviour of composites controls made with and without microgel and PEG or pNIPAM-hydrazide ferrofluid. * indicates statistical significance ($p<0.05$).

Figure 4.8 shows that all composites containing microgels swell initially on day one while composites without microgel deswell. On subsequent days the microgel-containing composites deswell statistically less ($p<0.05$) than the 0M controls for both the PEG-SPION and hzd-SPION composites.

4.6.2 Swelling Based on Composite Incubation Temperature

The swelling of composites was investigated at room temperature (approximately 22°C, 8$M_{0.56a}$-PEG FF-8H 100 Dex-T22), body temperature (37°C, 8$M_{0.56a}$-PEG FF-8H 100 Dex-T37) and the temperature observed after heating of the composites at 37°C with an AMF (43°C, 8$M_{0.56a}$-PEG FF-8H 100 Dex-T43). The composites contained 8 wt% $M_{0.56a}$ microgel, 8 wt% hydrogel, and 5 wt% SPIONs. Figure 4.9 shows the initial swelling observed over the first few hours of the swelling test while Figure 4.10 summarizes swelling over five days of incubation at various temperatures. A complete set of swelling results can be found in Appendix C (Figure C.5).

Figure 4.9 shows that all the gels swell initially. The T22 composites swell initially and remain significantly more swollen than those incubated at the higher temperatures over the course of the test (shown in Figure 4.10). Figure 4.9 also shows that the T43 composites deswellmuch faster than the T37 composites, which is why they are statistically less swollen ($p<0.05$) on day one compared to the composites (as shown in Figure 4.10). Figure 4.10 shows that over the course of the rest of the test (days two to five) the gels T37 and T43 composites remain deswollen by approximately 15%, significantly less than the T22 gels ($p<0.05$) but similar between themselves.

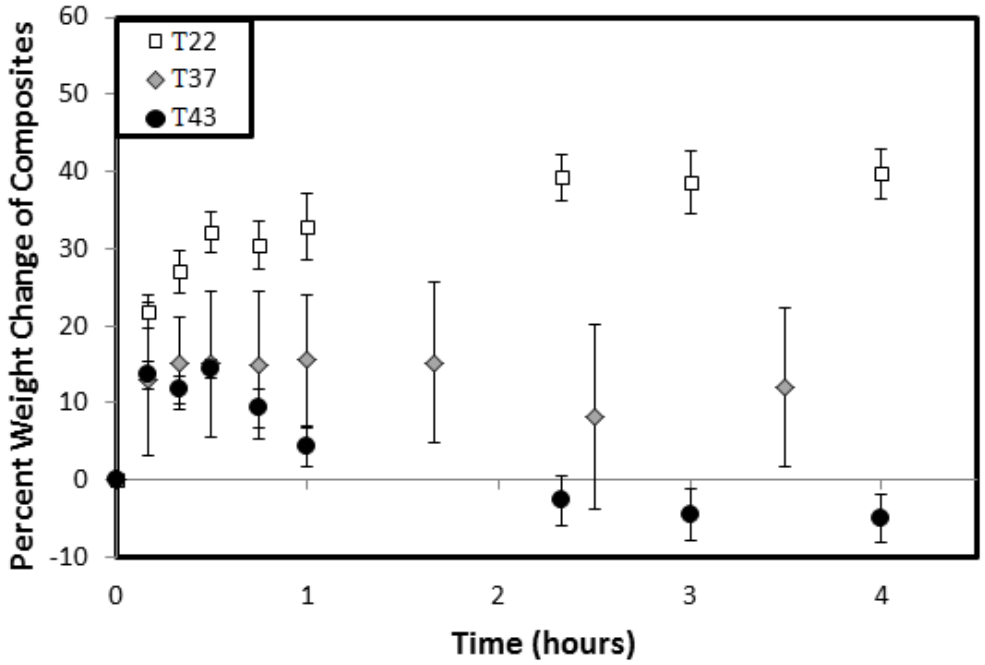

Figure 4.9: Initial swelling behaviour of composites based on a constant temperature of incubation.

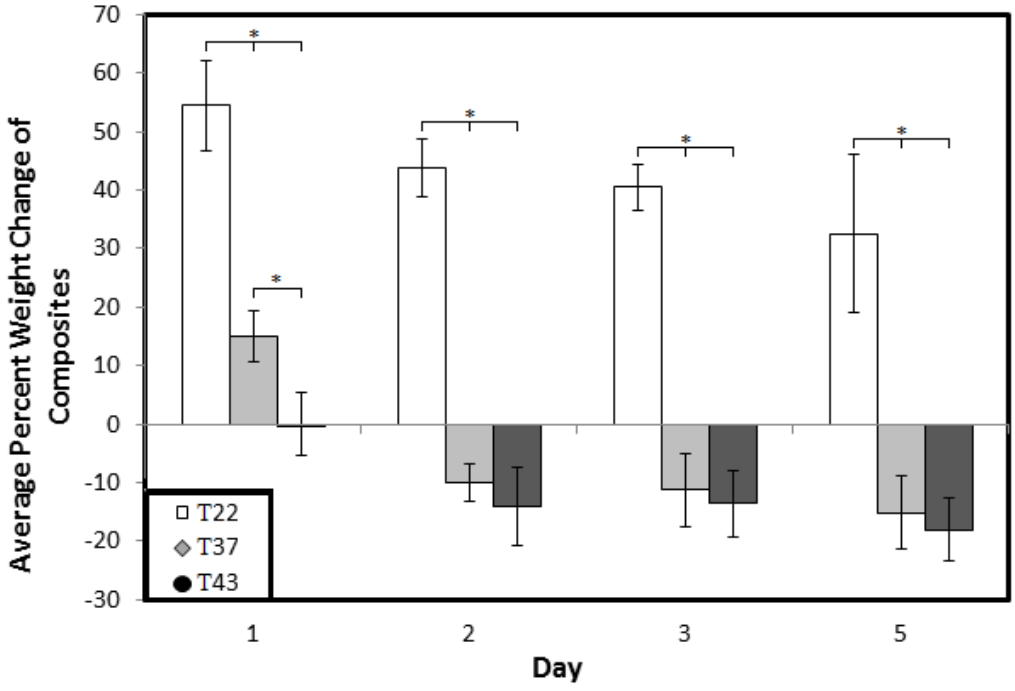

Figure 4.10: 5-day swelling behaviour of composites based on a constant temperature of incubation. * indicates if the differences in composite swelling was statistically significant ($p < 0.05$).

4.6.3 Swelling Based on Composite Microgel Fraction

The swelling of $M_{0.56a}$- PEG FF-8H 100 Dex-T37 composites were investigated for composites made with 0 wt% (0M- PEG FF-8H 100 Dex-T37), 4 wt% ($4M_{0.56a}$- PEG FF-8H 100 Dex-T37), 6 wt% ($6M_{0.56a}$- PEG FF-8H 100 Dex-T37) and 12 wt% ($12M_{0.56a}$- PEG FF-8H 100 Dex-T37) microgel content. All composites contained 8 wt% hydrogel and 5 wt% SPIONS. Figure 4.11 shows the initial swelling observed over the first few hours of the swelling test while Figure 4.12 summarizes swelling over five days of incubation at 37°C. A complete set of swelling results can be found in Appendix C (Figure C.6).

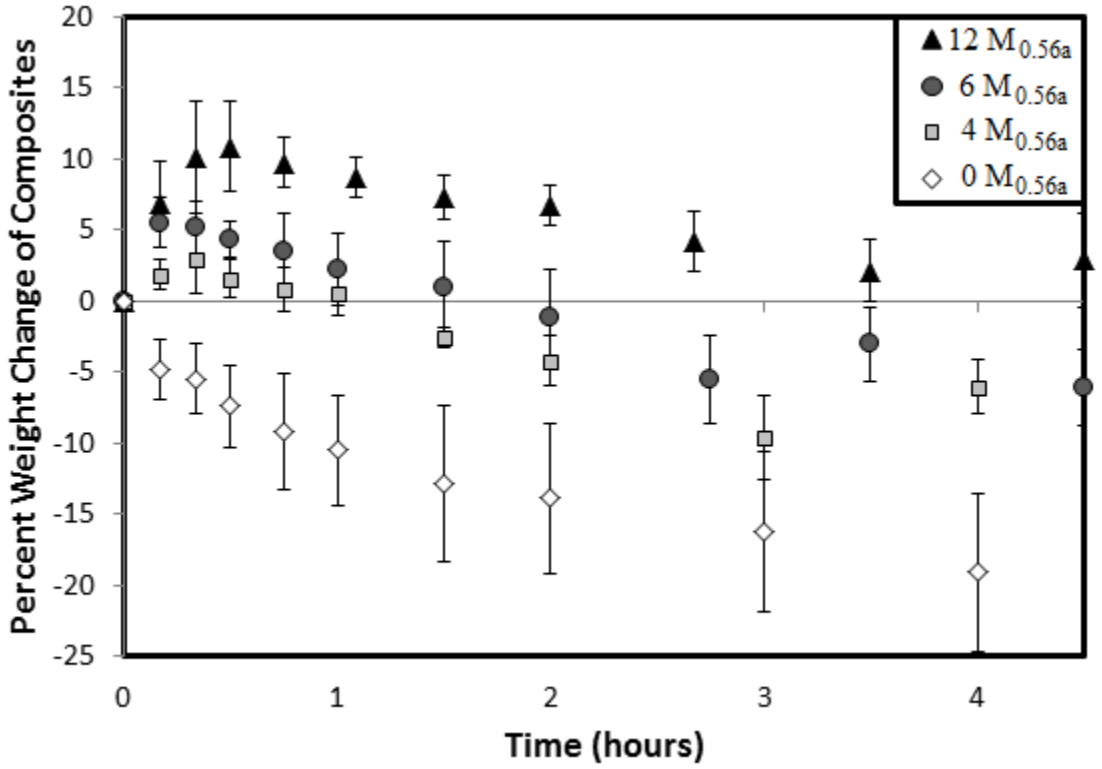

Figure 4.11: Initial swelling behaviour of composites based on microgel content.

Figure 4.11 shows that all the gels swell initially, with higher microgel contents corresponding to higher initial swelling both in magnitude and duration (although the $4M_{1.8}$ and $6M_{1.8}$ composites

are not statistically different and the statistical difference in swelling for $12M_{1.8}$ microgel composite does not persist past 24 hours, $p<0.05$). $0M_{1.8}$ composites deswell immediately and remain deswollen over the course of the test (shown in Figure 4.12).

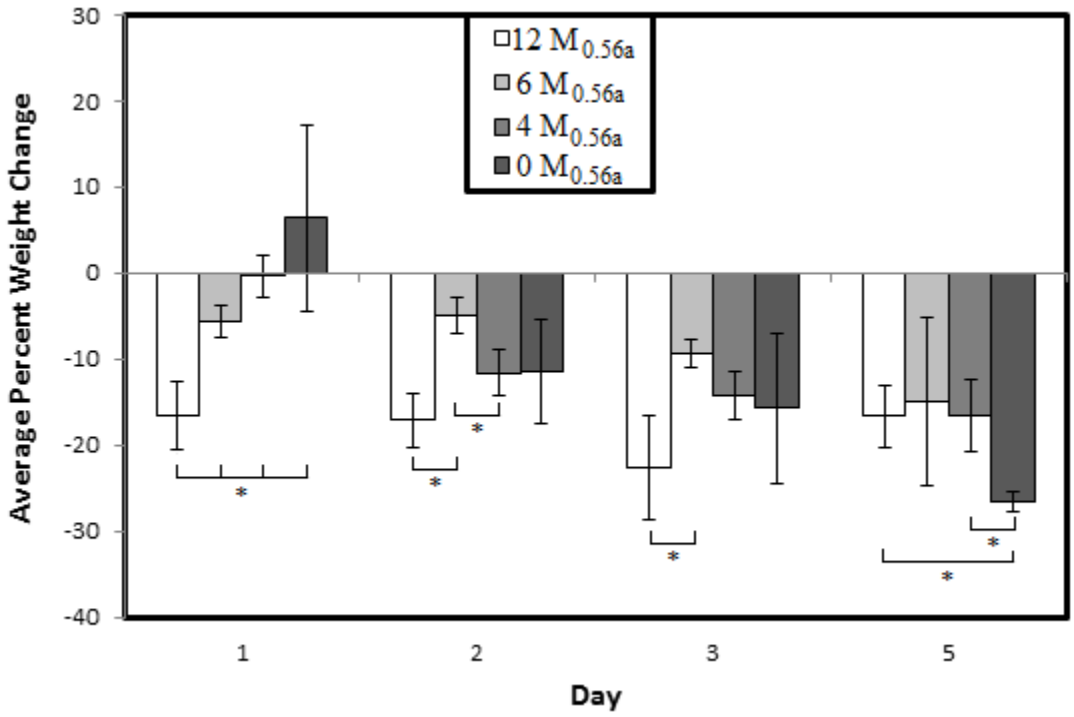

Figure 4.12: 5-day swelling behaviour of composites based on microgel content. * indicates statistical significance ($p<0.05$).

Figure 4.12 shows that over the course of the rest of the test (days two to five) the composites deswell by approximately 10-20%, but there is no statistically significant difference between composite swelling as a function of microgel content after the first day. Differences between $4M_{1.8}$ and $0M_{1.8}$ composites remain statistically significant until day three, and differences between $4M_{1.8}$ and $6M_{1.8}$ on day two are significant, while other differences between $4M_{1.8}$, $6M_{1.8}$, and $12M_{1.8}$ or $0M_{1.8}$, $6M_{1.8}$ and $12M_{1.8}$ are not significant ($p<0.05$). On day five, the $12M_{1.8}$ composite appears to have deswollen significantly (to approximately -25% from -15%);

however this is likely due to mechanical degradation of the composite, not deswelling of the network, given that composites prepared with higher microgel contents tend to degrade faster.

4.6.4 Swelling Based on CMC-aldehyde: Dextran-aldehyde Ratio in Hydrogel

The swelling of $6M_{1.8}$- PEG FF-6H CMC-T37 composites was investigated for composites made with 0%, 25%, 50%, 75% and 100% CMC aldehyde (6H 0 CMC, 6H 25 CMC, 6H 50 CMC, 6H 75 CMC and 6H 100 CMC) with the balance of the aldehyde component being made up of dextran-aldehyde (dextran B) . All composites contained 6 wt% hydrogel, 6 wt% $M_{1.8}$ microgel and 5 wt% PEG-SPIONS. Figure 4.13 shows the initial swelling observed over the first few hours of the swelling test, Figure 4.14 shows pictures comparing the size of composites before and after 24 hours of incubation in 37°C PBS, and Figure 4.15 summarizes swelling over five days of incubation at 37°C. A complete set of swelling results can be found in Appendix C (Figure C.7).

Figure 4.13 shows that composites prepared with higher CMC-aldehyde contents swell significantly more than dextran-rich composites. The 0 CMC composite (100 Dex) swells initially then deswells to approximately -10% of its original mass. All other composites experienced statistically significant differences in swelling, increasing with increasing CMC-aldehyde content.

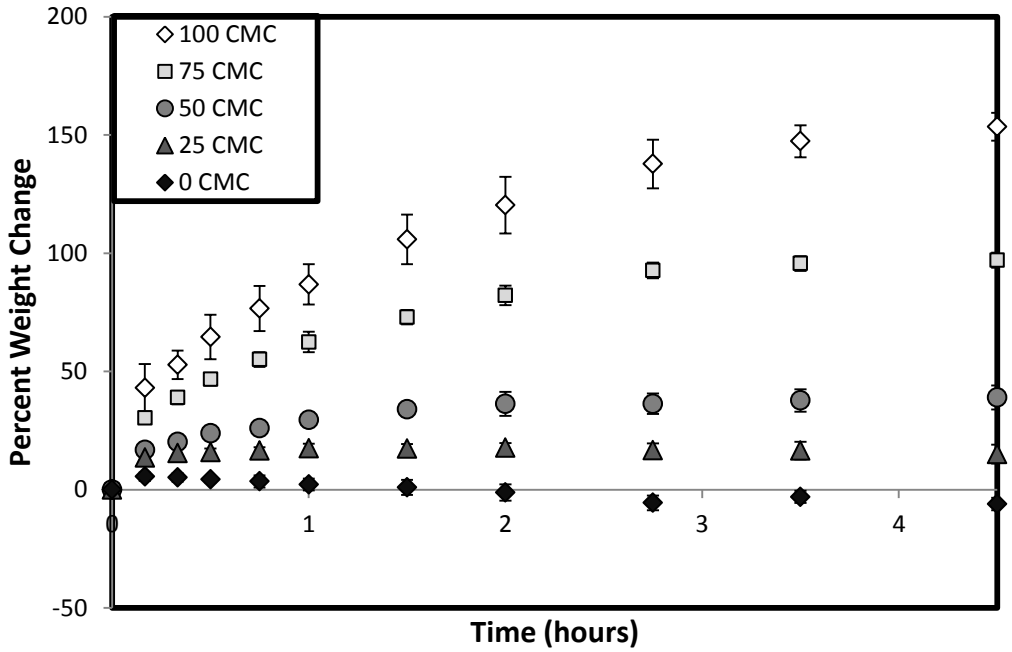

Figure 4.13: Initial swelling behaviour of composites prepared with different aldehyde-functionalized dextran: CMC ratios.

Figure 4.14 shows photographs of composites immediately after their removal from their moulds (immediately after gelation, before any solvent exposure) and after 24 hours of incubation in PBS at 37°C. Visually, there is not much difference between the composites immediately after removal from their moulds. Any difference present can be attributed to differences in camera angle and slight damage caused to the composites when they were removed from the moulds. After incubation in PBS, the composites show an increase in size as their CMC-aldehyde content increases. The 0 CMC composite also appear to have deswelled over the 24 hour period of incubation, while the 100 CMC composite almost doubled in size. These results are consistent with the average percent increase in mass results reported in Figure 4.15.

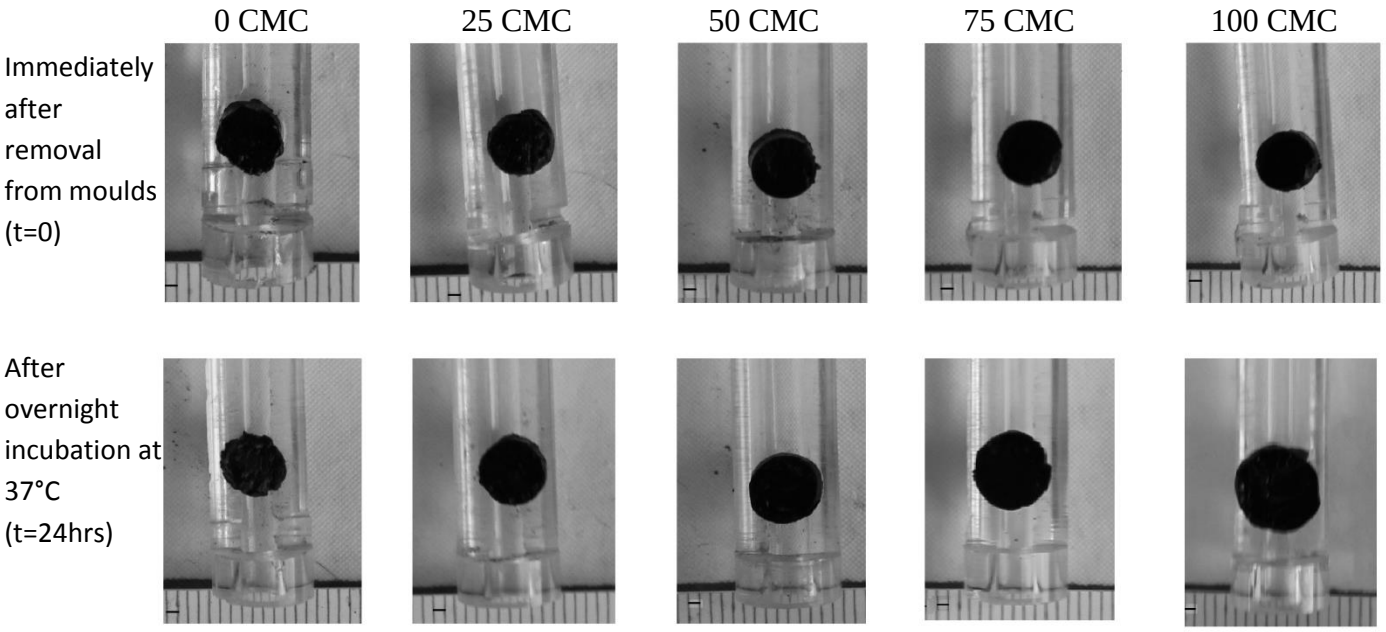

Figure 4.14: Visual comparison of swelling of hydrogel composites made with varying amounts of CMC-aldehyde before and after 24 hours of incubation in PBS at 37°C.

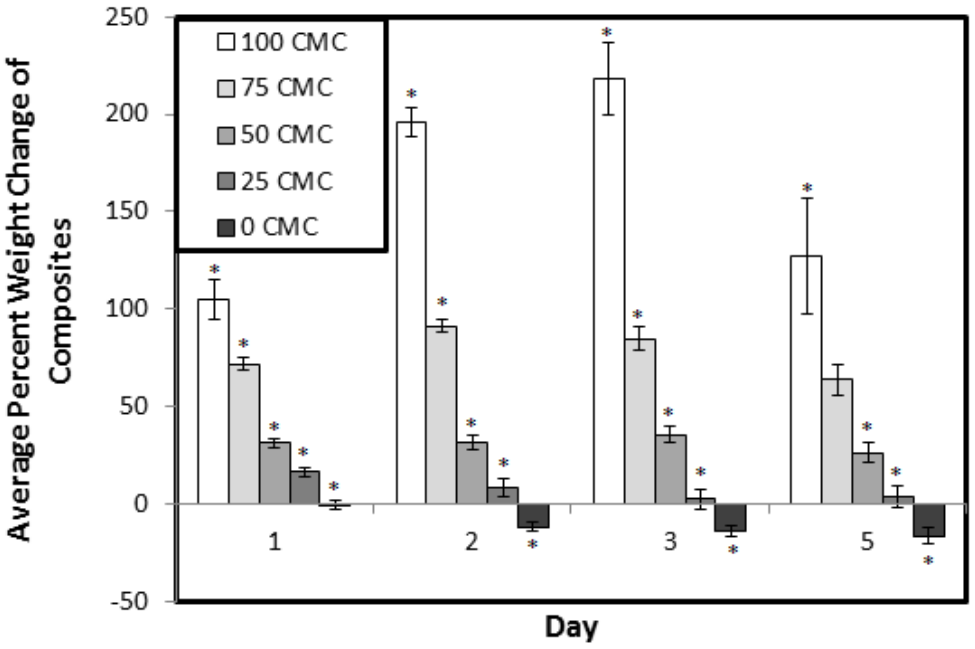

Figure 4.15: 5-day swelling behaviour of composites made with varying amounts of CMC-aldehyde. * indicates statistical significance between the bar and the ones immediately before and/or after it ($p<0.05$).

Figure 4.15 shows that the composites exhibit statistically significantly different swelling over five days of incubation at 37°C ($p<0.05$), with higher swelling corresponding to higher CMC-B contents. Of particular interest are the swelling behaviour changes for 25 CMC and 0 CMC. 0 CMC experiences zero-net swelling on the first day of testing, while 25 CMC swells only very slightly (16%). On the second day, 0 CMC has deswollen significantly (- 12%) while 25 CMC is less swollen (8%). Finally, on day three and five of the test, 0 CMC is still deswollen (-14%) while 25 CMC undergoes zero-net swelling.

Between days three and five, 100 CMC appears to have deswollen rather significantly (goes from approximately 218% positive percent weight change to 128% positive weight change); however this is likely due to mechanical degradation of the composite, not deswelling of the network.

4.6.5 Discussion

pNIPAM exhibits an entropically-driven lower critical solution temperature (LCST) of around 32°C (Pelton 2000). Patenaude and Hoare demonstrated that when pNIPAM-hydrazide and dextran-aldehyde are used to make a hydrazone crosslinked hydrogel, the bulk hydrogel matrix will deswell if incubated above this LCST. Outside of the first few hours of testing, this deswelling behaviour is observed consistently with pNIPAM-hydrazide/ dextran-aldehyde composites that also incorporate p(NIPAM-NIPMAM) microgels and/or SPIONs.

The initial swelling behaviour (i.e. swelling over the first few hours following incubation in PBS) of the composites is sensitive to microgel and SPION content. Upon incubation at 37°C in PBS, composites that do not contain microgels deswell immediately as the pNIPAM-hydrazide collapses. When a composite contains microgels, it initially swells as the slightly-hydrophilic

microgels rapidly take up water and then deswells slowly as bulk hydrogel network (much more slowly) contracts. This result clearly demonstrates the advantages of microgels for facilitating much more rapid swelling responses than bulk hydrogels. Higher microgel contents result in higher initial swelling as well as a slightly slower rate of composite collapse, possibly due to the fact that the presence of microgels would interrupt the cooperative interactions between pNIPAM chains that drive thermal deswelling. This would mean the more microgels that are present, the slower the rate of deswelling would be expected. Incorporation of SPIONs into the network could similarly disrupt the pNIPAM interactions, which would explain why the $8M_{0.56a}$-PEG FF composites deswelled slower than the $8M_{0.56a}$-0 FF control composites.

Bulk hydrogel swelling behaviour was also dependent on composite incubation temperature. Upon incubation at 22°C, the composites swelled quickly and remained swollen over the course of the test; both the microgel and pNIPAM-hydrazide components are well below their volume phase transition temperatures at this temperature, which promotes water uptake and swelling. Upon incubation at 37°C, the composites swell slightly (due to their microgel content), then deswell as the temperature sensitive-bulk hydrogel collapses due to the pNIPAM-hydrazide VPTT. Incubation at 43°C is also followed initially by (a slightly lower degree of) swelling, but the composites collapse more quickly, likely due to a combination of faster composite heating and a higher driving force for collapse at a temperature further above the VPTT. Note that the VPTT of these pNIPAM-hydrazide hydrogels is quite broad, such that increasing the temperature further above the single quoted VPTT value does significantly affect swelling. Appendix C, Figure C.8 shows the changes in composite swelling as they are moved between 25°C and 37°C incubation temperatures.

Use of aldehyde functionalized CMC has been previously demonstrated to result in hydrogels which swell significantly at physiological temperature(Sivakumaran, Maitland, and Hoare 2011),(Patenaude and Hoare 2012b). This behaviour was successfully exploited to create composites with a wide range of swelling behaviours swelling from approximately +220% increase to a -20% decrease in composite mass, at the extremes. This difference in swelling can be attributed to the anionic functional groups on CMC, which are absent on dextran-aldehyde, that create an osmotic pressure gradient across the gel/solvent interface, driving solvent into the gel and significantly increasing gel swelling due to Donnan equilibrium effects (Ricka and Tanaka 1984). Of particular note, the 25 CMC hydrogel that exhibits zero net swelling as of day two is of significant interest for preparation of the nanocomposites, as the hydrogel phase in this case neither swells nor compresses as a function of time to fill any free volume created upon a microgel phase transition.

4.7 Composite Degradation

Degradation studies on composites made with 0, 4, 8 and 12 wt% $M_{0.56a}$ (8 wt% hydrogel and 5 wt% PEG-SPIONs in all cases) were carried out in PBS (pH=7.4), pH=3 HCl and pH=1 HCl at 37 °C. The acid conditions were selected due to the known acid lability of the hydrazone bond, enabling gel degradation in an accelerated section allowing better comparisons between the different hydrogels tested. Table 4.2 shows the half-lives of degradation (i.e. the time until the composites had degraded to 50% of their original weight) of composites prepared with varying microgel contents. Error is based on the standard deviation in weights of the multiple composites tested (n=6).

Table 4.2: Half-lives of composites with different microgel compositions at pH= 7.4, 3 and 1. * indicates statistical significance ($p<0.05$).

	$t_{0.5}$		
	pH=7.4 (PBS)	pH= 3 (HCl)	pH=1 (HCl)
0 $M_{0.56a}$	24 ± 9 days	9 ± 2 days*	5.0 ± 0.9 hrs
4 $M_{0.56a}$	21 ± 5 days	19 ± 2 days*	5.6 ± 1.5 hrs
8 $M_{0.56a}$	100 ± 10 days*	30 ± 5 days *	9.8 ± 0.5 hrs*
12 $M_{0.56a}$	23 ± 4 days	4 ± 2 days*	4.1 ± 1.3 hrs

No statistically significant difference in degradation time is observed at pH=1 between the $0M_{0.56a}$, $4M_{0.56a}$ and $12M_{0.56a}$ composites, while the $8M_{0.56a}$ composite takes significantly longer to degrade at pH=1. The pH=3 results are all different with statistical significance, with the $8M_{0.56a}$ composites taking the longest to degrade, followed by the $4M_{0.56a}$ composites, the $0M_{0.56a}$ composites, and the fastest degrading $12M_{0.56a}$ composites. At pH 7.4, once again, no statistically significant difference in degradation time is observed in PBS (pH=7.4), between the $0M_{0.56a}$, $4M_{0.56a}$, and $12M_{0.56a}$ composites while the composites take significantly longer to degrade.

4.7.1 Discussion

Hydrogels formed via hydrazone crosslinking degrade as the hydrazone bonds undergo acid-catalyzed hydrolysis. The rate of degradation depends on the acid concentration and how easily the acid catalyst can reach the hydrazone bonds (Vetrik et al. 2011). $M_{0.56}$ microgels have water contents of 88 ±3 % at 37°C, calculated by comparing the completely collapsed particle size to the particle size at 37°C and assuming 2 mol of water are present for every more polymer in the collapsed state. This means there is a significantly higher polymer fraction inside the microgel phase as opposed to the hydrogel phase (8 wt% initially for all hydrogels tested). As such, incorporation of these denser microgels into the composite network would be expected to

provide some protection from degradation, by limiting the acid catalyst's ability to reach and degrade the hydrazone bonds. This protection would only be present up to a maximum value, however, as extremely high microgel contents disrupt the formation of the hydrazone-crosslinked network, resulting in a weaker bulk hydrogel phase that would degrade faster because fewer hydrazone bonds would have to be hydrolyzed before degradation occurred. This prediction is supported by the degradation data, particularly at pH=3, where the $8M_{0.56a}$ composites degraded slower than the $4M_{0.56a}$ composites which degraded slower than the $0M_{0.56a}$ composites while the $12M_{0.56a}$ composites degraded rapidly.

4.8 Cell Cytotoxicity

The cell compatibility of all the composite precursors was tested using a MTT metabolic assay and 3T3 mouse fibroblast cells. Figure 4.16 shows the cell viability of fibroblasts incubated with the hydrogel precursors (dextran-aldehyde, CMC-aldehyde and pNIPAM-hydrazide) and Figure 4.17 shows cell viability for the nano-scale composite additives (hzd-SPIONS, PEG-SPIONs and p(NIPAM-NIPMAM) microgels).

As shown in Figure 4.16, limited to no cytotoxicity was observed for the hydrogel precursors up to 2000 μg/mL, a concentration much higher than would be expected to be seen in any *in vivo* applications. Figure 4.17 also shows that limited to no cytotoxicity was observed for the pNIPAM-hydrazide and PEG functionalized SPIONs as well as the p(NIPAM-NIPMAM) microgels up to 2000 μg/mL.

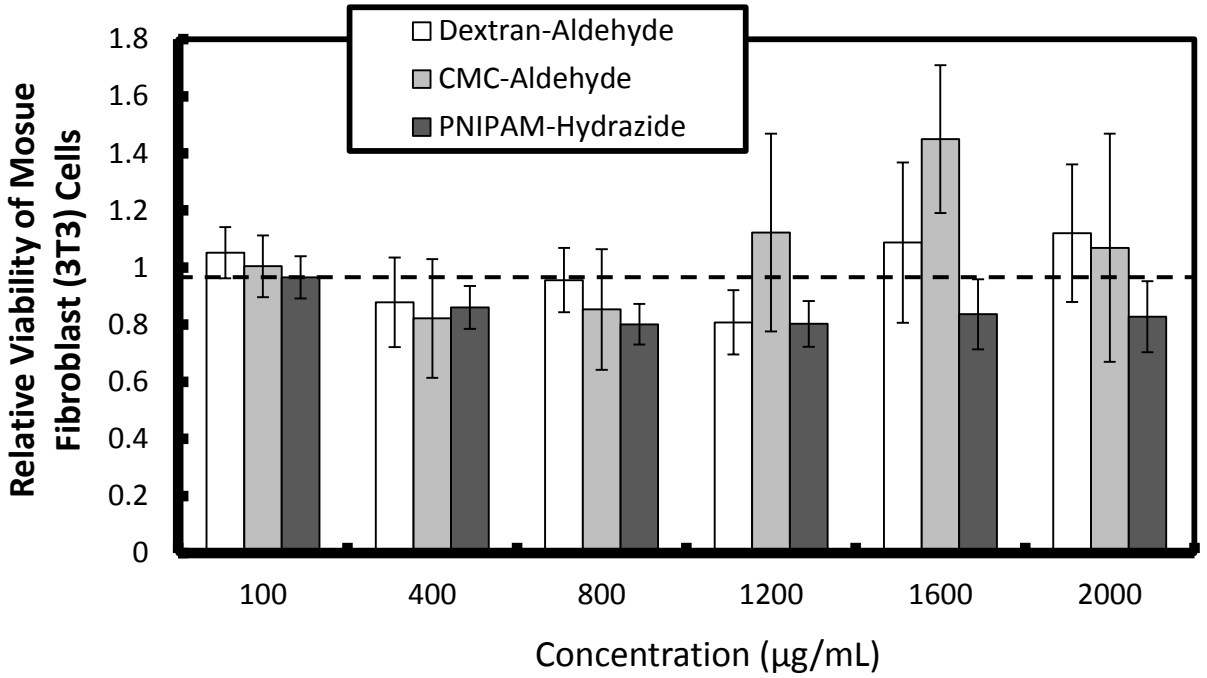

Figure 4.16: Cell viability of 3T3 mouse fibroblast cells exposed to hydrogel precursors. Dashed line represents the viability of control cells not exposed to any polymer solutions.

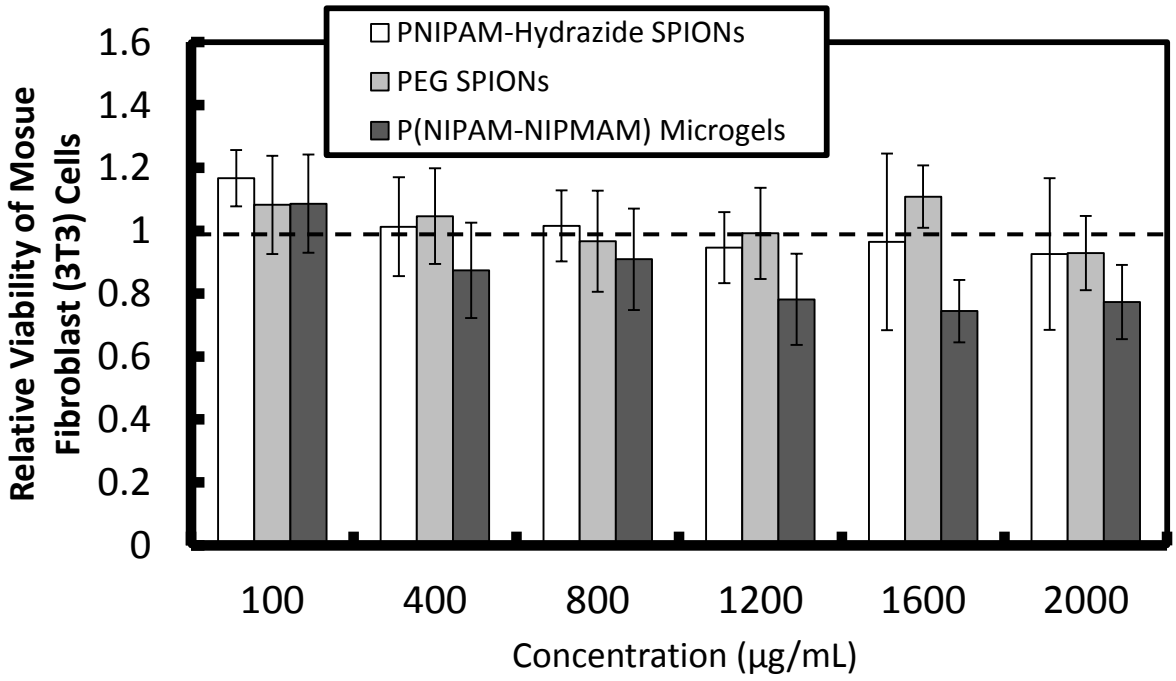

Figure 4.17: Cell viability of 3T3 mouse fibroblast cells exposed to SPION and microgel composite additives. Dashed line represents the viability of control cells not exposed to any polymer solutions.

4.8.1 Discussion

Overall, all components of the composite show limited or no cytotoxicity towards mouse fibroblast cells. The lowest cell viabilities observed were for $M_{0.56}$ (74 ± 10%) and pNIPAM-hydrazide (80 ± 7%) at the highest concentrations tested, but these values are not of major concern because limited to no cytotoxicity *in vivo* tends to be associated with *in vitro* cell viabilities greater than 75% (Fu and Kao 2011). Furthermore, the concentrations tested are much higher than would be expected to be seen in any *in vivo* applications given the rapid gelation (<30 seconds for all composites tested, such that minimal if any polymer diffusion from the injection site would occur prior to gelation) and relatively slow degradation of the composites shown in the previous sections. Although only one p(NIPAM-NIPMAM) microgel formulation was tested, it is reasonable to assume that cytotoxicity of the other microgels would be similar due to the chemical and physical similarities between them.

Chapter 5: Drug Release

Pulsatile release tests were completed on 20 composites including: (1) composites containing 8 wt% hydrogel, 8 wt% $M_{0.56a}$ microgel and 5 wt% SPIONs test at 37°C (the baseline incubation temperature), (2) composites made without SPIONs or microgel, (3) composites incubated at room temperature and at 43°C (well below and above the VPTT of the p(NIPAM-NIPMAM) microgels), (4) composites made using hzd-SPIONs, with and without microgel, (5) composites made with microgels with different VPTT profiles (from those that were mostly collapsed by 37°C to those that did not collapse until 39°C), (6) composites made with different microgel contents (from 0 wt% to 10 wt%), and finally (7) composites made with varying proportions of CMC-aldehyde to control the bulk hydrogel swelling behaviour.

The following sections describe the results for experiments (1) –(7) in turn. Each different subsection includes the pulsatile and cumulative release results for each test, followed by a discussion of the results.

5.1 Initial Release Studies

The release of fluorescein (0.33 kDa), 4kDa FITC-Dex and 70kDa FITC dextran was investigated at 37°C in PBS in the absence of magnetic heating from composites containing 12 wt% $M_{0.56a}$ microgel, 5 wt% PEG-SPIONs, 8 wt% pNIPAM-hydrazide/dextran-aldehyde hydrogel and 1 wt% of each respective fluorescent probe. These results are shown in Figure 5.1.

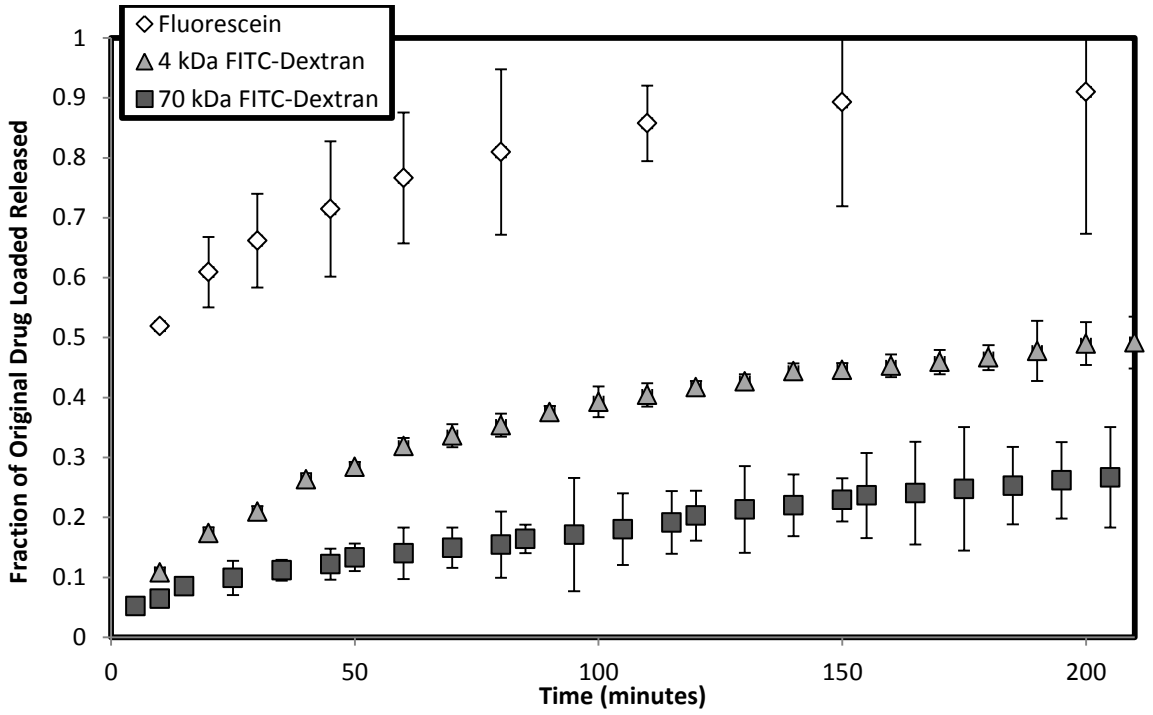

Figure 5.1: Release of fluorescein, 4 kDa FITC-Dex and 70 kDa FITC-Dex from hydrogel-microgel-SPION composites.

As expected for diffusion-based release (Appendix C, Figure C.9 shows the linearity of plots of concentration vs $t^{1/2}$ expected for diffusion-based release for all three model drugs), release scaled with the molecular weight of the fluorescent probe used, with the smallest probe (fluorescein) releasing the fastest (nearly 100% release in 4 hours) and the largest probe (FITC-Dex 70 kDa) releasing the slowest (~ 20% release in 4 hours). Based on these results, we chose to use FITC-Dex 4kDA for all further tests, facilitating slow enough diffusional (i.e. "off state") release to facilitate longer term pulsing while showing fast enough release that a significant drug dose could be administered in a reasonably short pulse time.

The release rate of 4kDa FITC-Dex for the first day of a pulsatile release test from the $8M_{0.56a}$- PEG FF-8H 100 Dex-T37 composites containing 1 wt% 4kDa FITC-Dex is shown in Figure 5.2.

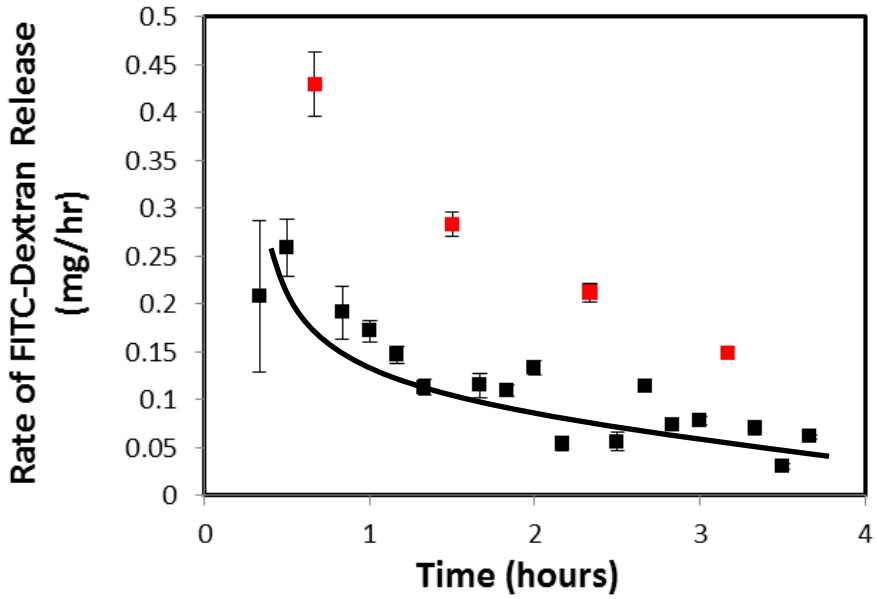

Figure 5.2: Release rate of 4 kDa FITC-Dex during the first day of a pulsatile release test. 8 wt% hydrogel, 8 wt% $M_{0.56a}$ microgel, 5 wt% PEG-SPIONs, 1 wt% 4 kDa FITC-Dex were used.

The red points represent the release rate observed from the gels during 10 minutes of exposure to an alternating magnetic field (AMF). The figure demonstrates that the AMF increases the drug release rate from the composite in a pulsatile manner over multiple cycles. Table 5.1 reports the predicted release rate (based on the baseline, diffusional release curve), observed release rate (after the 10 minute magnetic pulse) and percent increase in release rate for the test illustrated in Figure 5.2. For this test, the average percent increase in release rate observed from the control composites (i.e. gels with the same composition, incubated at the same temperature, but not exposed to any AMF) was -2.5 ± 4 %.

Table 5.1: Predicted release rate, actual release rate and percent increase in predicted release rate for the first day of a pulsatile release test on a composite containing 8 wt% hydrogel, 8 wt% $M_{0.56a}$, 5 wt% PEG-SPIONs and 1 wt% 4kDa FITC-Dex. 10 minute pulse lengths.

Pulse Time Point	Predicted Release Rate (mg/hr)	Actual Release Rate (mg/hr)	Percent Increase in Predicted Release Rate
40 minutes	0.21 ± 0.04	0.43 ± 0.03	109 ± 20 %
90 minutes	0.12 ± 0.01	0.28 ± 0.01	135 ± 9 %
140 minutes	0.089 ± 0.007	0.21 ± 0.01	137 ± 11 %
190 minutes	0.063 ± 0.005	0.149 ± 0.002	136 ± 11 %

As observed, the percentage increase in predicted release rate for each pulse is statistically the same, although the average rate of drug release decreases as a function of time due to the background $t^{1/2}$ release kinetics related to diffusion through the composite in the absence of a pulse. The pulsatile release results for subsequent days of testing on these composites, as well as the cumulative release results from these composites are shown in Section 5.2.

5.1.1 Discussion

Hoare et al showed that incorporation of p(NIPAM-NIPMAM-AAm) microgels (VPTT approximately 40°C) into a composite ethyl cellulose membrane containing magnetic nanoparticles resulted in pulsatile drug release when application of an AMF raised the composite temperature above the microgel VPTT. This caused the microgels to collapse and transformed the ethyl cellulose membrane into a porous structure that had a higher permeability, allowing for increased drug release (Hoare et al. 2009). A similar mechanism is used to explain the preceding and following results and is illustrated in Figure 5.3.

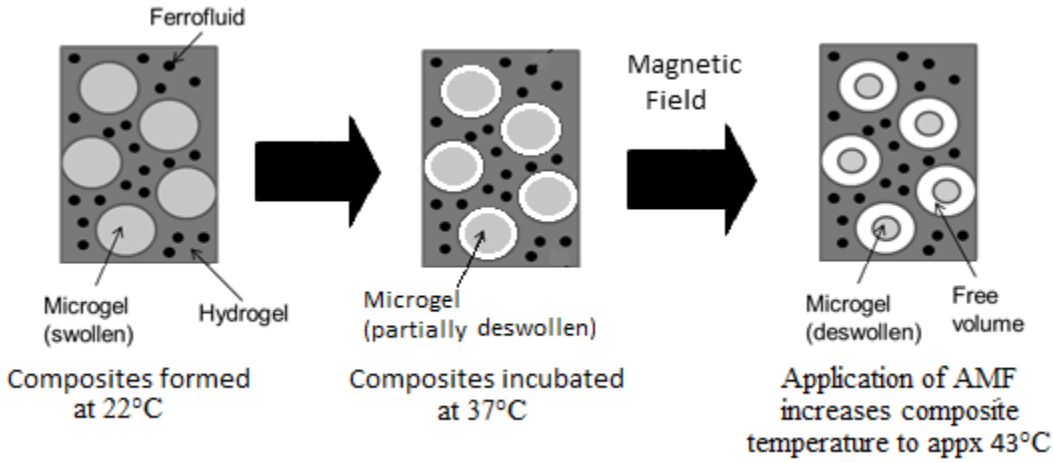

Figure 5.3: Schematic of proposed magnetic hydrogel-microgel nanocomposite structure before and after magnetic pulsing.

The composites are formed at room temperature (approximately 22°C) with fully swollen microgels. When the composites are transferred to a 37°C water bath, the microgels partially deswell, creating a small amount of free volume in the composite. Compared to diffusing through the swollen microgel or hydrogel phases, this water filled pore network provides a pathway through which the drug can more easily diffuse, although the swelling or deswelling of the bulk hydrogel may alter the magnitude of the free volume generated (a factor to be explored later in this thesis). Upon application of an AMF, the composite heats up above the microgel VPTT, causing the microgels to collapse completely, creating a larger amount of free volume. If the microgels are present at sufficiently high volume fractions, this free volume may result in a percolated network that would lead to significantly increased drug release over the course of the magnetic triggering. When the AMF is removed, the composites cool via convection and the microgels reswell, decreasing the pore network to its lesser, pre-pulse state.

As demonstrated in Figure 5.2 a significant increase in release rate is observed from these composites due to the application of an AMF. Further tests were completed to confirm that the

mechanism shown in Figure 5.3 was valid and to determine how pulsatile release could be controlled and improved.

5.2 Release from No Microgel and No Ferrofluid Controls

Composites made from hydrogel , microgel, PEG-SPIONs and 1wt % 4 kDA FITC-Dex ($8M_{0.56a}$- PEG FF-8H 100 Dex-T37) were compared with composites made without microgel (0M- PEG FF-8H 100 Dex-T37), and composites made with without SPIONs ($8M_{0.56a}$- 0 FF-8H 100 Dex-T37). We hypothesize that pulsatile release will be more effective for composites containing microgel because the microgels' collapse will create more free volume within the composite (facilitating more pulsatile release) and that the composites that do not contain any SPIONs will not exhibit any pulsatile release behaviour. Figure 5.4 and Table 5.2 describe the pulsatile release of 4 kDa FITC-Dex from the composites while Figure 5.5 and

Table 5.3 describe the burst and cumulative of 4 kDa FITC-Dex release.

5.2.1 Pulsatile Release

Pulsatile release tests were completed on composites with and without SPIONs ($8M_{0.56a}$-PEG FF and $8M_{0.56a}$-0 FF) and with and without microgel ($8M_{0.56a}$- PEG FF and 0M- PEG FF) as controls. Figure 5.4 shows that no statistically significant change in release was observed upon application of the AMF for the $8M_{0.56a}$-0 FF composites. The figure also demonstrates that $8M_{0.56a}$- PEG FF composites experienced a significantly greater percent increase in release rate due to the application of the magnetic field compared to 0M- PEG FF composites ($p<0.05$). As such, the microgel does significantly contribute to the pulsatile release kinetics observed. The loss of 2 out of 4 0M- PEG FF composites by day five of the test (one experienced significant

mechanical degradation and the other was dropped and destroyed) made pulsatile testing on the fifth day impossible for that test, so the 0M- PEG FF test was ended earlier than the others.

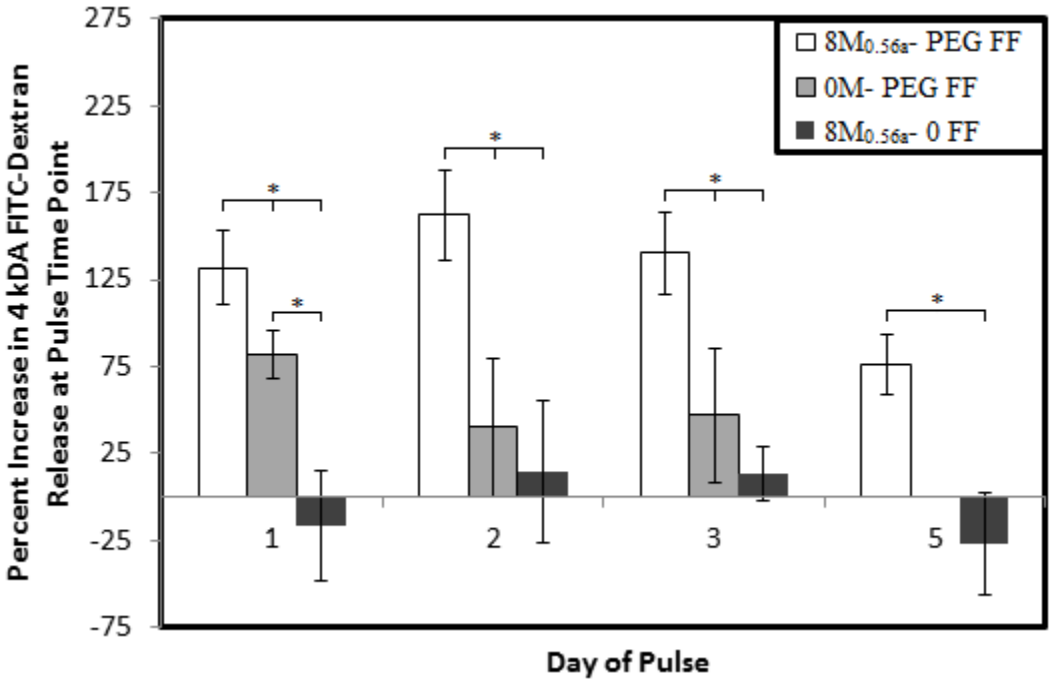

Figure 5.4: Percent increase in 4kDa FITC-Dex release rate observed from control composites made with and without microgel and ferrofluid due to exposure to an alternating magnetic field. * indicates statistical significance ($p<0.05$).

Table 5.2 shows the excess mass of FITC-Dex-4kDa that was released over the course of the AMF pulses relative to the baseline (diffusion-based) release. The increased mass released was significantly higher for the $8M_{0.56a}$- PEG FF composite than the other composites on all days. For the $8M_{0.56a}$- PEG FF composite, each day of testing saw an order of magnitude decrease in the extra mass of drug released during pulsing, although as Figure 5.4 shows, the percentage increase in release upon pulsing relative to the baseline remains relatively constant.

Table 5.2: Excess 4kDa FITC-Dex released over the duration of the magnetic pulse for control composites made with and without microgel or ferrofluid.

	Extra Drug Released During Pulses (µg)			
Test Name	Day 1	Day 2	Day 3	Day 5
$8M_{0.56a}$- PEG FF	25 ± 3	0.8 ± 0.1	0.16 ± 0.04	0.01 ± 0.005
0M- PEG FF	16 ± 3	0.01 ± 0.09	0.01 ± 0.08	NA
$8M_{0.56a}$- 0 FF	-6 ± 9	0.05 ± 0.2	0.03 ± 0.04	-0.01 ± 0.04

5.2.2 Cumulative Release

The burst (diffusion only) release from the composites is shown in Figure 5.5. Significantly more release was observed from the 0M- PEG FF and $8M_{0.56a}$- 0 FF composites compared to the $8M_{0.56a}$- PEG FF composites, but there was statistically no difference between the burst release profiles of the 0M- PEG FF and $8M_{0.56a}$- 0 FF controls.

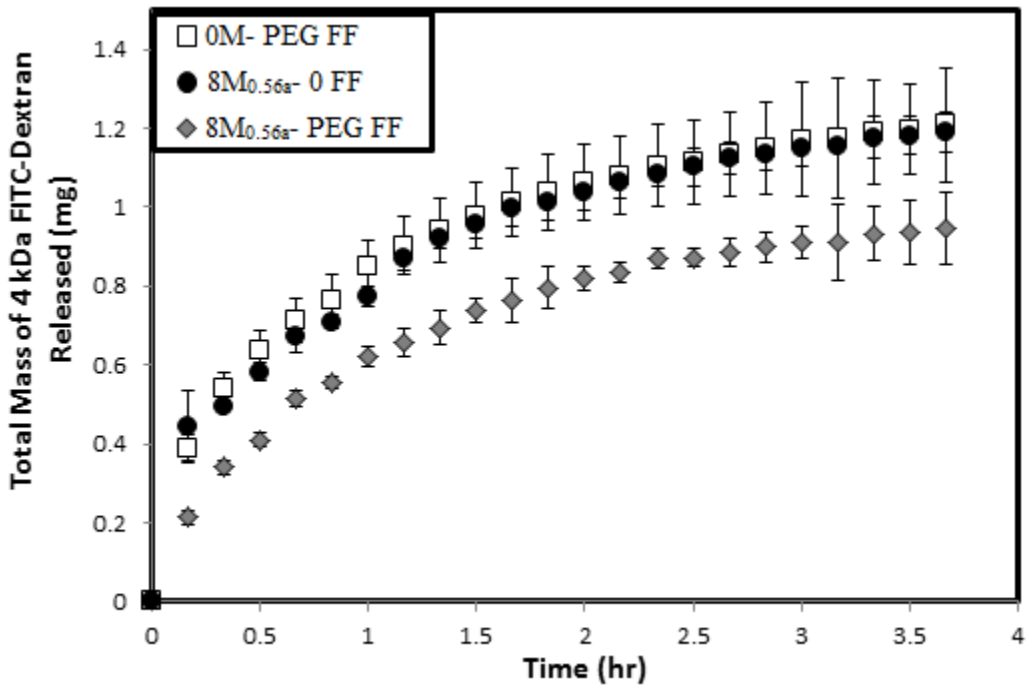

Figure 5.5: Initial burst release of 4kDa FITC-Dex (in the absence of a magnetic pulse i.e. diffusion only release) from control composites with and without microgel or ferrofluid.

Table 5.3 shows the cumulative release from these composites over the first 24 hours of testing. Similar to the results above, the release from the 0M- PEG FF and $8M_{0.56a}$- 0 FF controls is statistically higher than from the $8M_{0.56a}$- PEG FF composites but they are not significantly different from each other. The difference in overall mass released persists until the end of the tests.

Table 5.3: Cumulative release of 4 kDA FITC-Dex from control composites (not exposed to a magnetic pulse – release by diffusion alone) with and without microgel or ferrofluid over five days of testing. * indicates statistical significance ($p<0.05$). All samples marked NA were not possible to measure due to gel degradation.

Test Name	**Total Mass of 4 kDa FITC-Dex Released** After 1 hr (mg)	After 4 hr (mg)	After 24 hr (mg)	After 48 hr (mg)	After 96 hr (mg)
$8M_{0.56a}$- PEG FF	0.60± 0.09*	0.97 ± 0.12*	1.04 ± 0.06*	1.06 ± 0.1*	1.07 ± 0.15*
0M- PEG FF	0.84 ± 0.07	1.21 ± 0.11	1.32 ± 0.09	1.34 ± 0.09	NA
$8M_{0.56a}$- 0 FF	0.8 ± 0.2	1.19 ± 0.05	1.32 ± 0.07	1.28 ± 0.09	1.29 ± 0.07

5.2.3 Discussion

As expected, in the absence of SPIONs, the composites are not magnetic and do not exhibit any statistically significant pulsatile release behaviour when exposed to an AMF (i.e. no heating is initiated within the hydrogel). The fact that the mass of 4 kDa FITC-Dex released from the $8M_{0.56a}$- 0 FF composites is higher than that the $8M_{0.56a}$- PEG FF composites could be explained by the fact that the presence of the SPIONs in the hydrogel composites makes the composites denser, providing an extra barrier to diffusion in the $8M_{0.56a}$- PEG FF composites, slowing release. The difference in release between the $8M_{0.56a}$- PEG FF and $0M_{0.56a}$- PEG FF composites can be explained by two factors. First, without any microgels in the network, the 0M-PEG FF has a lower diffusional barrier to release compared to the $8M_{0.56a}$- PEG FF composites,

promoting faster release. Second, the 0M- PEG FF composites deswell immediately upon incubation at 37°C while the $8M_{0.56a}$- PEG FF composites swell significantly (see Figure 4.6) The deswelling of the 0M- PEG FF composites on the first day of release could result in drug being 'squeezed' out of the composite as the thermosensitive bulk hydrogel deswells and expels water, resulting in higher release compared to the swollen $8M_{0.56a}$- PEG FF composites.

0M- PEG FF composites exhibit some pulsatile behaviour, likely caused by increased diffusion due to increased composite temperature or drug being 'squeezed' out of the composite when the thermosensitive bulk hydrogel deswells and expels water due to the increase in temperature. There is also previous literature suggesting that magnetic heating can induce drug release in non-thermoresponsive composites via a mechanism attributed to local mechanical stressing of the hydrogel as the SPIONs move slightly in the magnetic field, which could also be happening in this thermoresponsive system (Brazel 2009). However, the pulsatile release from the 0M- PEG FF composites (in terms of both percentage increase in release rate relative to the baseline and the magnitude of extra mass released due to the AMF) is less than observed with the $8M_{0.56a}$- PEG FF composites, which supports the mechanism described in Figure 5.3.

5.3 Drug Release from hzd-SPION-based Composites With and Without Microgel

Composites were fabricated with different SPION types (hzd- and PEG-SPIONs) with and without microgel to determine the effect of crosslinking the SPION into the network on the observed pulsatile release properties as well as the impact of microgel content on pulsatile release. $8M_{0.56a}$- PEG FF-8H 100 Dex-T37 (PEG-SPIONs, 8 wt% microgel) and 0M- PEG FF-8H 100 Dex-T37 (PEG-ferrofluid, no microgel) were compared with $8M_{0.56a}$- hzd FF-8H 100 Dex-T37 composites (hzp-SPIONs, 8 wt% microgel), and 0M- hzd FF-8H 100 Dex-T37 (hzd-

SPIONs, no microgel). All composites contained 8 wt% hydrogel (100% dextran-aldehyde for the B component), 5 wt% SPIONs and 1 wt% 4 kDa FITC-Dextran and were incubated at 37°C. We hypothesize that pulsatile release will not be significantly different for composites using PEG vs hzd-SPIONs and that it will be more effective for composites containing microgel. Figure 5.6 and Table 5.4 describe the pulsatile release of 4 kDa FITC-Dex from the composites while Figure 5.7 and Table 5.5 describe the burst and cumulative of 4 kDa FITC-Dex release.

5.3.1 Pulsatile Release

Pulsatile release tests were completed on composites with PEG-SPION and hzd-SPIONs with and without microgel. Figure 5.6 shows that on the first day, AMF pulsing results in increases in release rate, with $8M_{0.56a}$- PEG FF and $8M_{0.56a}$- hzd FF (microgel containing) composites showing statistically significantly higher increases in percent increase in release rate than those for 0M- PEG FF and 0M- hzd FF composites (prepared without microgel), but no significant difference ($p<0.05$) between $8M_{0.56a}$- PEG FF and $8M_{0.56a}$- hzd FF . The pulse results from day two and three also show that composites containing microgel experienced a greater percent increase in release due to the application of the magnetic field compared to composites that did not contain any microgel, although there is again no significant difference between the PEG-FF and hzd-FF prepared samples. Interestingly, the 0M- hzd FF composites underwent rapid mechanical degradation upon application of the magnetic field (see Appendix C, Figure C.11) and are thus excluded from the day three data on Fig. 5.6.

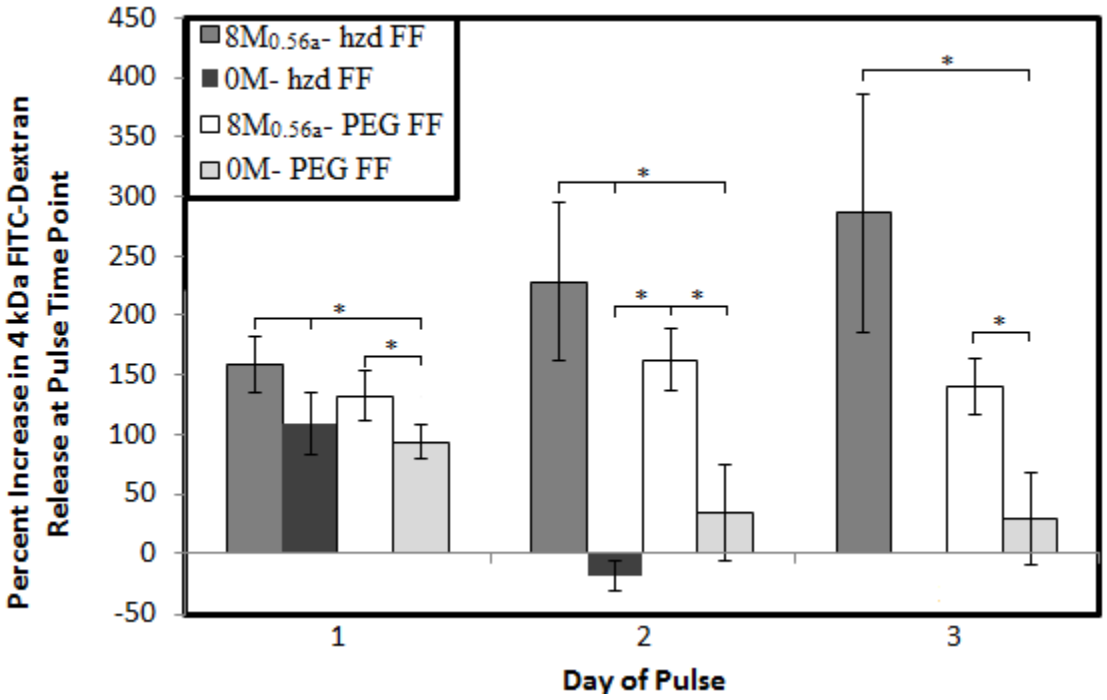

Figure 5.6: Percent increase in 4kDa FITC-Dex release rate observed from composites made with PEG-SPIONs and hzd-SPIONs with and without microgel due to exposure to an alternating magnetic field. * indicates statistical significance (p=0.05).

Table 5.4 shows extra mass of FITC-Dex that was released over the course of the AMF pulses. The increased mass released was significantly higher for the microgel containing-composites than the microgel-free composites on days 2 and 3. Although the percent increases in release rate reported in Figure 5.6 suggest that more pulsatile release was observed from the $8M_{0.56a}$- hzd FF composites compared to the $8M_{0.56a}$- PEG FF composites, the extra mass released is not statistically different on days 2 or 3, although statistically more extra mass release was observed on day one from the $8M_{0.56a}$- hzd FF. For the microgel-containing composites, each day of testing saw approximately one order of magnitude decrease in the extra mass of drug released during pulsing.

Table 5.4: Excess drug released over the duration of the magnetic pulse for composites made with PEG-SPIONs and hzd-SPIONs with and without microgel.

	Extra Drug Released During Pulses (µg)		
Test Name	Day 1	Day 2	Day 3
$8M_{0.56a}$- PEG FF	25 ± 3	0.8 ± 0.1	0.16 ± 0.04
0M- PEG FF	16 ± 3	0.01 ± 0.09	-0.01 ± 0.08
$8M_{0.56a}$- hzd FF	46 ± 6	0.6 ± 0.2	0.12 ± 0.02
0M- hzd FF	38 ± 9	-0.04 ± 0.2	NA

5.3.2 Cumulative Release

The burst release from the composites is shown in Figure 5.7. Initially, significantly less release was observed from the microgel containing composites relative to the microgel-free composites. This difference did not persist past 4 hours for the hzd-FF composites but persisted past 24 hours for the PEG-FF composites (see Table 5.5). Initially, the $8M_{0.56a}$- PEG FF exhibited similar release to the $8M_{0.56a}$- hzd FF , but after 4 hours the release from $8M_{0.56a}$- hzd FF composites was significantly higher than that from the $8M_{0.56a}$- PEG FF composites (see Table 5.5).

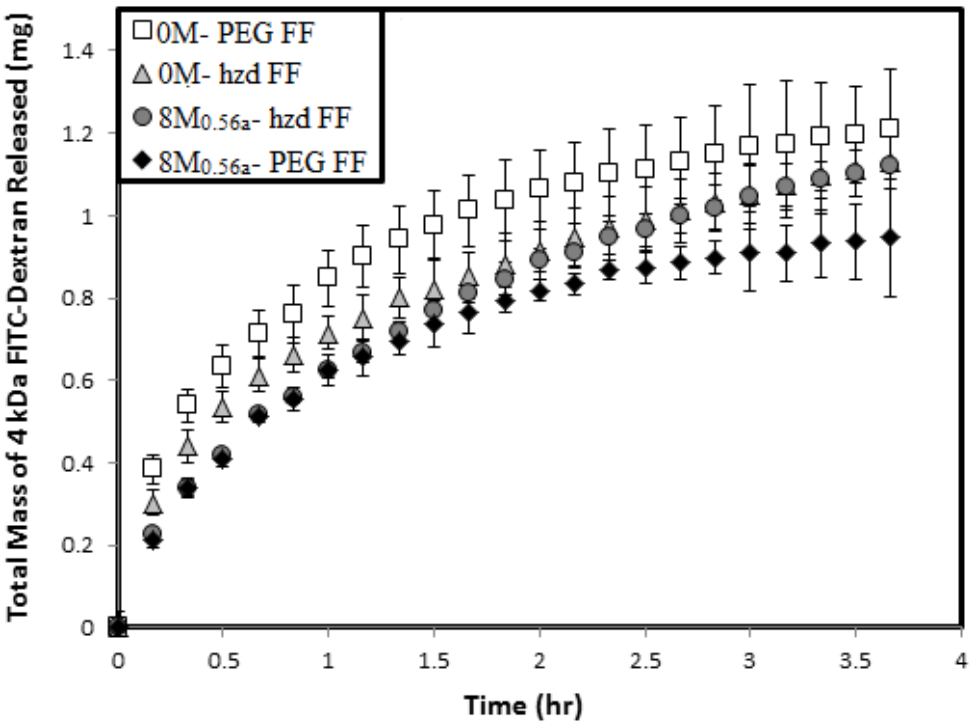

Figure 5.7: Initial burst release of 4 kDa FITC-Dex (in the absence of a magnetic pulse-diffusion only) from composites made with PEG-SPIONs and hzd-SPIONs with and without microgel.

Table 5.5: Cumulative release of 4 kDa FITC-Dex from composites made with PEG-SPIONs and hzd-SPIONs with and without microgel (not exposed to a magnetic pulse – release by diffusion alone) over 5 days of testing. All samples marked NA were not possible to measure due to gel degradation prior to the stated measurement time.

Test Name	**Total Mass of 4 kDa FITC-Dex Released** After 1 hr (mg)	After 4 hr (mg)	After 24 hr (mg)	After 48 hr (mg)	After 96 hr (mg)
$8M_{0.56a}$- PEG FF	0.60± 0.09	0.97 ± 0.12	1.04 ± 0.06	1.06 ± 0.10*	1.07 ± 0.15
0M- PEG FF	0.84 ± 0.07	1.21 ± 0.11	1.32 ± 0.09	1.34 ± 0.09	NA
$8M_{0.56a}$- hzd FF	0.62± 0.02	1.12 ± 0.06	1.37 ± 0.10	1.39 ± 0.05	NA
0M- hzd FF	0.71± 0.04	1.13± 0.07	1.27 ± 0.15	NA	NA

5.3.3 Discussion

Composites made with hzd- SPIONs exhibit pulsatile behaviour, which is consistent with the work published by Campbell et al. which reported repeated pulsatile release of the cationic, local anaesthetic bupivacaine upon application of an oscillating magnetic field to composites similar to the 0M- hzd FF composites used here (Campbell, 2013). Little to no difference was observed between the PEG and hzd-FF composites in terms of their release behaviours, aside from the slightly faster cumulative release observed for hzd-FF composites (Table 5.5). The percent increases in release rate reported in Figure 5.6 suggest that more pulsatile release was observed from the $8M_{0.56a}$- hzd FF composites compared to the $8M_{0.56a}$- PEG FF composites, while the extra mass released is not statistically different on days 2 or 3 and actually appears to be lower for the pNIPAM-hydrazide composites. This can be explained by the fact that the baseline rate of release from the $8M_{0.56a}$- hzd FF composites is lower on subsequent days than for the $8M_{0.56a}$- PEG FF composites; this lower baseline release results in an inflated percent increase in release rate.

Again, the pulsatile release both $0M_{0.56a}$ composites (in terms of percent increase in pulsatile release rate) is significantly less than the $8M_{0.56a}$ composites for the two days for which testing was possible. This result also supports the mechanism described in Figure 5.3.

The 0M- hzd FF composites exhibited rapid mechanical degradation upon repeated exposure to ten minute AMF pulses. Due to the fact that the hydrogel network directly incorporated the SPIONs, it is possible that vibration of the SPIONs in the AMF caused vibration of the network resulting in mechanical degradation. Less degradation could be expected (and was observed) from the $8M_{0.56a}$- hzd FF composites because the interspersion of the (more highly crosslinked) microgels in the network may have the potential to dissipate or absorb some of the

vibrational energy from the SPIONs. The same level of degradation would not be expected from the $8M_{0.56a}$- PEG FF composites (and was not observed) because the SPIONs were entrapped within the network, not incorporated into it, so vibrational energy would not be transferred into the network bonds to the same degree.

Similar to the results discussed in Section 5.2.3, the mass of 4 kDa FITC-Dex released from the 0M- hzd FF composites was initially higher than $8M_{0.56a}$- had FF composites, likely due to the fact the microgel phase has a higher resistance to drug diffusion, providing an extra barrier to drug release. The 0M- hzd FF composites also experienced significant deswelling on the first day of release (see

Figure 4.8) which could result in drug being 'squeezed' out of the composite as the thermosensitive bulk hydrogel deswells and expels water. This explanation is further supported by the fact that the 0M- PEG FF composite appears to deswell more than the 0M- hzd FF composites and also experiences a higher initial burst release (Figure 4.8 and Figure 5.7). In comparison, the composites prepared with microgel swell on the first day, with the $8M_{0.56a}$- hzd FF composites returning to a state of 0 net swelling over days two and three while $8M_{0.56a}$- PEG FF composites deswell to approximately -10% of their original weight. This swelling behaviour could account for why the $8M_{0.56a}$- hzd FF composite releases more drug than the $8M_{0.56a}$- PEG FF composite after 24 hours; the collapse of $8M_{0.56a}$- PEG FF network would make diffusion of 4 kDa FITC-Dextran from the network slower, while the net-zero swelling environment of the $8M_{0.56a}$- hzd FF composites would promote diffusion (because the pore network created by microgel collapse between 25°C and 37°C would not be occluded by the swollen or collapsed hydrogel).

5.4 Release from Composite Incubated At Different Base Temperatures

Composites were incubated and exposed to AMF at different temperatures to determine the effect of incubation temperature on release behaviour. All composites contained 8 wt% hydrogel (100% dextran-aldehyde for the B component), 8 wt% $M_{0.56a}$ microgel, 5 wt% PEG-SPIONs, 1 wt% 4 kDa FITC-Dextran ($8M_{0.56b}$- PEG FF-8H 100 Dex-Tx, where x is 37, 43 or 22). We hypothesize that pulsatile release will be more effective at a 37°C baseline temperature (around the VPTT of the microgels) compared to 22°C (well below the microgel VPTT) or 43°C (above the microgel VPTT) because the microgels at 37°C will undergo the biggest size change and thus induce the largest pulsatile release. Figure 5.8 and Table 5.6 describe the pulsatile release of 4 kDa FITC-Dex from the composites while Figure 5.9 and Table 5.7 describe the burst and cumulative of 4 kDa FITC-Dex release.

5.4.1 Pulsatile Release

Pulsatile release tests were completed on composites with a fixed composition but maintained at different incubation temperatures. Figure 5.8 shows that on the first day, AMF pulsing produces percent increases in release rate in the T37 and T43 composites that are not significantly different from each other ($p<0.05$) but are significantly higher than those observed in the T22 composites. Pulsatile release from the T43 composites is statistically insignificant on days two and three. Although pulsatile release behaviour persists for the T22 composite for days two and three, the percent increase in release rate of the T37 composites is significantly higher. There is no statistical difference in the pulse behaviour of the three composites on the fifth day of testing, with all three facilitating rather small pulse releases.

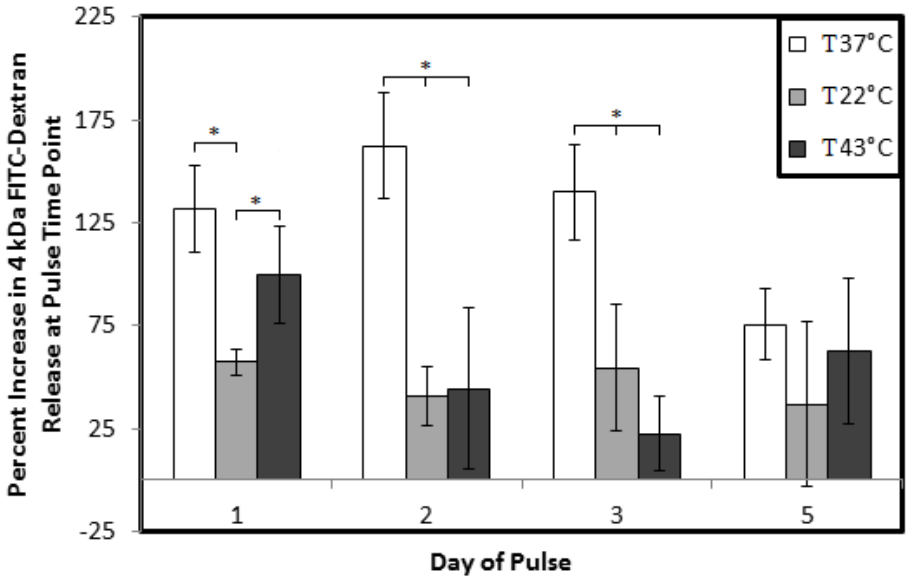

Figure 5.8: Percent increase in 4kDa FITC-Dex release rate observed from composites incubated at different temperatures due to exposure to an alternating magnetic field. * indicates statistical significance (p=0.05).

Table 5.6 shows extra mass (relative to the baseline, diffusion-only release) of FITC-Dex-4kDa that was released over the course of the AMF pulses. Similar to the above results, the excess mass released was significantly higher for the composites incubated at 37°C and 43°C than the composite pulsed at baseline room temperature (22°C) but are not statistically different from each other on day one. For days two and three, the increased mass released was significantly higher for the composites incubated at 37°C than the composites incubated at 43°C or 22°C, the latter two of which are not statistically different from each other. There is no difference in mass released on day five between all the composites tested.

Table 5.6: Excess 4kDa FITC-Dex released over the duration of the magnetic pulse for composites incubated at different temperatures.

	Extra Drug Released During Pulses (µg)			
Test Name	Day 1	Day 2	Day 3	Day 5
T37	25 ± 3	0.8 ± 0.1	0.16 ± 0.04	0.01 ± 0.005
T43	27 ± 5	0.1 ± 0.2	0.025 ± 0.015	0.01 ± 0.04
T22	13 ± 2	0.47 ± 0.08	0.14 ± 0.02	0.04 ± 0.08

5.4.2 Cumulative Release

The burst release from the composites is shown in Figure 5.9. Initially, higher burst release was observed with increasing temperature (i.e. the T22 composites experienced less burst release than T37 composites which showed less burst release than T43 composites). Statistically ($p<0.05$) there was no difference in the mass of 4 kDa FITC-Dex released from different composites after 24 hours (i.e. the cumulative mass released on days two, three and five were not statistically different for T22, T37 and T43 composites)(see Table 5.7). Also shown in Figure 5.9 is the burst release from the 0M- PEG FF control composite, which shows higher, but statistically indistinguishable burst release relative to the T43 composite.

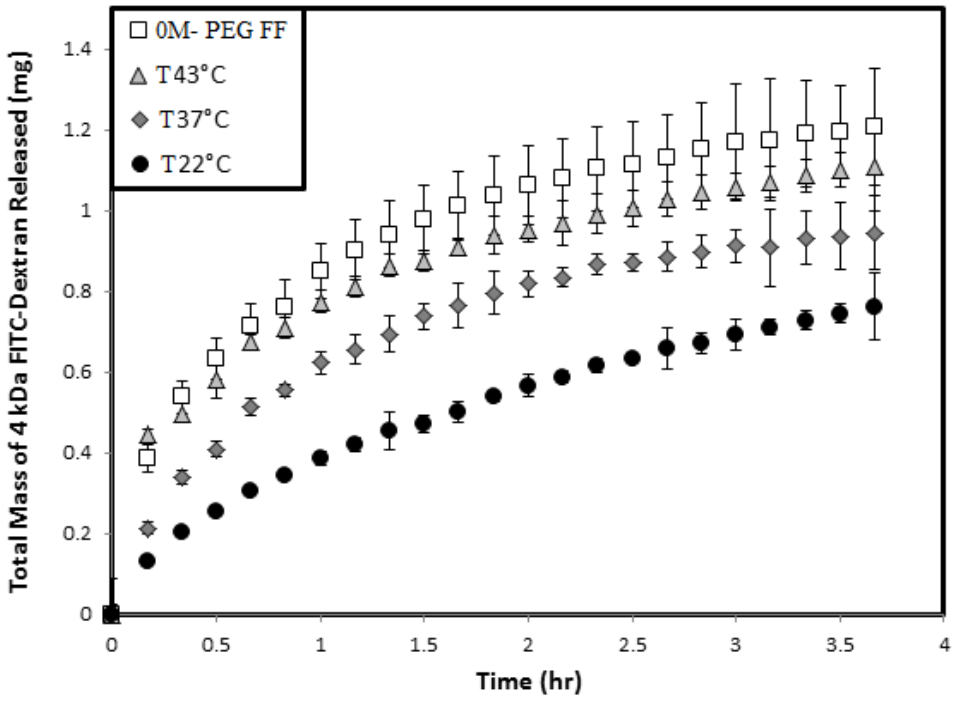

Figure 5.9: Initial burst release of 4kDa FITC-Dex (in the absence of a magnetic pulse-diffusion only) from composites incubated at different temperatures. Burst release from 0M-PEG FF (a composite incubated at 37°C, but not containing microgel) is shown for comparison.

Table 5.7: Cumulative release of 4 kDa FITC-Dex from composites incubated at different temperatures (not exposed to a magnetic pulse – release by diffusion alone) over five days of testing. All samples marked NA were not possible to measure due to gel degradation at this time point.

Test Name	**Total Mass of 4 kDa FITC-Dex Released** After 1 hr (mg)	After 4 hr (mg)	After 24 hr (mg)	After 48 hr (mg)	After 96 hr (mg)
T43	0.77 ± 0.03	1.11 ± 0.04	1.3 ± 0.1	1.06 ± 0.1	1.07 ± 0.15
T37	0.60± 0.09	0.97 ± 0.12	1.04 ± 0.06	1.20 ±0.09	1.24 ± 0.15
T22	0.38 ± 0.01	0.76 ± 0.02	1.14 ± 0.08	1.28 ± 0.09	1.29 ± 0.08
0M-PEG FF	0.84 ± 0.07	1.21 ± 0.11	1.32 ± 0.09	1.34 ± 0.09	NA

5.4.3 Discussion

The proposed mechanism responsible for the differences in the pulsatile behaviours of the composites based on temperature of incubation is illustrated in Figure 5.10. All composites were formed at room temperature, a temperature at which the microgels would be fully swollen (Figure 5.10 (a) i,(b) i, and (c) i). The microgels contained in the composites that are incubated at 37°C undergo slight deswelling to create a small pore network (Figure 5.10 (a) ii) while the microgels in the composites incubated at 22°C remain swollen (Figure 5.10 (b) ii) and no excess free volume is created. The microgels in the composites incubated at 43°C deswell almost completely (Figure 5.10 (c) ii), resulting in a larger pore network and a lot of excess free volume. Upon application of the magnetic field, the microgels in the 37°C composites would be expected to deswell significantly (Figure 5.10 (a) iii), resulting in the greatest change in free volume and pulsatile release potential, while the microgels in the 22°C composites would be expected to slightly deswell (Figure 5.10 (b) ii), resulting in some free volume increase and pulsatile release, and the microgels in the 43°C composites would deswell very little if at all (Figure 5.10 (c) iii), causing almost no change in the composite's pore network and pulsatile release potential. Based on this mechanism, one would predict the highest pulsatile response from the 37°C composites,

with less or no pulsatile release expected from 22°C and 43°C composites. As shown in Figure 5.6, this is the exact behaviour that was observed from the composites on days two and three.

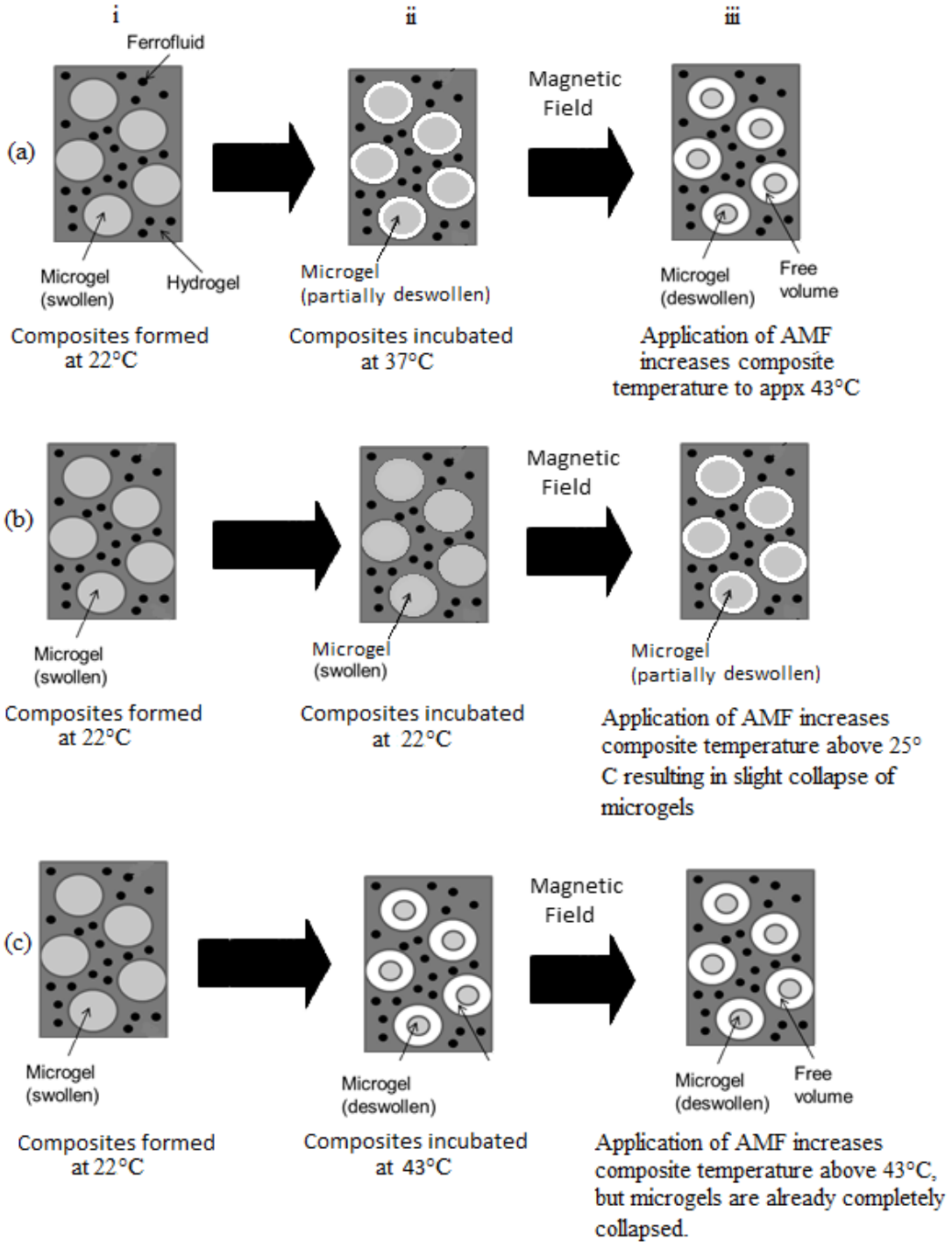

Figure 5.10: Schematic of proposed magnetic hydrogel-microgel nanocomposite structure before and after magnetic pulsing at different incubation temperatures.

On day one, more pulsatile release was observed from the T37 and T43 composites than the composite incubated at T22, but there was no difference between the two higher temperature tests. This could be due to the fact that the T43 composite experienced zero net swelling on the first day of testing (Figure 4.10) while the T37 composite swelled significantly. It is possible that the swelling of the 37°C composites caused the free volume created by microgel desweling to be at least partially occluded by the swollen hydrogel matrix, limiting the pulsatile drug release. Supporting this explanation is the fact that the deswelling behaviour of the T37 and T43 composites is very similar on days two and three, and pulsatile release from the T37 composites (in terms of both percent increase in pulsatile release rate and extra mass released due to the AMF) is higher than the T43 composites.

The relative cumulative release from the composites can be explained by three factors. First of all, diffusion of drug from the composite would be expected to be slower at lower temperatures; this is observed in the data as release at T22 is lower than at T37 which is lower than at T43 baseline temperature. The Stokes-Einstein equation can be used to estimate the diffusivity of solutes in water and is shown below.

$$\boldsymbol{D_A = \frac{kT}{6\pi\eta r_H}} \qquad \textbf{(8)}$$

where K is the Boltzmann constant (1.38 x 10^{-23} J/K), T is the absolute temperature in Kelvin, and η is the dynamic viscosity of water at T. The change in diffusivity of a solute due to temperature increase (not considering changes in composite swelling, microgel collapse or mechanical properties) can be predicted by the following equation (Brandl et al. 2010):

$$\boldsymbol{\frac{D_{A2}}{D_{A1}} = \frac{T_2\eta_1}{T_1\eta_2}} \qquad (9)$$

This equation predicts a change in diffusivity between 37°C (D_{A2}) and 22°C (D_{A1}) of 1.24x and a change in diffusivity between 37°C (D_{A2}) and 43°C (D_{A1}) of 0.88x. By fitting a simplified Fick's 2nd Law equation to the experimental burst release results (see Appendix, Figure C.10), approximate diffusivities were determined. The observed change in diffusivity between 37°C and 22°C was almost double what Equation 9 predicted (at 2.45 x) and the change from 37°C and 43°C was 25% less than predicted by Equation 9 (at 0.65x). This suggests that the difference in diffusivities observed is significantly different than what diffusion alone would predict, suggesting that the thermoresponsivity of the microgels and bulk hydrogel is playing a role in this result.

The second factor that could drive this difference is the creation of a pore network within the composite due to microgel deswelling. As illustrated in Figure 5.10 ii, the pore network is expected to be minimal or non-existent for the composites at T22, slightly larger for the T37 composites, and the largest for the T43 composites; this would suggest release rates should scale as T43 > T37 > T22 baseline temperatures, as shown. Finally, occlusion of the pore network by composite swelling, observed on day one at T22 and T37 would further slow release from these composites while negligible swelling, observed on day one at T43 would result in fully open pore network.

5.5 Effect of Microgel VPTT on Drug Release

Composites were fabricated with 8wt% microgel content using microgels with different VPTTs to determine the effect of VPTT behaviour of the microgel on release. All composites contained 8 wt% hydrogel (100% dextran-aldehyde for the B component), 8 wt% microgel, 5

wt% PEG-SPIONs, 1 wt% 4 kDa FITC-Dextran and were incubated at 37°C ($8M_x$- PEG FF-8H 100 Dex-T37, where x is 1.8, 1, 0.56b, or 0.27). We hypothesize that microgels with VPTT values closer to the middle of the temperature range used in the experiment will undergo the biggest size change and thus induce the largest pulsatile release. Figure 5.11 and Table 5.9 describe the pulsatile release of 4 kDa FITC-Dex from the composites while Figure 5.12 and Table 5.10 describe the burst and cumulative release of 4 kDa FITC-Dex.

5.5.1 Pulsatile Release

The temperature at which each microgel's effective diameter had decreased by half (from their size at 26°C) is listed in Table 5.8 (based on data from Figure 4.3).

Table 5.8: Microgel VPTTs (temperature at which different p(NIPAM-NIPMAM) microgels' effective diameters have decreased by 50% from their size at 26°C) and diameter changes between 25°C, 37°C and 43°C for each microgel tested. * indicates statistical significance ($p<0.05$).

Test Name	NIPMAM: NIPAM Ratio	Microgel VPTT	Change in Microgel Effective Diameter (nm)	
			From 25°C to 37°C	From 37°C to 43°C
$M_{1.8}$	1.8 : 1	38.6°C	-620 ± 120*	-591 ± 41*
M_1	1 : 1	37.9°C	-429 ± 57*	-248 ± 25^^
$M_{0.56b}$^	0.56 : 1	36.2°C	-1202 ± 112*	-272 ± 26
$M_{0.27}$	0.27 : 1	35.6°C	-1000 ± 30*	-135 ± 18*

^$M_{0.56a}$ has a VPTT of 36.5°C.
^^ This size difference is based on the size of M_1 at 40°C instead of 43°C because the microgels aggregated before 43°C. The difference in size experienced by the microgels in the composite (where aggregation would not occur) is likely higher than this reported value.

Figure 5.11 shows that on the first day, AMF pulsing produces increases in release rate in all composites that are not statistically different from each other. Data from all subsequent days shows that application of the AMF results in a more significant increase in release rates for composites made with the $M_{1.8}$ and M_1 microgels (which have VPTT values above 37°C)

compared to the composites made with $M_{0.56b}$ and $M_{0.27}$ microgels (which have VPTT values below 37°C). This VPTT behaviour is illustrated in Figure 4.3, which shows that $M_{0.56b}$ and $M_{0.27}$ microgels are much more collapsed by 37°C compared to $M_{1.8}$ and M_1 microgels. The trend of higher pulsatile response corresponding to VPTTs over 37°C persists on day two, but the $M_{1.8}$ microgels facilitate in statistically significantly higher percent increase in release rate over the M_1 microgels on days 3 and 5. Although using $M_{0.56b}$ microgels appears to produce a slightly higher percent increase in release rate over the $M_{0.27}$ microgels, this difference is not statistically significant on any day. It is also worth noting that negligible pulsatile behaviour was observed from the $M_{0.56b}$ and $M_{0.27}$ microgel-containing composites on day five.

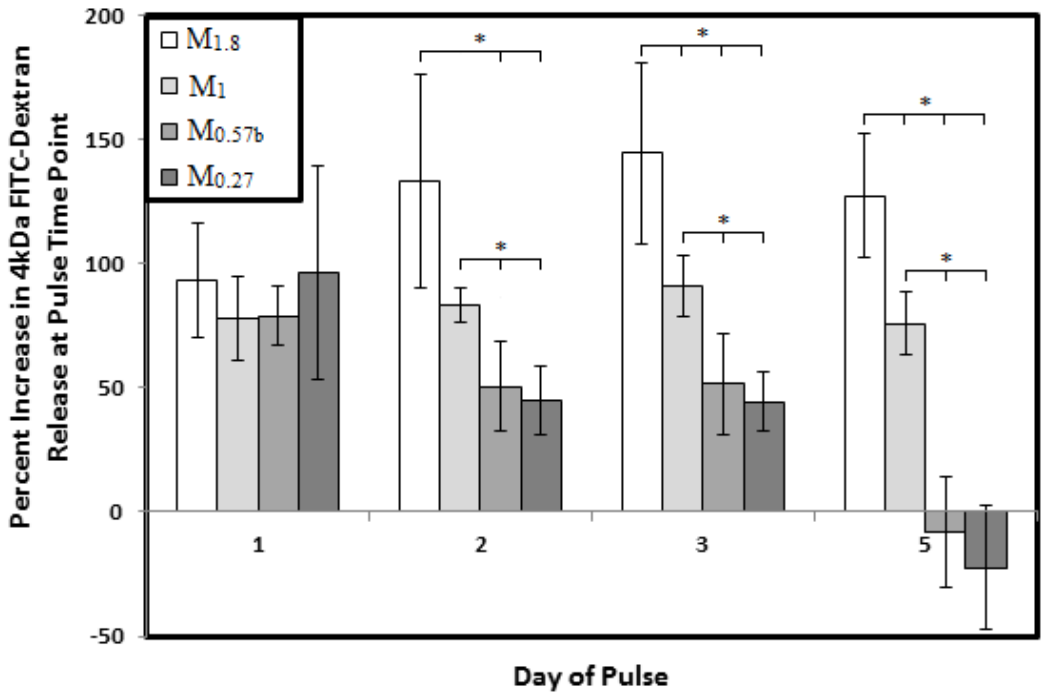

Figure 5.11: Percent increase in 4kDa FITC-Dex release rate observed from composites made with microgels with different VPTTs due to exposure to an alternating magnetic field. * indicates statistical significance (p=0.05).

Table 5.9 lists the excess mass of 4 kDa FITC-Dex released over the course of the pulses. $M_{1.8}$ composites do appear to release more 4 kDa FITC-Dex over the course of the pulses compared to M_1 composites as well, but unlike the percent increases in 4kDa FITC-Dex release rate the extra mass of 4 kDa FITC-Dex released over the course of the pulse is not statistically different from the M_1 recipe composites. The $M_{1.8}$ and M_1 recipe composites do exhibit a statistically higher mass of drug released over the course of the AMF pulses compared to the $M_{0.56b}$ and $M_{0.27}$ composites on days two, three and five. A higher mass of 4 kDa FITC-Dex also appears to be released from the $M_{0.56b}$ composites compared the M_1 composites, although this difference is only statistically significant on day three.

Table 5.9: Excess 4kDa FITC-Dex released over the duration of the magnetic pulse for composites made with microgels with different VPTTs.

	Extra Drug Released During Pulses (µg)			
Test Name	Day 1	Day 2	Day 3	Day 5
$M_{1.8}$	21 ± 5	0.42 ± 0.07	0.13 ± 0.04	0.022 ± 0.003
M_1	18 ± 2	0.35 ± 0.02	0.10 ± 0.01	0.024 ± 0.004
$M_{0.56b}$	20 ± 2	0.10 ± 0.02	0.018 ± 0.008	-0.025 ± 0.03
$M_{0.27}$	14 ± 5	0.07 ± 0.04	0.003 ±0.0005	-0.04 ± 0.05

5.5.2 Cumulative Release

The relative decreases in microgel effective diameter between 25°C (approximately the temperature at which the gels are fabricated) and 37°C (the temperature at which the cumulative release was observed for) is shown in Table 5.8. The decreases in size are all statistically different from each (p=0.05).

Burst release from the composites is shown in Figure 5.12 The burst release appears to be higher for the composites made with microgels that have lower VPTTs (i.e. have deswollen

more by 37°C), although the burst release from the M_1 composite is the only profile that is statistically significant (i.e. lower) from the other microgels over the entire 5 day test (see Table 5.10). The burst release curves also appear to be higher for composites that experience a higher absolute decrease in particle diameter between 25°C and 37°C ($M_{0.56} > M_{0.27} > M_{1.8} > M_1$, see Table 5.8).

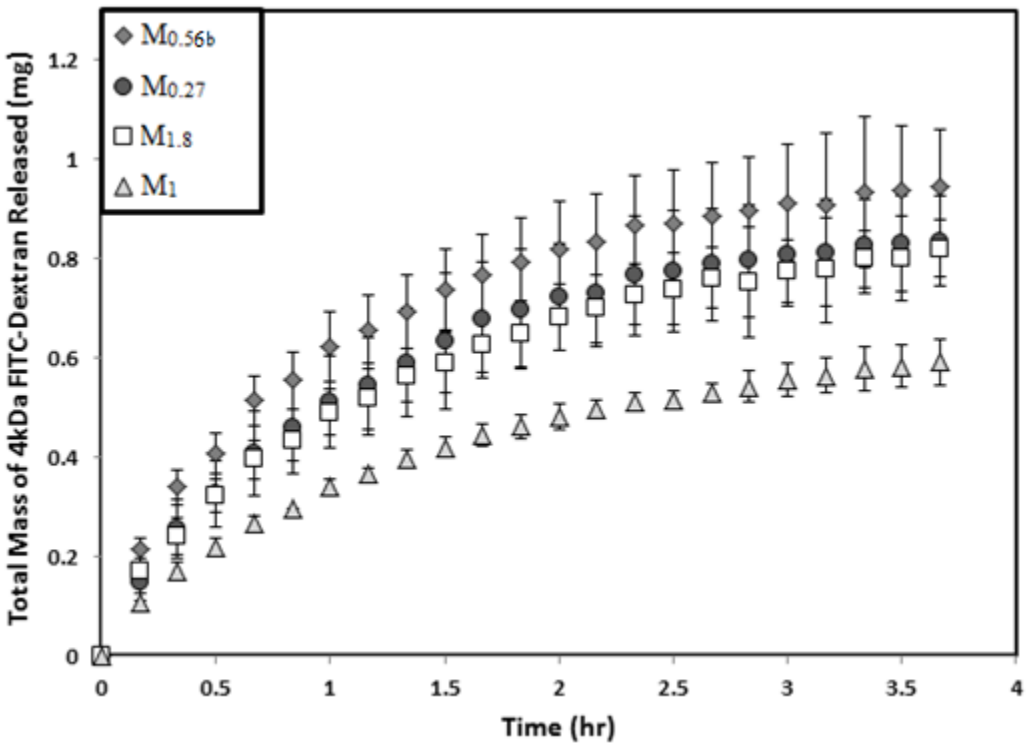

Figure 5.12: Initial burst release of 4kDa FITC-Dex (in the absence of a magnetic pulse-diffusion only) from composites made with microgels with different VPTTs.

Table 5.10: Cumulative release from composites made with microgels with different VPTTs (not exposed to a magnetic pulse – release by diffusion alone) over five days of testing.

Test Name	**Total Mass of 4 kDa FITC-Dex Released** After 1 hr (mg)	After 4 hr (mg)	After 24 hr (mg)	After 48 hr (mg)	After 96 hr (mg)
M_1	0.34± 0.01	0.59 ± 0.05	0.76 ± 0.08	0.78 ± 0.08	0.80 ± 0.04
$M_{1.8}$	0.49 ± 0.05	0.82 ± 0.06	1.03 ± 0.10	1.06 ± 0.10	1.07 ± 0.09
$M_{0.27}$	0.51± 0.09	0.83± 0.09	0.93 ± 0.8	0.95 ± 0.07	0.96 ± 0.07
$M_{0.57b}$	0.62± 0.03	0.95 ± 0.09	1.32 ± 0.14	1.06 ± 0.10	1.07 ± 0.08

5.5.3 Discussion

The proposed mechanism responsible for the differences in the pulsatile behaviours of the composites made with microgels with different VPTTs is illustrated in Figure 5.13. In short, composites with higher VPTT microgels would be expected to exhibit more pronounced pulsatile release because the difference between their baseline state (37°C, microgels slightly deswollen) and their activated state (43°C, microgels completely deswollen) is greater than for a composite containing a microgel that had collapsed to a greater degree before the magnetic induction was started.

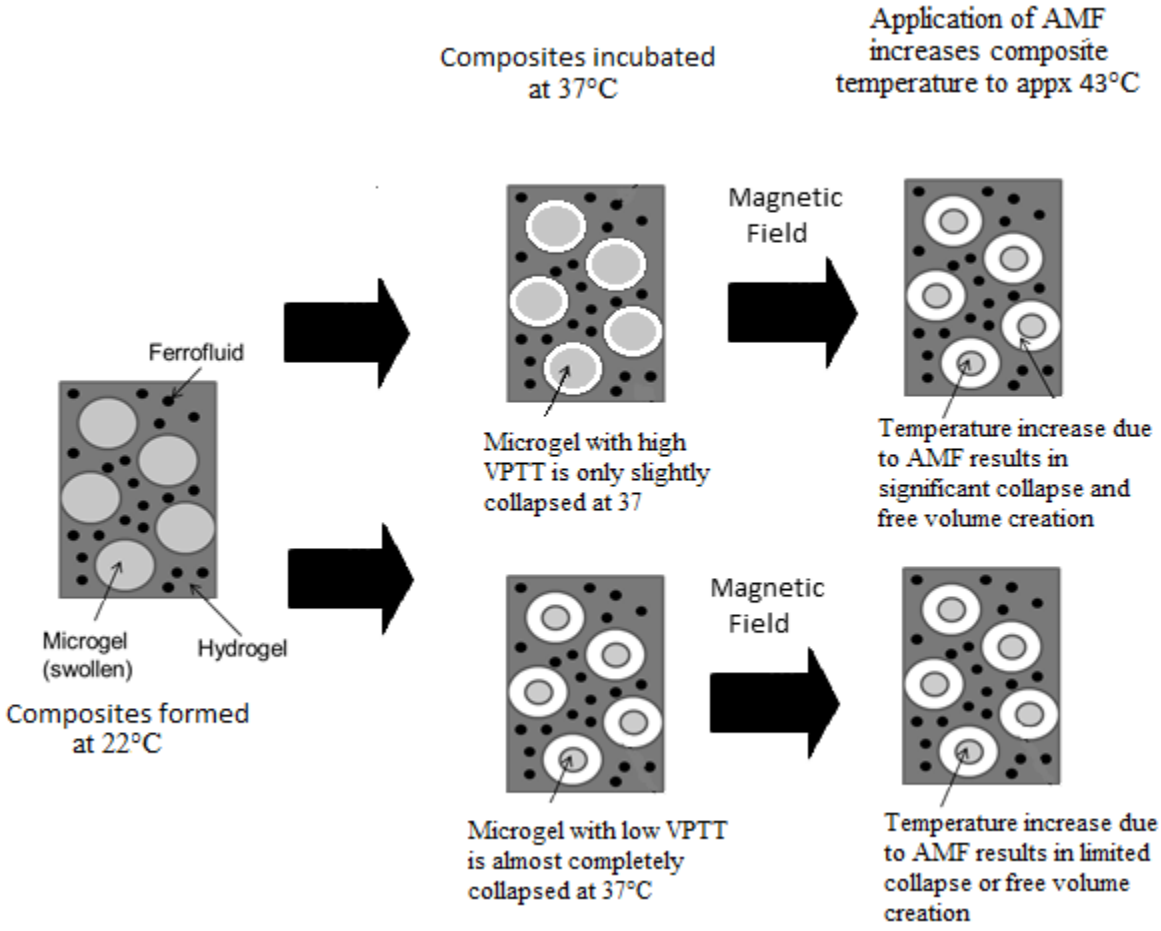

Figure 5.13: Schematic of proposed magnetic hydrogel-microgel nanocomposite structure before and after magnetic pulsing for composites with microgels with different VPTT behaviours.

This explanation is supported by the data which shows that composites made with microgels with VPTTs that are higher than the baseline incubation temperature of 37°C ($M_{1.8}$ and M_1 composites) have significantly higher pulsatile release (in terms of both the mass of drug released upon magnetic induction and the percent increase in release rate observed relative to the diffusion-only baseline) compared to the microgels with VPTTs that are below the incubation temperature ($M_{0.56b}$ and $M_{0.27}$ composites). It also helps to explain the cumulative release data. Burst release appears to be lower for composites made with microgels that have deswollen less between fabrication (at 22°C and incubation at 37°C). For example, the composites made with $M_{0.56b}$ microgels (which decrease in diameter by 1,202 ± 112 nm between 22°C and 37°C) exhibit much more release over the course of the first few days of testing than the M_1 microgels (which decrease in diameter by 429 ± 57nm between 22°C and 37°C) likely due to the fact that the free volume pore network created in the $M_{0.56b}$ composites upon incubation at 37°C is significantly greater than that created in the M_1 composites.

These results suggest that the burst release and pulsatile release could be independently controlled by varying initial microgel size and microgel VPTT.

5.6 Effect of Microgel Content on Drug Release

Composites were fabricated with 0 – 10 wt% microgel content using $M_{1.8}$ microgels. All composites contained 8 wt% hydrogel (100% dextran-aldehyde for the B component), 5 wt% PEG-SPIONs, 1 wt% 4 kDa FITC-Dextran and were incubated at 37°C (x$M_{1.8}$- PEG FF-8H 100 Dex-T37, where x is 10, 8, 6, or 4). We hypothesize that higher microgel contents will lead to higher pulsatile release responses. Figure 5.14 and Table 5.11 describe the pulsatile release of 4

kDa FITC-Dex from the composites while Figure 5.15 and Table 5.12 describe the burst and cumulative of 4 kDa FITC-Dex release.

5.6.1 Pulsatile Release

Figure 5.14 shows that on the first day, AMF pulsing produces increases in release rate in all composites that are not statistically different from each other. Data from all subsequent days suggests that application of the AMF results in a larger percent increase in release rates for composites containing with a higher microgel content. The percent increase in release rate is statistically significant between all composites on day two. This difference persists on day three, although the difference in percent increase in release rate for the $8M_{1.8}$ and $6M_{1.8}$ composites is not statistically significant. On day five, there is no statistical difference observed in the pulsatile behaviour between the $10M_{1.8}$, $8M_{1.8}$, and $6M_{1.8}$ composites, however the percent increase in release rate for the $10M_{1.8}$ and $8M_{1.8}$ composites is still significantly higher than from the $4M_{1.8}$ composite. The pulsatile release from $0M_{1.8}$ composites (microgel free composites previously referred to as 0M-PEG FF) are included in Figure 5.14. There is no statistical difference ($p<0.05$) between the $0M_{1.8}$ and any other microgel content composite on day one. One days two and three, pulsatile release from the $0M_{1.8}$ is not statistically different from zero or from the $4M_{1.8}$ or $6M_{1.8}$ composites.

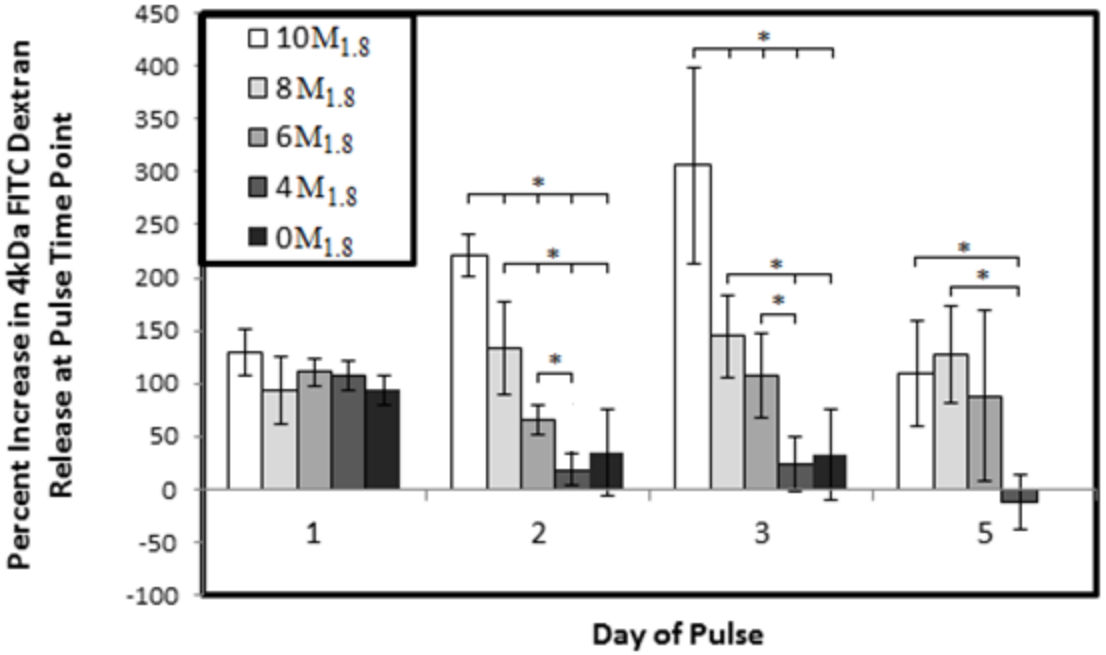

Figure 5.14: Percent increase in 4kDa FITC-Dex release rate observed from composites made with different microgel contents due to exposure to an alternating magnetic field. * indicates statistical significance (p=0.05).

Composites with higher microgel contents appear to release more 4 kDa FITC-Dex over the course of the pulses as well, as shown in Table 5.11. However, unlike the percent increases in FITC-release rate, the mass of 4 kDa FITC-Dex released (relative to the diffusion-only control) over the course of the pulse is not statistically different for the $10M_{1.8}$, 8 $M_{1.8}$ and $6M_{1.8}$ composites after day two. The difference in mass released is not statistically different between $6M_{1.8}$ and $4M_{1.8}$ on day two, but pulsatile release from the $4M_{1.8}$ composites is significantly lower than all composites containing higher microgel contents on days three and five (and indeed indistinguishable from a composite prepared with no microgels at all time points).

Table 5.11: Excess 4kDa FITC-Dex released over the duration of the magnetic pulse for composites made with different microgel contents.

	Extra Drug Released During Pulses (µg)			
Test Name	Day 1	Day 2	Day 3	Day 5
$10M_{1.8}$	25 ± 6	0.71 ± 0.07	0.12 ± 0.03	0.021 ± 0.007
$8M_{1.8}$	21 ± 5	0.42 ± 0.07	0.13 ± 0.05	0.018 ± 0.03
$6M_{1.8}$	27 ± 3	0.28 ± 0.04	0.12 ± 0.04	0.03 ± 0.01
$4M_{1.8}$	21 ± 3	0.22 ± 0.08	0.013 ± 0.004	-0.01 ± 0.02
$0M_{1.8}$	16 ± 3	0.01 ± 0.09	0.01 ± 0.08	NA

5.6.2 Cumulative Release

The burst release from the composites is shown in Figure 5.15. Initially, higher burst release was observed with lower microgel contents (0M- PEG FF from an earlier set of tests is shown for comparison). No difference is initially seen between the $8M_{1.8}$ and $10M_{1.8}$gels, or the $4M_{1.8}$ and $6M_{1.8}$ gels. Statistically ($p<0.05$) there was no difference in the mass of 4 kDa FITC-Dex released from different composites after 24 hours (i.e. the cumulative mass released on days two, three and five were not statistically different for composites with different microgel contents) (see Table 5.12).

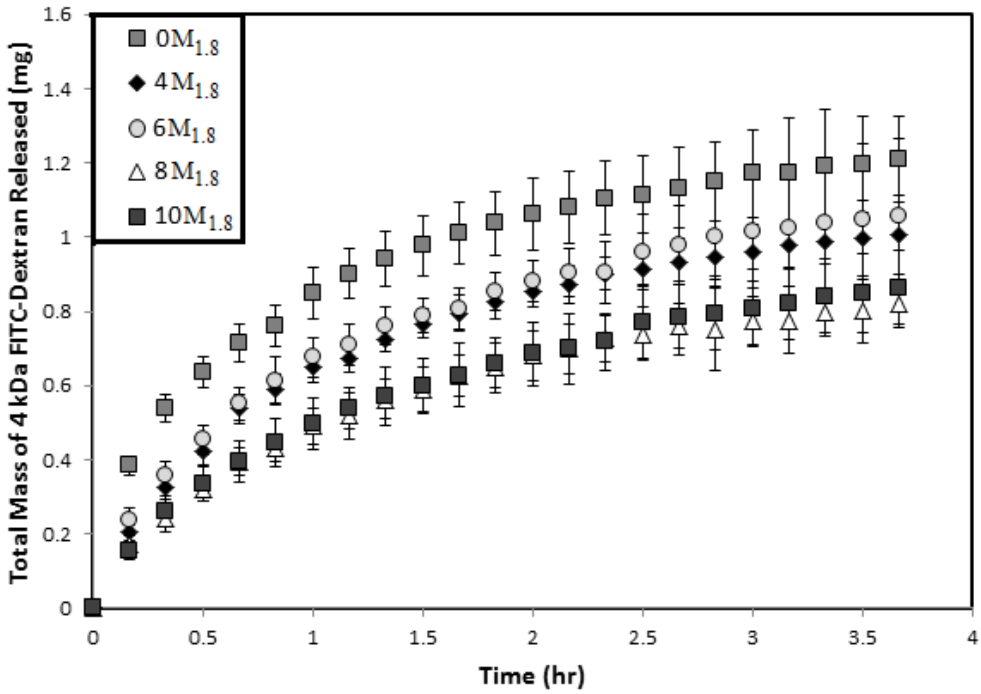

Figure 5.15: Initial burst release (in the absence of a magnetic pulse-diffusion only) of 4kDa FITC-Dex from composites with different microgel contents.

Table 5.12: Cumulative release from composites with different microgel contents (not exposed to a magnetic pulse – release by diffusion alone) over five days of testing. All samples marked NA were not possible to measure due to gel degradation at this time point

	Total Mass of 4 kDa FITC-Dex Released				
Test Name	After 1 hr (mg)	After 4 hr (mg)	After 24 hr (mg)	After 48 hr (mg)	After 96 hr (mg)
$10M_{1.8}$	0.50 ± 0.07	0.86 ± 0.11	1.02 ± 0.16	1.04 ± 0.07	1.04 ± 0.06
$8M_{1.8}$	0.49 ± 0.05	0.82 ± 0.06	1.03 ± 0.10	1.06 ± 0.10	1.07 ± 0.085
$6M_{1.8}$	0.68± 0.05	1.1± 0.2	1.13 ± 0.08	1.20 ± 0.09	1.24 ± 0.15
$4M_{1.8}$	0.62 ± 0.03	1.06 ± 0.09	1.21 ± 0.06	1.22 ± 0.19	1.23 ± 0.10
$0M_{1.8}$	0.84 ± 0.07	1.21 ± 0.11	1.3 ± 0.1	1.34 ± 0.09	NA

5.6.3 Discussion

Higher microgel content appears to correspond to increased pulsatile release capability in terms of both the extra mass released due to AMF application and the percent increase in release rate. This is expected because higher microgel content would correspond to more free volume

creation upon application of the AMF. Interestingly, there is a significant increase in pulsatile release between 4 wt% microgel and 6 wt% microgel samples, particularly at later days. The volume fraction of microgel in the composite, the volume fraction of the gel that becomes free volume at 37°C and 43°C (according to microgel volume changes) and the increase in free volume fraction due to AMF activation is listed in Table 5.13 (assuming no accommodation to pore network formation by the surrounding hydrogel). It is possible that the 6 wt% microgel (4.2 vol% microgel or 0.8 % change in pore network vol%) represents a critical value in terms of facilitating sufficient free volume for pulsatile release to occur.

Table 5.13: The volume fraction of the composite corresponding to microgel, the volume fraction of the gel that becomes free volume at 37°C and 43°C and the increase in free volume fraction due to AMF activation.

Wt% Microgel	$10M_{1.8}$	$8M_{1.8}$	$6M_{1.8}$	$4M_{1.8}$	$0M_{1.8}$
Vol % Microgel	7.023	5.619	4.214	2.809	0
Vol% Pore Network at 37°C (change between 25°C and 37°C)	5.612	4.489	3.367	2.245	0
Vol% Pore Network at 43°C (change between 25°C and 43°C)	6.953	5.562	4.172	2.781	0
Change in Vol% Pore Network Between 37°C and 43°C	1.341	1.073	0.805	0.537	0

The burst release behaviour of the composites suggests that higher microgel contents correspond to lower initial release of drug. This could be due to the fact that compared to the bulk hydrogel phase, the microgel phase has a higher density and thus higher resistance to drug diffusion, with higher microgel content composites having an extra barrier to release. The slowed release could also be due to the fact that initially, higher microgel content composites experience more swelling, as shown in Figure 4.12. More swelling could result in occlusion of the pore

network created due to the partial collapse of the microgels at 37°C. The higher swelling experienced by the composites could also explain why the pulsatile release behaviour observed on day one is lower on a percentage basis and no statistical difference in release is observed based on microgel content: the swelling of the composites limits pulsatile release from all composites, but is more limiting to higher microgel contents that experience more swelling. The impact of composite swelling on pulsatile release and burst release behaviour is discussed in more detail in Section 5.7.

5.7 Effect of Hydrogel Swelling on Drug Release

Composites were fabricated with varying CMC-aldehyde contents to control bulk hydrogel swelling and to determine the effect of bulk composite swelling behaviour on pulsatile release. All composites contained 6wt% hydrogel (0-100% CMC-aldehyde for the B component), 6 wt% $M_{1.8}$ microgel, 5 wt% PEG-SPIONs, 1 wt% 4 kDa FITC-Dextran and were incubated at 37°C (8$M_{1.8}$- PEG FF-8H x CMC-T37, where x is 100, 75, 50, 25 or 0). We hypothesize that hydrogels that neither swell nor deswell as a function of time will facilitate improved pulsatile release behaviour due to their improved ability to preserve the free volume created upon microgel collapse. Figure 5.16 and Table 5.14 describe the pulsatile release of 4 kDa FITC-Dex from the composites while Figure 5.17 and Table 5.15 describe the burst and cumulative release of 4 kDa FITC-Dex.

5.7.1 Pulsatile Release

Figure 5.16 shows that on the first day, AMF pulsing facilitates increases in the observed release rate in all composites tested, with composites that swell less experiencing significantly

higher percent increases in release rate. Specifically, the percent increases in release rate for the 0 CMC and 25 CMC composites were statistically higher than the 100, 75 and 50 CMC composites ($p<0.05$). Similarly, on day two, the percent increases in release rate for the 0 and 25 CMC composites were not statistically different from each other but were higher than 100, 75 and 50 CMC composites. On day three, the percent increases in release rate for the 0 CMC composite is lower than the 25 CMC composites. The percent increases in release rate for the 25 and 50 CMC composites are not statistically different from each other but are significantly higher than those from the 75 and 100 CMC composites on day 3. On day five, the percent increases in release rate are highest for the 25 CMC composites. The 50 and 0 CMC composites also exhibit statistically significant percent increases in release rate (although there is no statistical difference between the two) while negligible pulsatile behaviour was observed from the 100 and 75 CMC composites on day five.

Composites that swell significantly (especially 100, 75 and 50 CMC) or deswell significantly (0 CMC on days 2-5) (see Figure 4.15 for swelling data) appear to release less 4 kDa FITC-Dex over the course of the pulses, as shown in Table 5.14. On day one, the excess mass of 4 kDa FITC-Dex released over the course of the pulse is not statistically different for the 50, 75 or 100 CMC composites but the excess release from the 0 and 25 CMC composites is significantly higher ($p<0.05$). On days 2-5, the excess drug released from the 25 and 50 CMC composites is higher than for the 0, 75 or 100 CMC composites (although statistical difference is not seen on day two between 25 and 0 CMC composites).

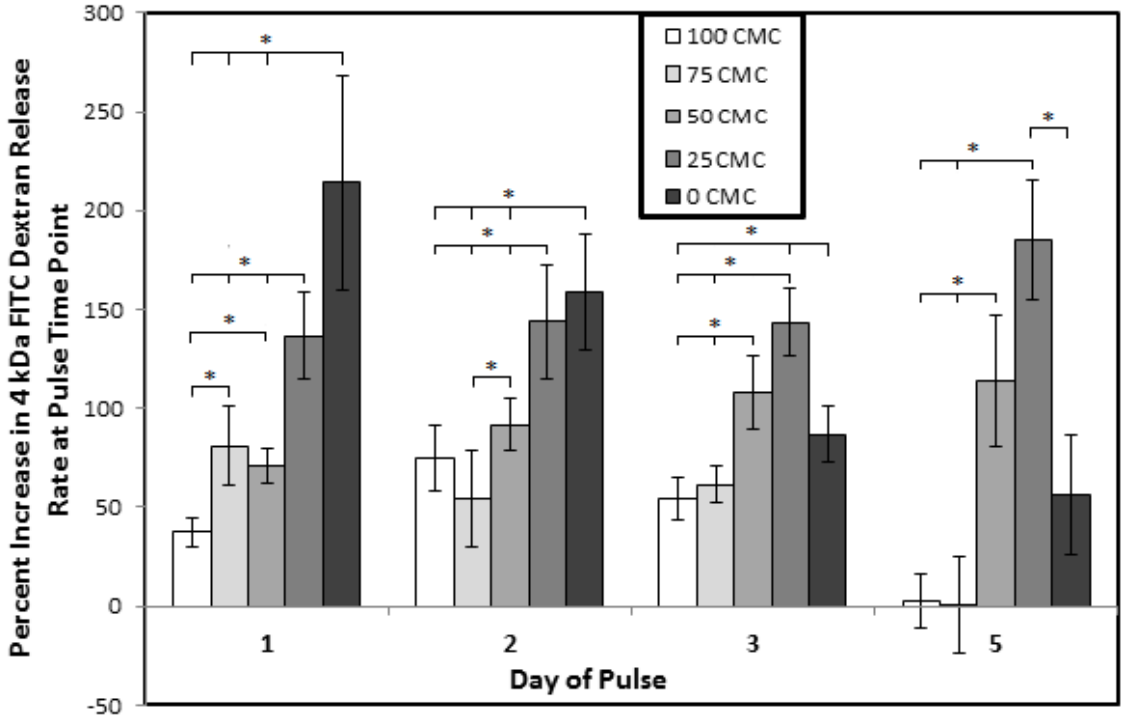

Figure 5.16: Percent increase in 4kDa FITC-Dex release rate observed from composites with different swelling profiles due to exposure to an alternating magnetic field. * indicates statistical significance (p=0.05).

Table 5.14: Excess 4kDa FITC-Dex released over the duration of the magnetic pulse for composites with different swelling behaviours.

	Extra Drug Released During Pulses (µg)			
Test Name	Day 1	Day 2	Day 3	Day 5
100 CMC	15 ± 1	0.29 ± 0.08	0.049 ±0.014	-0.041 ± 0.07
75 CMC	15 ± 4	0.28 ± 0.11	0.034 ±0.006	-0.024 ± 0.05
50 CMC	15 ± 2	0.58 ± 0.09	0.16 ±0.02	0.074 ± 0.018
25 CMC	41 ± 5	0.57 ± 0.12	0.19 ±0.02	0.098± 0.017
0 CMC	36 ± 9	0.38 ± 0.1	0.04 ±0.01	0.029 ± 0.014

5.7.2 Cumulative Release

The burst release from the composites is shown in Figure 5.17. Initially, higher burst release was observed from composites that experienced less swelling (0, 25 and 50 CMC composites). Statistically ($p<0.05$) there was no difference in the mass of 4 kDa FITC-Dex released from different composites after 24 hours (i.e. the cumulative mass released on days two, three and five were not statistically different for 25, 50, 75 or 100 CMC) with the exception of the deswollen 0 CMC composites, which release less than all other composites over the course of the five day test (see Table 5.15).

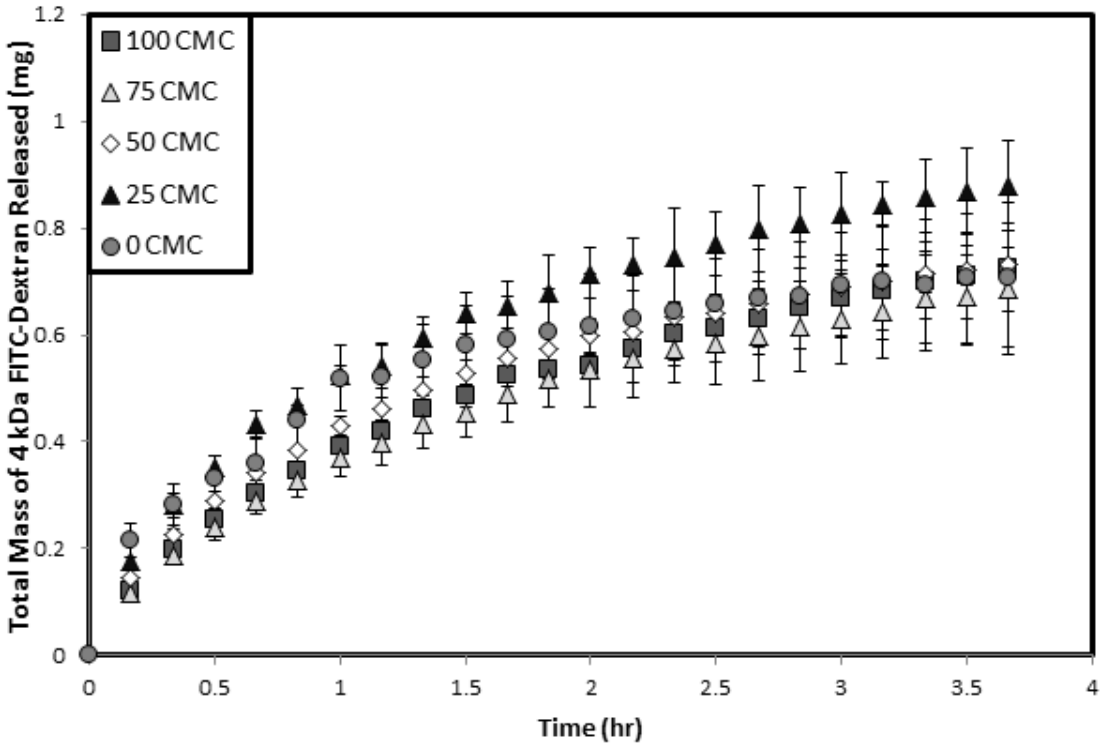

Figure 5.17: Initial burst release of 4kDa FITC-Dex (in the absence of a magnetic pulse-diffusion only) from composites with different swelling behaviours.

Table 5.15: Cumulative release of 4 kDa FITC-Dex from composites with different swelling profiles (not exposed to a magnetic pulse – release by diffusion alone) over the first 24 hours of testing.

Test Name	**Total Mass of 4 kDa FITC-Dex Released** After 1 hr (mg)	After 4 hr (mg)	After 24 hr (mg)	After 48 hr (mg)	After 96 hr (mg)
100 CMC	0.39 ± 0.01	0.73 ± 0.08	0.93 ± 0.8	0.96 ± 0.08	0.97 ± 0.04
75 CMC	0.37± 0.03	0.69 ± 0.11	0.90 ± 0.11	0.94 ± 0.06	0.96 ± 0.05
50 CMC	0.43± 0.02	0.73 ± 0.03	0.90 ± 0.09	0.94 ± 0.04	0.95 ± 0.05
25 CMC	0.53± 0.02	0.88± 0.09	0.93 ± 0.8	1.10 ± 0.04	1.11 ± 0.08
0 CMC	0.51 ± 0.06	0.71 ± 0.12	0.77 ± 0.04	0.80 ± 0.06	0.81 ± 0.07

5.7.3 Discussion

The proposed mechanism responsible for the differences in the pulsatile release behaviour of the composites made with different amounts of CMC-aldehyde to control swelling behaviour is shown in Figure 5.18. In short, if the bulk hydrogel swells significantly upon incubation at 37°C, pulsatile release is limited because the bulk hydrogel matrix swells to occlude any pore network created by microgel deswelling (both at 37°C and 43°C after magnetic induction). Pulsatile release is similarly limited for composites if their bulk hydrogel matrix deswells, in which the free volume created also be consumed in this case by the collapse of the surrounding network into the free volume created. Optimum pulsatile release is observed for composites with limited or no swelling or deswelling behaviour.

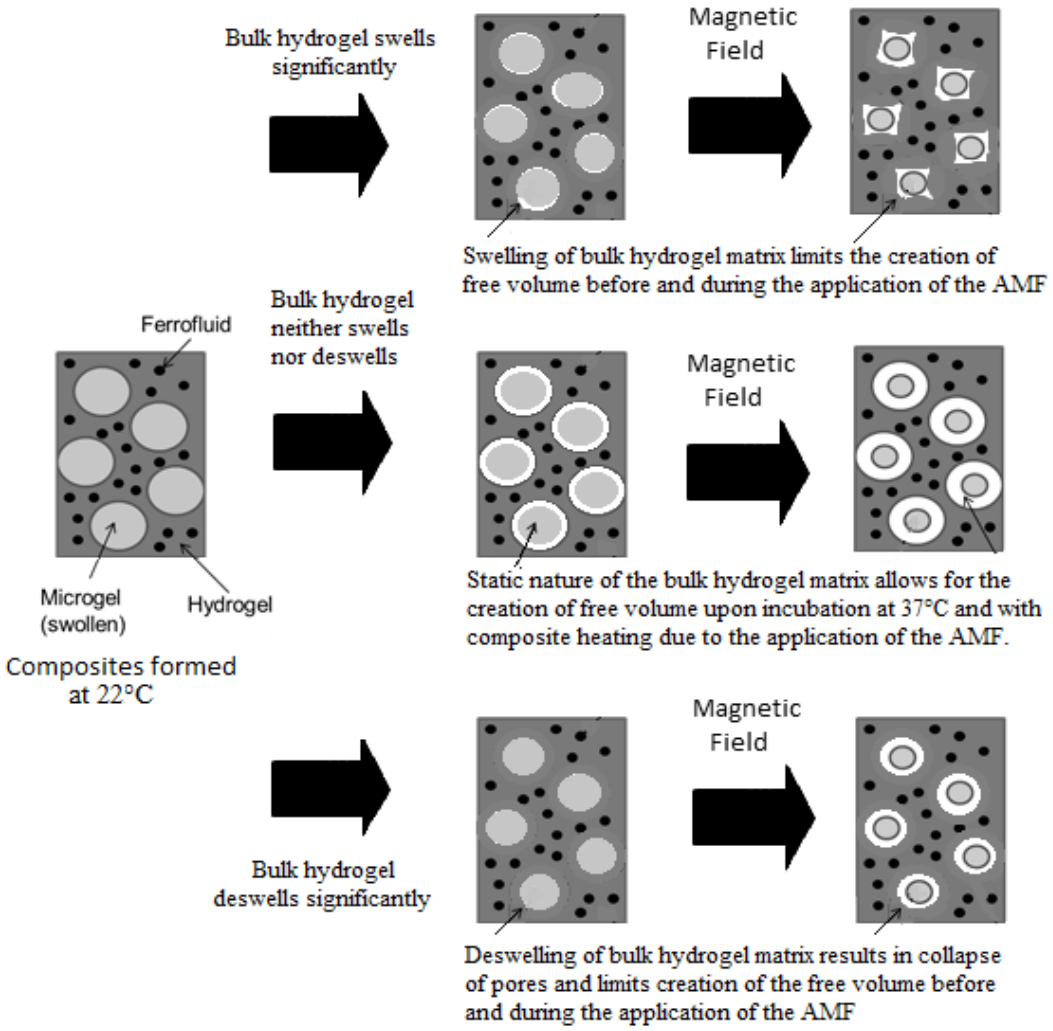

Figure 5.18: Schematic of proposed magnetic hydrogel-microgel nanocomposite structure before and after magnetic pulsing for composites with different swelling behaviours.

This explanation is supported by the data which shows that composites which experience the closest to zero swelling in the bulk hydrogel phase exhibit improved pulsatile release both in terms of the extra mass released and the percent increase in release rate due to AMF application. By the third day of testing, the composite that initially showed zero net swelling (0 CMC) has deswelled significantly, while the initially swollen 25 CMC has zero net swelling (see Figure

4.15). This switch in swelling characteristics corresponds to a switch in pulsatile release behaviour, by which both the excess mass released (relative to the diffusion-only baseline) and the percent increase in release rate due to AMF application to the 25 CMC composites become higher than that achieved with the 0 CMC composites.

As mentioned in previous sections, this mechanism also helps explain why pulsatile release behaviour is not significantly different on the first day of testing for several comparative release tests (for example for composites pulsed at 37°C vs 43°C or composites with different microgel contents). These composites swell initially on the first day, which would limit the formation of the pore network (i.e. free volume) upon microgel collapse and thus limit the magnitude of pulsatile release observed.

The initial burst release of drug from the composites also seems to support this mechanism, with composites exhibiting little to no swelling (i.e. 0 CMC and 25 CMC) initially releasing more drug compared to the composites that demonstrate higher initial swelling, likely due to occlusion of the pore network by swollen hydrogel matrix (and/or actual compression of the microgels in the case of the highly swelling CMC-rich hydrogels). By the end of the first day of testing, there is no further statistical difference in the cumulative mass of drug released (i.e. the highly swelling CMC-rich composites catch up to the less swelling dextran-rich composites in terms of total release). This observation can be attributed to the lower resistance to diffusion facilitated by the swollen hydrogel networks, resulting in a higher baseline release rate from the swollen composites versus the unswollen or deswollen networks after the initial burst release subsides.

Chapter 6: Conclusions and Recommendations

By embedding magnetic nanoparticles and temperature-sensitive microgels into a hydrogel matrix, pulsatile drug release can be achieved with the application of a highly penetrative but non-invasive alternating magnetic field.

Incorporation of p(NIPAM-NIPMAM) microgels into the composites improves pulsatile release by providing a barrier to diffusion that is removed upon thermal collapse of the particles with heating caused by the AMF. This was true for networks with SPIONs physically entrapped within them as well as networks in which the SPION was integrated directly into the hydrogel structure.

The volume phase transition temperature of p(NIPAM-NIPMAM) microgels can be controlled by modifying the NIPAM: NIPMAM ratio, with more NIPMAM corresponding to higher microgel VPTTs. By tailoring microgel VPTT to be greater than 37°C, improved pulsatile behaviour can be achieved. Bulk release of drug can also be controlled by limiting the magnitude of microgel deswelling between the incubation temperature and fabrication temperature. Limiting initial microgel collapse corresponds to the creation of a lower volume fraction pore network when the microgels collapse between the temperature of fabrication and the temperature of incubation, leading to less burst release of drug. Higher microgel content also results in higher pulsatile release.

Pulsatile and burst release from composites can be controlled by modifying the bulk hydrogel swelling properties. Composites that experience little to no swelling exhibit better pulsatile release while composites that swell or collapse significantly exhibit a lower burst release, but also exhibit less pulsatile release behaviour.

The chemistry used to prepare the bulk hydrogel allows for the composite to be injected, unlike previous devices which would require surgical implantation. All composite precursors exhibit limited cytotoxicity, which suggests this composite would be a viable vehicle for *in vivo* drug delivery.

Further development of these materials would aim to minimize drug diffusion from the composite in the absence of the AMF. This could be accomplished by better controlling initial microgel size (i.e. to limit the magnitude of microgel collapse between 25°C and 37°C) by manipulating the comonomer ratio in the microgels or by increasing resistance to diffusion in the hydrogel phase (i.e. by using higher weight percent hydrogel or more functionalized pre-polymers to increase crosslink density). Further investigating the effect of pulse duration, SPION concentration, drug size and the hydrogel crosslinking density on pulsatile release could lead to better control over the pulsatile drug release kinetics.

References

Andhariya, N., B. Chudasama, R. V. Mehta, and R. V. Upadhyay. 2011. "Biodegradable thermoresponsive polymeric magnetic nanoparticles: a new drug delivery platform for doxorubicin." *Journal of Nanoparticle Research* no. 13:1677-1688.

Aqil, A., S. Vasseur, E. Duguet, C. Passirani, J. P. Benoit, A. Roch, R. Muller, R. Jerome, and C. Jerome. 2008. "PEO coated magnetic nanoparticles for biomedical application." *European Polymer Journal* no. 44:3191-3199.

Ashley, G. W., J. Henise, R. Reid, and D. V. Santi. 2013. "Hydrogel drug delivery system with predictable and tunable drug release and degradation rates." *Proc Natl Acad Sci U S A* no. 110 (6):2318-23.

Asmarandei, I., G. Fundueanu, M. Cristea, V. Harabagiu, and M. Constantin. 2013. "Thermo- and pH-sensitive interpenetrating poly(N isopropylacrylamide)/carboxymethyl pullulan network for drug delivery." *J Polym Res* no. 2013 (20):293-306.

Babes, L., B. Denizot, G. Tanguy, J. J. Le Jeune, and P. Jallet. 1999. "Synthesis of Iron Oxide Nanoparticles Used as MRI Contrast Agents: A Parametric Study." *J Colloid Interface Sci* no. 212 (2):474-482.

Bachelet-Violette, L., A. K. A. Silva, M. Maire, A. Michel, O. Brinza, P. Ou, V. Ollivier, A. Nicoletti, C. Wilhelm, D. Letourneur, C. Menager, and F. Chaubet. 2014. "Strong and specific interaction of ultra small superparamagnetic iron oxide nanoparticles and human activated platelets mediated by fucoidan coating." *RSC Advances* no. 4:4864-4871.

Barbucci, R., A. Magnani, and M. Consumi. 2000. "Swelling behaviour of carboxymethylcellulose hydrogels in relation to cross-linking, pH and charge density." *Macromolecules* no. 33 (20):7475-7480.

Bean, C. P., and J. D. Livingston. 1959. "Superparamagnetism." *J. Appl. Phys* no. 30 (4):S120-S129.

Boistelle, R., and J. P. Astier. 1988. "Chrystallization mechanisms in solution." *Journal of Crystal Growth* no. 90:14-30.

Borek, F. 1961. "The fluorescent antibody method in medical and biological research." *Bull World Health Organ* no. 24 (2):249-56.

Brandl, F., F. Kastner, R. M. Gschwind, T. Blunk, J. Tessmar, and A. Gopferich. 2010. "Hydrogel-based drug delivery systems: comparison of drug diffusivity and release kinetics." *J Control Release* no. 142 (2):221-8.

Brazel, C. S. 2009. "Magnetothermally-responsive nanomaterials: combining magnetic nanostructures and thermally-sensitive polymers for triggered drug release." *Pharm Res* no. 26 (3):644-56.

Campardelli, R., G. Della Porta, L. Gomez, S. Irusta, E. Reverchon, and J. Santamaria. 2014. "Au-PLA nanocomposites for photothermally controlled drug delivery." *Journal of Materials Chemistry B* no. 2:409-417.

Campbell, S. B., M. Patenaude, and T. Hoare. 2013. "Injectable superparamagnets: highly elastic and degradable poly(N-isopropylacrylamide)-superparamagnetic iron oxide nanoparticle (SPION) composite hydrogels." *Biomacromolecules* no. 14 (3):644-53.

Chen, L., X. Fan, G. Jin, X. Wang, R. Qiu, G. Yi, Y. You, and Q. Xu. 2014. "Treatment of Rat with Traumatic Brain Injury and MR Tracing In Vivo via Combined Transplantation of Bone Marrow Stromal Cells Labeled with Superparamagnetic Iron Oxide and Schwann Cells." *Journal of Biomedical Nanotechnology* no. 10 (2):205-215.

Chin, A. B., and I. I. Yaacob. 2007. "Synthesis and characterization of magnetic iron oxide nanoparticles via w/o microemulsion and Massart's procedure." *Journal of Materials Processing Technology* no. 19:235-237.

Chiu, H. C., G. H. Hsiue, Y. P. Lee, and L. W. Huang. 1999. "Synthesis and characterization of pH-sensitive dextran hydrogels as a potential colon-specific drug delivery system." *J Biomater Sci Polym Ed* no. 10 (5):591-608.

Coons, A. H. 1958. "Fluorescent antibody methods." *Gen Cytochem Methods* no. 1:399-422.

Crangle, J. 1991. *Solid State Magnetism*. New York: Van Nostrand Reinhold.

Crompton, K. E., R. J. Prankerd, D. M. Paganin, T. F. Scott, M. K. Horne, D. I. Finkelstein, K. A. Gross, and J. S. Forsythe. 2005. "Morphology and gelation of thermosensitive chitosan hydrogels." *Biophys Chem* no. 117 (1):47-53.

del Monte, F., M. P. Morales, D. Levy, A. Fernandez, M. Ocana, A. Roig, E. Molins, K. O'Grady, and C.J. Serna. 1997. "Formation of ç-Fe2O3 Isolated Nanoparticles in a Silica Matrix." *Langmuir* no. 13 (14):3627-3634.

Demirel, G. B., and R. von Klitzing. 2013. "A new multiresponsive drug delivery system using smart nanogels." *Chemphyschem* no. 14 (12):2833-40.

Derjaguin, B.V., and L. D. Landau. 1941. "The theory of stability of highly charged lyophobic sols and coalescence of highly charged particles in electrolyte solutions." *Acta Physicochim. URSS* no. 14:633.

Du, B., A. Mei, P. Tao, B. Zhao, Z. Cao, J. Nie, J. Xu, and Z. Fan. 2009. "Poly[N-isopropylacrylamide-co-3-(trimethoxysilyl)-propylmethacrylate] Coated Aqueous Dispersed Thermosensitive Fe3O4 Nanoparticles." *J. Phys. Chem. C* no. 113:10090-10096.

Fu, Y., and W. J. Kao. 2011. "In situ forming poly(ethylene glycol)-based hydrogels via thiol-maleimide Michael-type addition." *J Biomed Mater Res A* no. 98 (2):201-11.

Fundueanu, G., M. Constantin, I. Asmarandei, S. Bucatariu, V. Harabagiu, P. Ascenzi, and B. C. Simionescu. 2013. "Poly(N-isopropylacrylamide-co-hydroxyethylacrylamide) thermosensitive microspheres: the size of microgels dictates the pulsatile release mechanism." *Eur J Pharm Biopharm* no. 85 (3 Pt A):614-23.

Gribanov, N. M., E. E. Bibik, O. V. Buzunov, and V. N. Naumov. 1990. "Physico-chemical regularities of obtaining highly dispersed magnetite by the method of chemical condensation." *Journal of Magnetism and Magnetic Materials* no. 85:7-10.

Hawkins, A. M., N. S. Satarkar, and J. Z. Hilt. 2009. "Nanocomposite degradable hydrogels: demonstration of remote controlled degradation and drug release." *Pharm Res* no. 26 (3):667-73.

Hertle, Y., and T. Hellweg. 2013. "Thermoresponsive copolymer microgels." *Journal of Materials Chemistry B* no. 1 (43):5874-5885.

Hoare, T., and D. S. Kohane. 2008. "Hydrogels in drug delivery: progress and challenges." *Polymer* no. 49:1993-2007.

Hoare, T., and R. Pelton. 2004. "Functional group distributions in carboxylic acid containing poly(N-isopropylacrylamide) microgels." *Langmuir* no. 20 (6):2123-33.

Hoare, T., and R. Pelton. 2007a. "Calorimetric analysis of thermal phase transitions in functionalized microgels." *J Phys Chem B* no. 111 (6):1334-42.

Hoare, T., and R. Pelton. 2007b. "Engineering glucose swelling responses in poly(N-isopropylacrylamide)-based microgels." *Macromolecules* no. 40 (3):670-678.

Hoare, T., and R. Pelton. 2008. "Charge-switching, amphoteric glucose-responsive microgels with physiological swelling activity." *Biomacromolecules* no. 9 (2):733-40.

Hoare, T., J. Santamaria, G. F. Goya, S. Irusta, D. Lin, S. Lau, R. Padera, R. Langer, and D. S. Kohane. 2009. "A magnetically triggered composite membrane for on-demand drug delivery." *Nano Lett* no. 9 (10):3651-7.

Hoare, T., D. Sivakumaran, C. F. Stefanescu, M. W. Lawlor, and D. S. Kohane. 2012. "Nanogel scavengers for drugs: local anesthetic uptake by thermoresponsive nanogels." *Acta Biomater* no. 8 (4):1450-8.

Hoare, T., B. P. Timko, J. Santamaria, G. F. Goya, S. Irusta, S. Lau, C. F. Stefanescu, D. Lin, R. Langer, and D. S. Kohane. 2011. "Magnetically triggered nanocomposite membranes: a versatile platform for triggered drug release." *Nano Lett* no. 11 (3):1395-400.

Hoare, T., S. Young, M. W. Lawlor, and D. S. Kohane. 2012. "Thermoresponsive nanogels for prolonged duration local anesthesia." *Acta Biomater* no. 8 (10):3596-605.

Hobbs, S. K., W. L. Monsky, F. Yuan, W. G. Roberts, L. Griffith, V. P. Torchilin, and R. K. Jain. 1998. "Regulation of transport pathways in tumor vessels: role of tumor type and microenvironment." *Proc Natl Acad Sci U S A* no. 95 (8):4607-12.

Hoffman, A.S. 2012. "Hydrogels for biomedical applications." *Advanced Drug Delivery Reviews* no. 64:18-23. doi: 10.1016/j.addr.2012.09.010.

Huang, S.;, J.; Ke, G.; Chen, and L. Wang. 2013. "One-pot synthesis of PDMAEMA-bound iron oxide nanoparticles for magnetofection." *Journal of Materials Chemistry B* no. 1 (43):5916-5924.

Jackson, D. K., S. B. Leeb, A. H. Mitwalli, P. Narvaez, D. Fusco, and E.C. Lupton. 1997. "Power Electronic Drives for Magnetically Triggered Gels." *IEEE TRANSACTIONS ON INDUSTRIAL ELECTRONICS* no. 44 (2):217-225.

Jokerst, J. V., T. Lobovkina, R. N. Zare, and S. S. Gambhir. 2011. "Nanoparticle PEGylation for imaging and therapy." *Nanomedicine (Lond)* no. 6 (4):715-28.

Jordan, A., R. Scholz, R. Wust, H. Schirra, T. Schiestel, G. Schmidt, and R. Felix. 1999. "Endocytosis of dextran and silan-coated magnetite nanoparticles and the effect of intracellular hyperthermia

on human mammary carcinoma cells in vitro." *Journal of Magnetism and Magnetic Materials* no. 194 (3):185-196.

Klaassen, C. D. 2013. *Casarett and Doull's toxicology: the basic science of poisons*. 8th ed. New York: McGraw-Hill Education.

Lak, A., J. Dieckhoff, F. Ludwig, J. M. Scholtyssek, O. Goldmann, H. Lunsdorf, D. Eberbeck, A. Kornowski, M. Kraken, F. J. Litterst, K. Fiege, P. Mischnick, and M. Schilling. 2013. "Highly stable monodisperse PEGylated iron oxide nanoparticle aqueous suspensions: a nontoxic tracer for homogeneous magnetic bioassays." *Nanoscale* no. 5 (23):11447-55.

Laurent, S., S. Dutz, U. O. Hafeli, and M. Mahmoudi. 2011. "Magnetic fluid hyperthermia: focus on superparamagnetic iron oxide nanoparticles." *Adv Colloid Interface Sci* no. 166 (1-2):8-23.

Laurent, S., D. Forge, M. Port, A. Roch, C. Robic, L. Vander Elst, and R. N. Muller. 2008. "Magnetic iron oxide nanoparticles: synthesis, stabilization, vectorization, physicochemical characterizations, and biological applications." *Chem Rev* no. 108 (6):2064-110.

Li, Y., J. Rodrigues, and H. Tomas. 2012. "Injectable and biodegradable hydrogels: gelation, biodegradation and biomedical applications." *Chem Soc Rev* no. 41 (6):2193-221.

Licciardi, M., C. Scialabba, G. Cavallaro, C. Sangregorio, E. Fantechi, and G. Giammona. 2013. "Cell uptake enhancement of folate targeted polymer coated magnetic nanoparticles." *J Biomed Nanotechnol* no. 9 (6):949-64.

Lin, J., W. Zhou, A. Kumbhar, J. Wiemann, J. Fang, E. Carpenter, and C. J. O'Connor. 2001. "Gold-Coated Iron (Fe@Au) Nanoparticles: Synthesis, Characterization, and Magnetic Field-Induced Self-Assembly." *2001* no. 159:26-31.

Liu, X. Q., S. W. Tao, and Y. S. Shen. 1997. "Preparation and characterization of nanocrystalline c -FeeO 3 by a sol-gel process." *Sensors and Actuators B* no. 40:161-165.

Lui, C. N., Y. P. Tsui, A. S. Ho, D. K. Shum, Y. S. Chan, C. T. Wu, H. W. Li, S. C. Tsang, and K. K. Yung. 2013. "Neural stem cells harvested from live brains by antibody-conjugated magnetic nanoparticles." *Angew Chem Int Ed Engl* no. 52 (47):12298-302.

Marshall, J. D., W. C. Eveland, and C. W. Smith. 1958. "Superiority of fluorescein isothiocyanate (Riggs) for fluorescent-antibody technic with a modification of its application." *Proc Soc Exp Biol Med* no. 98 (4):898-900.

Massart, R. 1981. "Preparation of Aqueous Magnetic Liquids in Alkaline and Acidic Media." *IEEE Transactions on Magnetics* no. 17 (2):1247-1248.

Matsumura, Y., and H. Maeda. 1986. "A new concept for macromolecular therapeutics in cancer chemotherapy: mechanism of tumoritropic accumulation of proteins and the antitumor agent smancs." *Cancer Res* no. 46 (12 Pt 1):6387-92.

Meenach, S. A., C. G. Otu, K. W. Anderson, and J. Z. Hilt. 2012. "Controlled synergistic delivery of paclitaxel and heat from poly(beta-amino ester)/iron oxide-based hydrogel nanocomposites." *Int J Pharm* no. 427 (2):177-84.

Milošević, I., S. Guillot, M. Tadic, M. Duttine, E. Duguet, K. Pierzchala, A. Sienkiewicz, L. Forro, and M. Sabougni. 2014. "Loading and release of internally self-assembled emulsions embedded in a magnetic hydrogel." *Applied Physics Letters* no. 104 (043701):1-5.

Naessens, M., A. Cerdobbel, W. Soetart, and E. J. Vandamme. 2005. "*Leuconstoc* dextransucrase and dextran: production, properties and applications." *Journal of Chemical Technology and Biotechnology* no. 80:845-860.

Ohtani, T., M. Murakami, A. Yamamoto, K. Takada, and S. Muranishi. 1991. "Effect of absorption enhancers on pulmonary absorption of fluorescein isothiocyanate dextrans with various molecular weights." *International Journal of Pharmaceutics* no. 77:141-150.

Ossipov, D. A., S. Piskounova, O. P. Varghese, and J. Hilborn. 2010. "Functionalization of hyaluronic acid with chemoselective groups via a disulfide-based protection strategy for in situ formation of mechanically stable hydrogels." *Biomacromolecules* no. 11 (9):2247-54.

Pascal, C., J. L. Pascal, and F. Favier. 1999. "Electrochemical Synthesis for the Control of ç-Fe2O3 Nanoparticle Size. Morphology, Microstructure, and Magnetic Behavior." *Chem. Mater.* no. 11:141-147.

Patenaude, M., S. Campbell, D. Kinio, and T. Hoare. 2014. "Tuning gelation time and morphology of injectable hydrogels using ketone-hydrazide cross-linking." *Biomacromolecules* no. 15 (3):781-90.

Patenaude, M., and T. Hoare. 2012a. "Injectable, Degradable Thermoresponsive Poly(Nisopropylacrylamide) Hydrogels." *ACS Macro Letters* no. 1:409−413.

Patenaude, M., and T. Hoare. 2012b. "Injectable, mixed natural-synthetic polymer hydrogels with modular properties." *Biomacromolecules* no. 13 (2):369-78.

Patenaude, M., N. M. Smeets, and T. Hoare. 2014. "Designing Injectable, Covalently Cross-Linked Hydrogels for Biomedical Applications." *Macromol Rapid Commun* no. 35 (6):598-617.

Patil, R. M., P. B. Shete, N. D. Thorat, S. V. Otari, K. C. Barick, A. Prasad, R. S. Ningthoujam, B. M. Tiwale, and S. H. Pawar. 2014. "Superparamagneticironoxide/chitosancore/shellsforhyperthermia application: Improvedcolloidalstabilityandbiocompatibility." *Journal of Magnetism and Magnetic Materials* no. 355:22-30.

Pavlov, A. M., B. G. De Geest, B. Louage, L. Lybaert, S. De Koker, Z. Koudelka, A. Sapelkin, and G. B. Sukhorukov. 2013. "Magnetically engineered microcapsules as intracellular anchors for remote control over cellular mobility." *Adv Mater* no. 25 (48):6945-50.

Pelton, R. 2000. "Temperature-sensitive aqueous microgels." *Adv Colloid Interface Sci* no. 85 (1):1-33.

Pelton, R.H., and P. Chibante. 1986. "Preparation of Aqueous Latices with NIsopropylacrylamide." *Colloids and Surfaces* no. 20:247-256.

Pouliquen, D., J. J. Le Jeune, R. Perdrisot, A. Ermias, and P. Jallet. 1991. "Iron oxide nanoparticles for use as an MRI contrast agent: pharmacokinetics and metabolism." *Magn Reson Imaging* no. 9 (3):275-83.

Pouponneau, P., J. C. Leroux, and S. Martel. 2009. "Magnetic nanoparticles encapsulated into biodegradable microparticles steered with an upgraded magnetic resonance imaging system for tumor chemoembolization." *Biomaterials* no. 30 (31):6327-32.

Rejman, J., V. Oberle, I. S. Zuhorn, and D. Hoekstra. 2004. "Size-dependent internalization of particles via the pathways of clathrin- and caveolae-mediated endocytosis." *Biochem J* no. 377 (Pt 1):159-69.

Ricka, J., and T. Tanaka. 1984. "Swelling of ionic gels: Quantitative performance of the donnan theory." *Macromolecules* no. 17 (12):2916-2921.

Rosenweig, R. E. 1985. *Ferrohydrodynamics*. New York: Cambridge University Press.

Rovers, S. A.; Hoogenboom, R.; Kemmere, M. F.; and Keurentjes, J. T. F. 2012. "Repetitive on-demand drug release by magnetic heating of iron oxide containing polymeric implants." *Soft Matter* no. 8:1623-1627.

Sahoo, Y., H. Pizem, T. Fried, D. Golodnitsky, L. Burstein, C. Sukenik, and G. Markovich. 2001. "Alkyl Phosphonate/Phosphate Coating on Magnetite Nanoparticles: A Comparison with Fatty Acids." *Langmuir* no. 17 (25):7907-7911.

Saltzman, W. M. 2001. *Drug Delivery: Engineering Principles for Drug Therapy*. New York: Oxford University Press.

Saraswathy, A., S. S. Nazeer, N. Nimi, S. Arumugam, S. J. Shenoy, and R. S. Jayasree. 2014. "Synthesis and characterization of dextran stabilized superparamagnetic iron oxide nanoparticles for in vivo MR imaging of liver fibrosis." *Carbohydr Polym* no. 101:760-8.

Satarkar, N. S., and J. Z. Hilt. 2008. "Magnetic hydrogel nanocomposites for remote controlled pulsatile drug release." *J Control Release* no. 130 (3):246-51.

Satarkar, N. S., W. Zhang, R. E. Eitel, and J. Z. Hilt. 2009. "Magnetic hydrogel nanocomposites as remote controlled microfluidic valves." *Lab Chip* no. 9 (12):1773-9.

Sivakumaran, D., D. Maitland, and T. Hoare. 2011. "Injectable microgel-hydrogel composites for prolonged small-molecule drug delivery." *Biomacromolecules* no. 12 (11):4112-20.

Smeets, N. M., and T. Hoare. 2013. "Designing Responsive Microgels for Drug Delivery Applications." *Journal of Polymer Science, Part A: Polymer Chemistry* no. 51 (14):3027-3043.

Stock, R. J., E. V. Cilento, and R. S. McCuskey. 1989. "A quantitative study of fluorescein isothiocyanate-dextran transport in the microcirculation of the isolated perfused rat liver." *Hepatology* no. 9 (1):75-82.

Tao, Y., X. Tong, Y. Zhang, J. Lai, Y. Huang, Y. R. Jiang, and B. H. Guo. 2013. "Evaluation of an in situ chemically crosslinked hydrogel as a long-term vitreous substitute material." *Acta Biomater* no. 9 (2):5022-30.

Timko, B. P., M. Arruebo, S. A. Shankarappa, McAlvinm J. B., O. S. Okonkwo, B. Mizrahi, C. F. Stefanescu, L. Gomez, J. Zhu, A. Zhu, J. Santamaria, R. Langer, and D. S. Kohane. 2014. "Near-infrared–actuated devices for remotely controlled drug delivery." *PNAS* no. 111 (4):1349-1354.

Todd, T., Z. Zhen, W. Tang, H. Chen, G. Wang, Y. J. Chuang, K. Deaton, Z. Pan, and J. Xie. 2014. "Iron oxide nanoparticle encapsulated diatoms for magnetic delivery of small molecules to tumors." *Nanoscale* no. 6 (4):2073-6.

Uhrich, K. E., S. M. Cannizzaro, R. S. Langer, and K. M. Shakesheff. 1999. "Polymeric systems for controlled drug release." *Chem Rev* no. 99 (11):3181-98.

Verwey, E. J. W., and J. T. G. Overbeek. 1948. *Theory of the stability of lyophobic colloids: the interaction of sol particles having an electric double layer*. Amsterdam, The Netherlands: Elsevier.

Vetrik, M., M. Pradny, M. Hruby, and J. Michalek. 2011. "Hydrazone-based hydrogel hydrolytically degradable in acidic environment." *Polymer Degradation and Stability* no. 96:756-759.

Vincent, B., J. Edwards, S. Emmett, and A. Jones. 1986. "Depletion flocculation in dispersions of sterically-stabilized particles." *Colloids and Surfaces* no. 18:261-281.

Wagner, S., J. Schnorr, H. Pilgrimm, B. Hamm, and M. Taupitz. 2002. "Monomer-coated very small superparamagnetic iron oxide particles as contrast medium for magnetic resonance imaging: preclinical in vivo characterization." *Invest Radiol* no. 37 (4):167-77.

Wan, J., X. Chen, Z. Wang, X. Yang, and Y. Qian. 2005. "A soft-template-assisted hydrothermal approach to single-crystal Fe3O4 nanorods." *Journal of Crystal Growth* no. 276:571-576.

Wee, S., and W. R. Gombotz. 1998. "Protein release from alginate matrices." *Adv Drug Deliv Rev* no. 31 (3):267-285.

Yang, X., E. Bakaic, T. Hoare, and E. D. Cranston. 2013. "Injectable polysaccharide hydrogels reinforced with cellulose nanocrystals: morphology, rheology, degradation, and cytotoxicity." *Biomacromolecules* no. 14 (12):4447-55.

Zarzycki, R., Z. Modrzejewska, and K. Nawrotek. 2010. "Drug Release From Hydrogel Matrices." *Ecological Chemistry and Engineering S* no. 17 (2):117-136.

Zhang, C., B. Wangler, B. Morgenstern, H. Zentgraf, M. Eisenhut, H. Untenecker, R. Kruger, R. Huss, C. Seliger, W. Semmler, and F. Kiessling. 2007. "Silica- and alkoxysilane-coated ultrasmall superparamagnetic iron oxide particles: a promising tool to label cells for magnetic resonance imaging." *Langmuir* no. 23 (3):1427-34.

Zhang, S., M. A. Anderson, Y. Ao, B. S. Khakh, J. Fan, T. J. Deming, and M. V. Sofroniew. 2014. "Tunable diblock copolypeptide hydrogel depots for local delivery of hydrophobic molecules in healthy and injured central nervous system." *Biomaterials* no. 35 (6):1989-2000.

Appendices

Appendix A: Materials and Methods

Table A.1: Summary of reagents used.

Chemical Name	Abbreviation	Supplier	Product Identification Number
2,2-azobisisobutyric acid dimethyl ester	AIBME	Wako Chemicals	2589-57-3
3T3 *Mus Musculus* Fibroblasts	3T3	ATCC: Cedarlane Laboratories Ltd. - Burlington, ON	CCL- 92
Acrylic Acid	AA	Sigma Aldrich – Oakville, ON	147230
Acrylamide	AAm	Sigma Aldrich – Oakville, ON	A3553
Adipic acid dihydrazide	ADH	Sigma Aldrich – Oakville, ON	A06638
Ammonium Hydroxide		Sigma Aldrich – Oakville, ON	320145
Ammonium Persulfate	APS	Sigma Aldrich – Oakville, ON	215589
Dextran from *Leuconstoc spp.*		Sigma Aldrich – Oakville, ON	31392
Dimethyl Sulfoxide	DMSO	Caledon Laboratory Chemicals – Georgetown, ON	4100-1
Dulbecco's Modified Eagle Medium (high glucose)	DMEM	Invitrogen Canada – Burlington, ON	11965
Ethylene Glycol	EG	Sigma Aldrich – Oakville, ON	324558
Fluorescein isothiocyanate-labelled dextran	FITC-Dextran	Sigma Aldrich – Oakville, ON	46944
Fetal Bovine Serum	FBS	Invitrogen Canada – Burlington, ON	10437
Iron (II) Chloride		Sigma Aldrich – Oakville, ON	372870
Iron (III) Chloride		Sigma Aldrich – Oakville, ON	157740
N'-ethyl-N-(3-dimethylaminopropyl)-	EDC	Sigma Aldrich – Oakville, ON	E7750

carbodiimide			
N-isopropylacrylamide, 97%	NIPAM	Thermo Fisher Scientific	412785000
N-isopropylmethacrylamide	NIPMAM	Sigma Aldrich – Oakville, ON	423548
N-N'-methylene bisacrylamide	MBA	Sigma Aldrich – Oakville, ON	146072
Penicillin Streptomycin	PS	Invitrogen Canada – Burlington, ON	15140
Poly(ethylene oxide)	PEO	Sigma Aldrich – Oakville, ON	372838
Sodium Periodate		Sigma Aldrich – Oakville, ON	311448
Thiazolyl Blue Tetrazolium Bromide	MTT	Sigma Aldrich – Oakville, ON	M5655
Thioglycolic Acid	TGA	Sigma Aldrich – Oakville, ON	T3758
Trypsin-EDTA		Invitrogen Canada – Burlington, ON	25200

Table A.2: Summary of pulsatile release tests and their components.

	Short Form	Hydrogel	Microgel	PEG-SPIONs	FITC Dextran	Incubation Temp
Microgel and Ferrofluid, Pulsed at 37°C, PEG-ferrofluid and MG	MG+FF 37°C PEG-FF +MG	192.8mg each NIP-A + DexB (8 wt%)	385.5mg Med-Low (8 wt%)	1.646 g of 15wt% Ferrofluid (5 wt%)	48.2mg (1 wt%)	37°C
No Microgel, PEG-Ferrofluid, No microgel	-MG PEG-FF, No MG	175.8mg each NIP-A + DexB (8 wt%)	**NA (0 wt%)**	1.646 g of 15wt% Ferrofluid (5 wt%)	48.2mg (1 wt%)	37°C
No SPION Control	-FF	192.8mg each NIP-A + DexB (8 wt%)	385.5mg Med-Low (8 wt%)	**NA (0 wt%)**	48.2mg (1 wt%)	37°C
pNIPAM-hydrazide-SPIONs**	NipA-FF	175.8mg Dex B + **2mL pNIPAM-hydrazide-**	**NA (0 wt%)**	**NA (0 wt%)**	48.2mg (1 wt%)	37°C

		SPIONs (8 wt%)				
pNIPAM-hydrazide-SPIONs** and Microgel	NipA-FF +MG	192.8mg Dex B + **2mL pNIPAM-hydrazide-SPIONs (8 wt%)**	385.5mg Med-Low (8 wt%)	**NA (0 wt%)**	48.2mg (1 wt%)	37°C
Pulsed at 25°C	25°C	192.8mg each NIP-A + DexB (8 wt%)	385.5mg Med-Low (8 wt%)	1.646 g of 15wt% Ferrofluid (5 wt%)	48.2mg (1 wt%)	**25°C**
Pulsed at 43°C	43°C	192.8mg each NIP-A + DexB (8 wt%)	385.5mg Med-Low (8 wt%)	1.646 g of 15wt% Ferrofluid (5 wt%)	48.2mg (1 wt%)	**43°C**
4 wt% Microgel	4 wt% MG	183.9 mg each NIP-A + DexB (8 wt%)	**183.9mg Med-Low (4 wt%)**	1.646 g of 15wt% Ferrofluid (5 wt%)	45.98mg (1 wt%)	37°C
6 wt% Microgel	6 wt% MG	188.2mg each NIP-A + DexB (8 wt%)	**282.4mg Med-Low (6 wt%)**	1.646 g of 15wt% Ferrofluid (5 wt%)	47.06mg (1 wt%)	37°C
10 wt% Microgel	10 wt% MG	197.5mg each NIP-A + DexB (8 wt%)	**493.8mg Med-Low (10 wt%)**	1.646 g of 15wt% Ferrofluid (5 wt%)	49.4mg (1 wt%)	37°C
Low Microgel LCST	Low MG	192.8mg each NIP-A + DexB (8 wt%)	**385.5mg Low MG (8 wt%)**	1.646 g of 15wt% Ferrofluid (5 wt%)	48.2mg (1 wt%)	37°C
Med Microgel LCST	Med MG	192.8mg each NIP-A + DexB (8 wt%)	**385.5mg Med MG (8 wt%)**	1.646 g of 15wt% Ferrofluid (5 wt%)	48.2mg (1 wt%)	37°C
High Microgel LCST	High MG	192.8mg each NIP-A + DexB (8 wt%)	**385.5mg Low MG (8 wt%)**	1.646 g of 15wt% Ferrofluid (5 wt%)	48.2mg (1 wt%)	37°C
100% CMC-B Used (High Swelling Test)	100% CMC B	137.9 mg each NIP-A + **CMCB** (6 wt%)	275.9mg High MG (6 wt%)	1.646 g of 15wt% Ferrofluid (5 wt%)	45.98 mg (1 wt%)	37°C
75% CMC-	75%	137.9 mg NIP-A	275.9mg	1.646 g of	45.98 mg	37°C

B Used (Med-High Swelling Test)	CMC B	**+ 103.4 mg CMCB, 34.5mg DexB** (6 wt%)	High MG (6 wt%)	15wt% Ferrofluid (5 wt%)	(1 wt%)	
50% CMC-B Used (Med Swelling Test)	75% CMC B	137.9 mg NIP-A **+ 68.95 mg CMCB, 68.95 mg DexB** (6 wt%)	275.9mg High MG (6 wt%)	1.646 g of 15wt% Ferrofluid (5 wt%)	45.98 mg (1 wt%)	37°C
25% CMC-B Used (Low-No Swelling Test)	75% CMC B	137.9 mg NIP-A **+ 34.5mg CMCB, 103.4mg DexB,** (6 wt%)	275.9mg High MG (6 wt%)	1.646 g of 15wt% Ferrofluid (5 wt%)	45.98 mg (1 wt%)	37°C
0% CMC-B Used (High Swelling Test)	0% CMC B	137.9 mg each NIP-A + **DexB** (6 wt%)	275.9mg High MG (6 wt%)	1.646 g of 15wt% Ferrofluid (5 wt%)	45.98 mg (1 wt%)	37°C

Appendix B: Calibration Curves

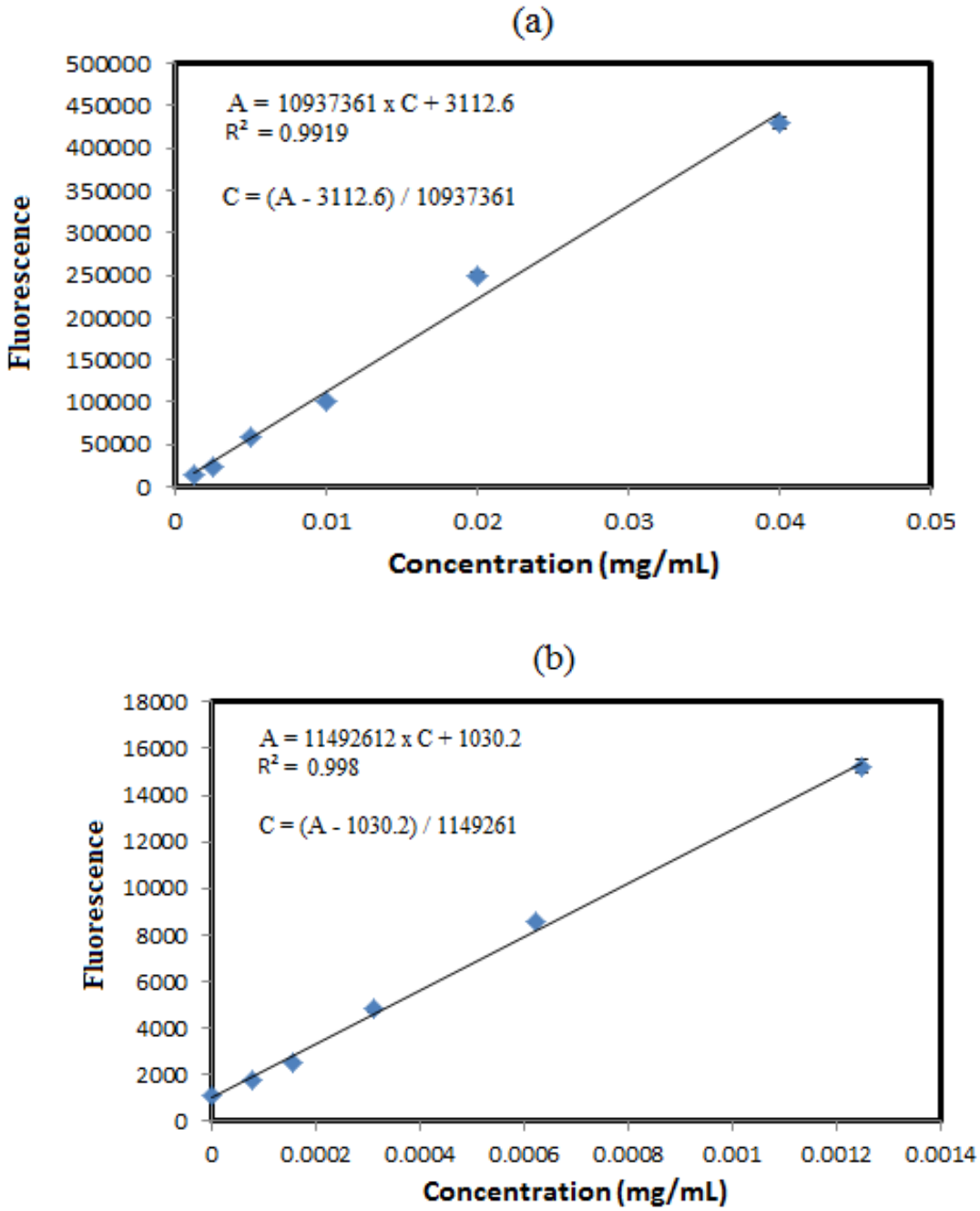

Figure B.1: 4 kDa FITC-Dextran calibration curves for (a) higher concentration range of 0.00125 – 0.04 mg/mL (seen on testing days 1 and 2) and (b) lower concentration range of 0 – 0.00125 mg/mL (seen on days 3 and 5).

Appendix C: Additional Data

i) pNIPAM-hydrazide GPC

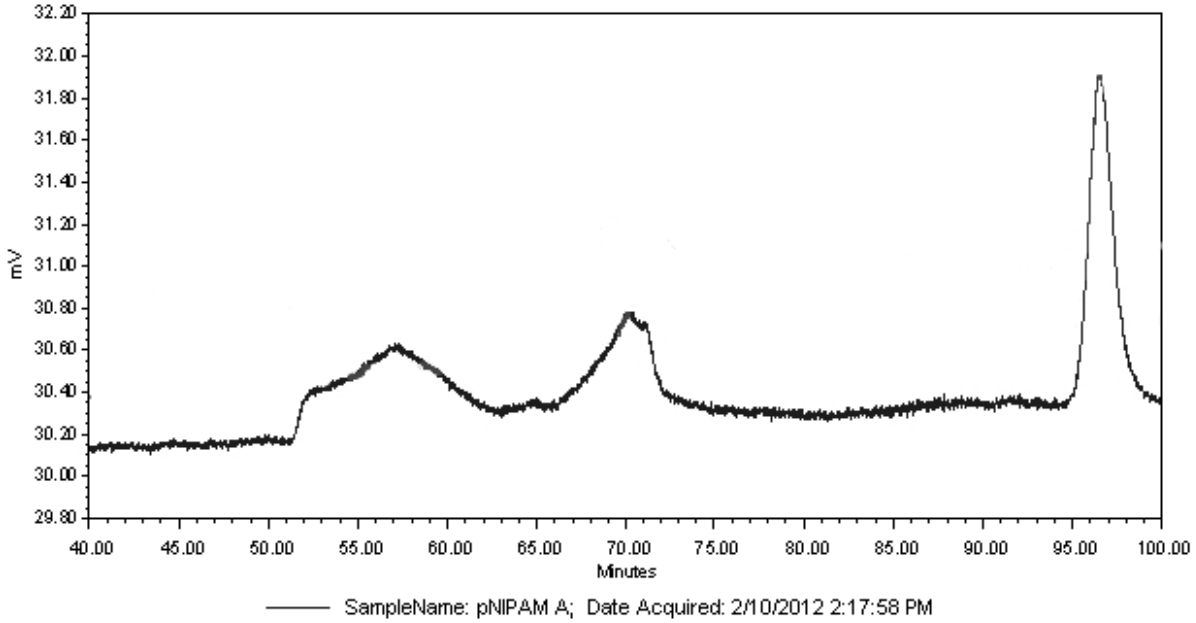

Figure C.1: GPC chromatograph of pNIPAM-hydrazide measured using a Polymer Labs PL-GPC 50, 10mM, pH=7 sodium phosphate buffer continuous phase and a PL Aquagel-OH mixed separation column. Calibrations were completed using PEG standards. Note: peak at appx 70min likely due to lack of use of charge screening molecules in the mobile phase. (Reproduced from Patenaude and Hoare 2012a with permission).

ii) Microgel VPTT Behaviour

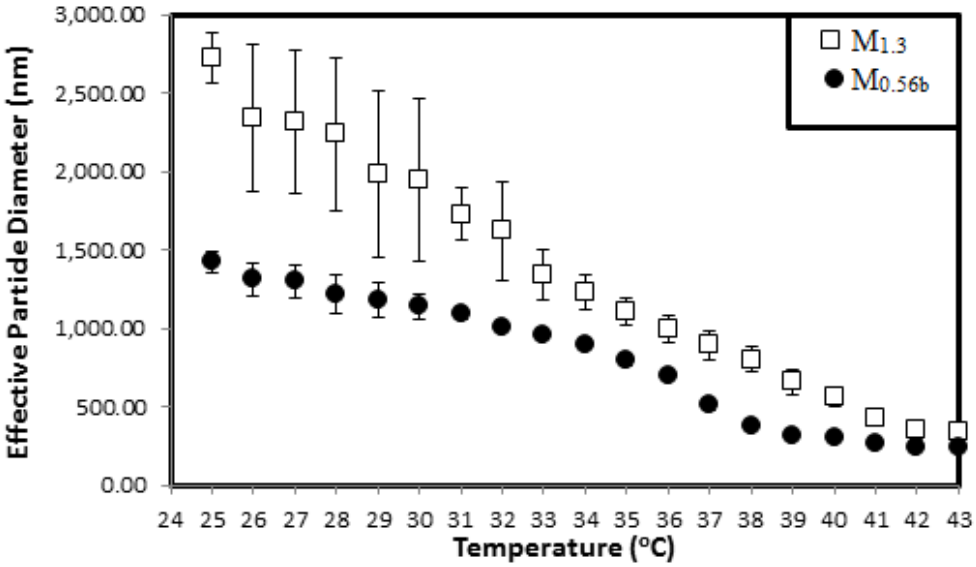

Figure C.2: VPTT behaviour of $M_{1.3}$ microgel ($M_{0.56b}$ shown for comparison).

iii) Long-term Composite Swelling Behaviour

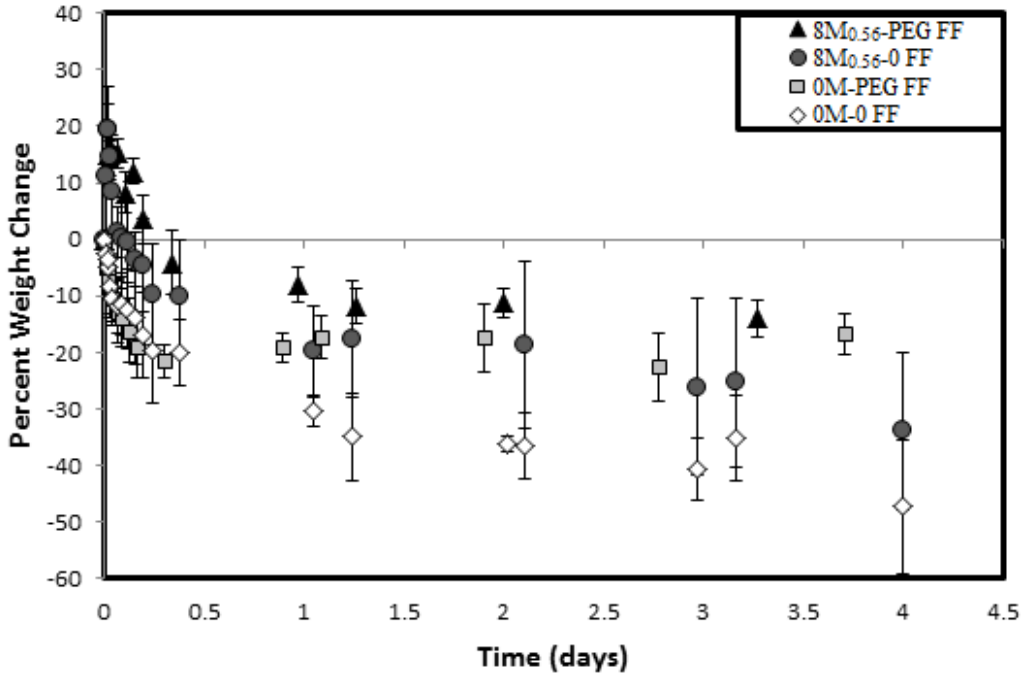

Figure C.3: Long term swelling behaviour of baseline composite and controls.

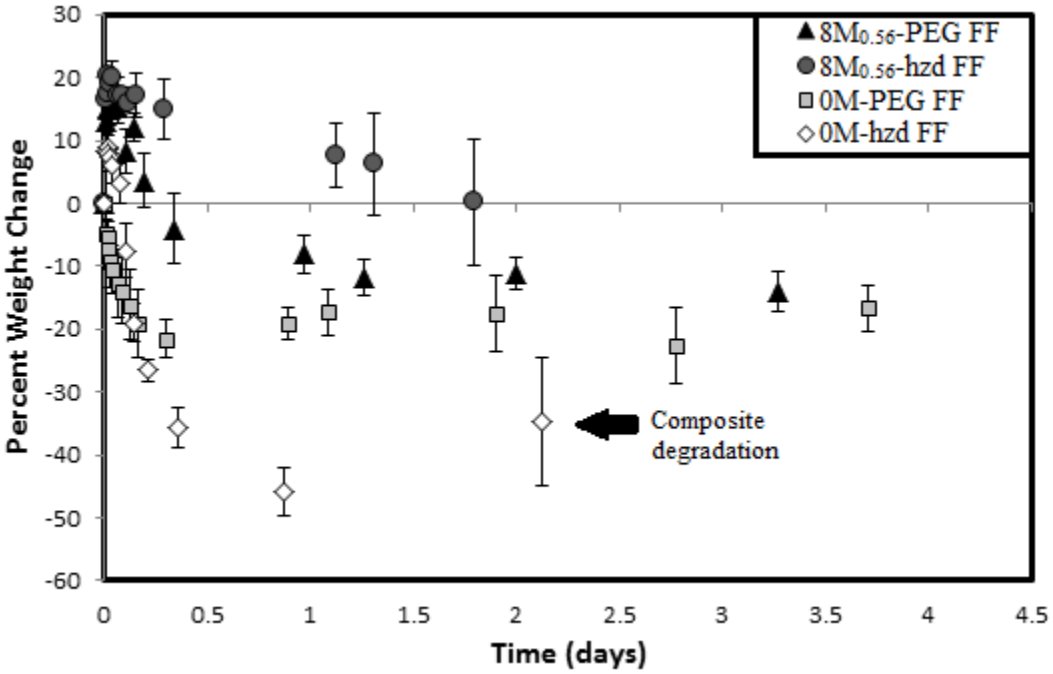

Figure C.4: Long term swelling behaviour of composites made with pNIPAM-hydrazide functionalized SPIONs.

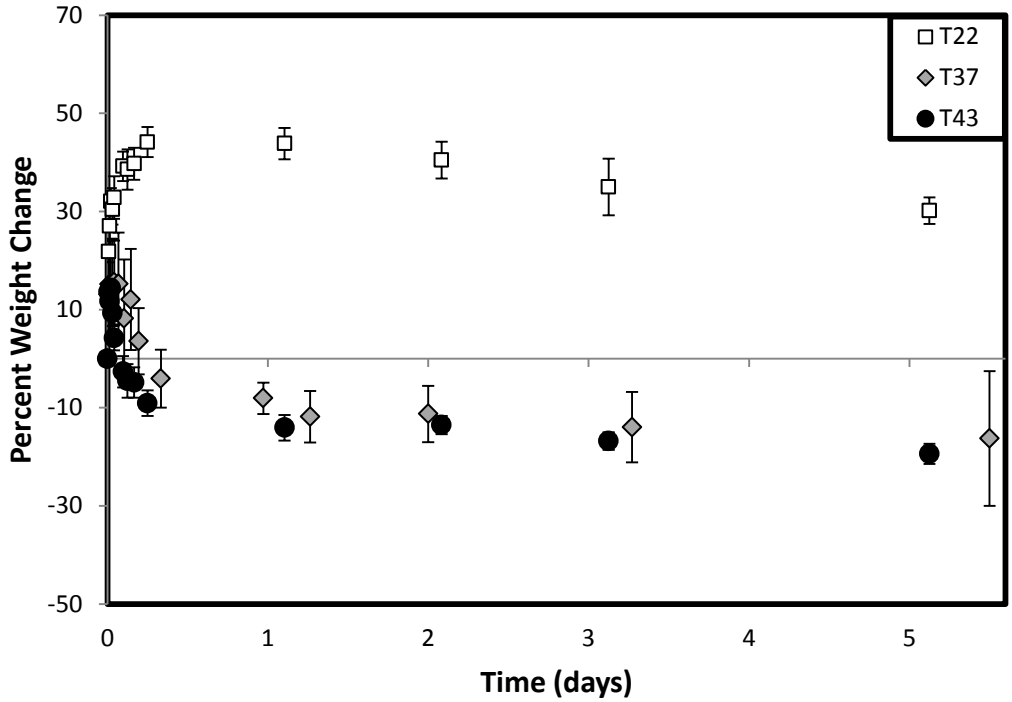

Figure C.5: Long term swelling behaviour of composites incubated at different temperatures. Slow decrease in T22 swelling likely due to composite degradation.

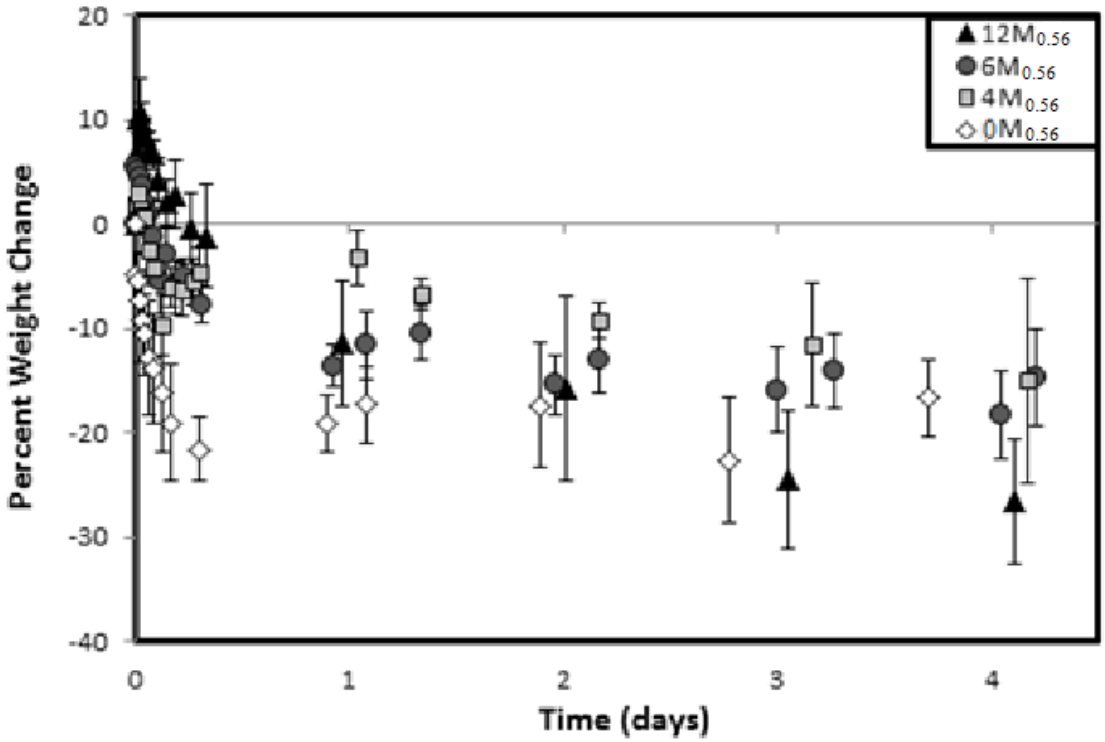

Figure C.6: Long term swelling behaviour of composites made with different microgel contents.

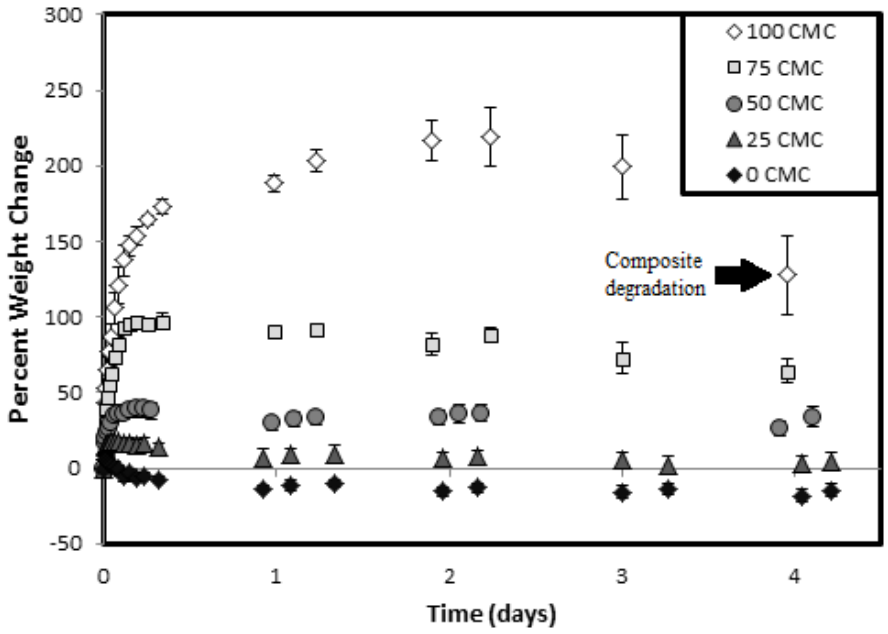

Figure C.7: Long term swelling behaviour of composites made with different percentages of CMC-aldehyde.

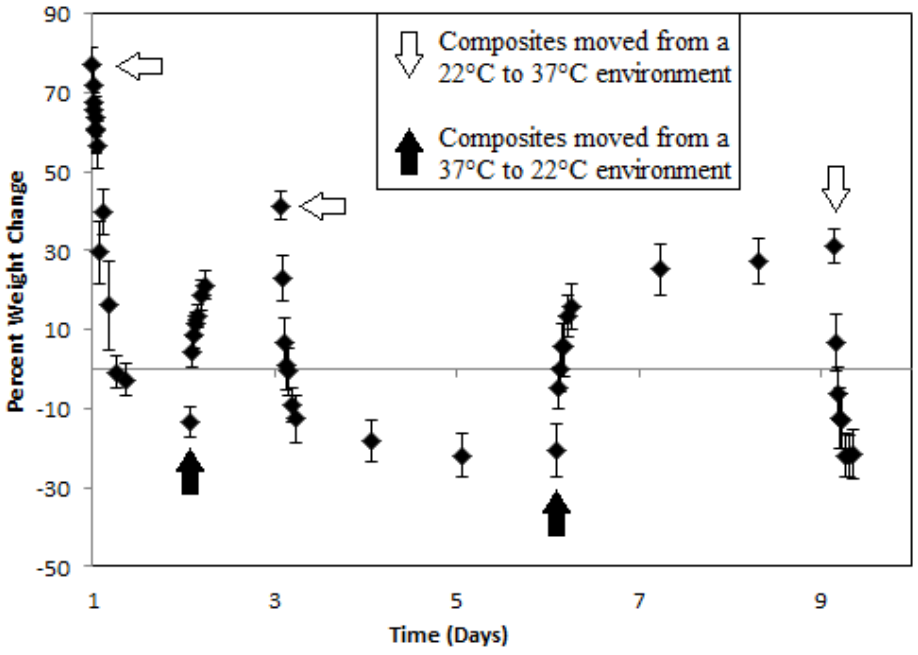

Figure C.8: Changes in swelling of 8wt% microgel, 8 wt% pNIPAM-hydrazide-dextran-aldehyde, PEG-SPION composites as they are moved between 25°C and 37°C incubation temperatures.

iv) Modelling of Burst Release

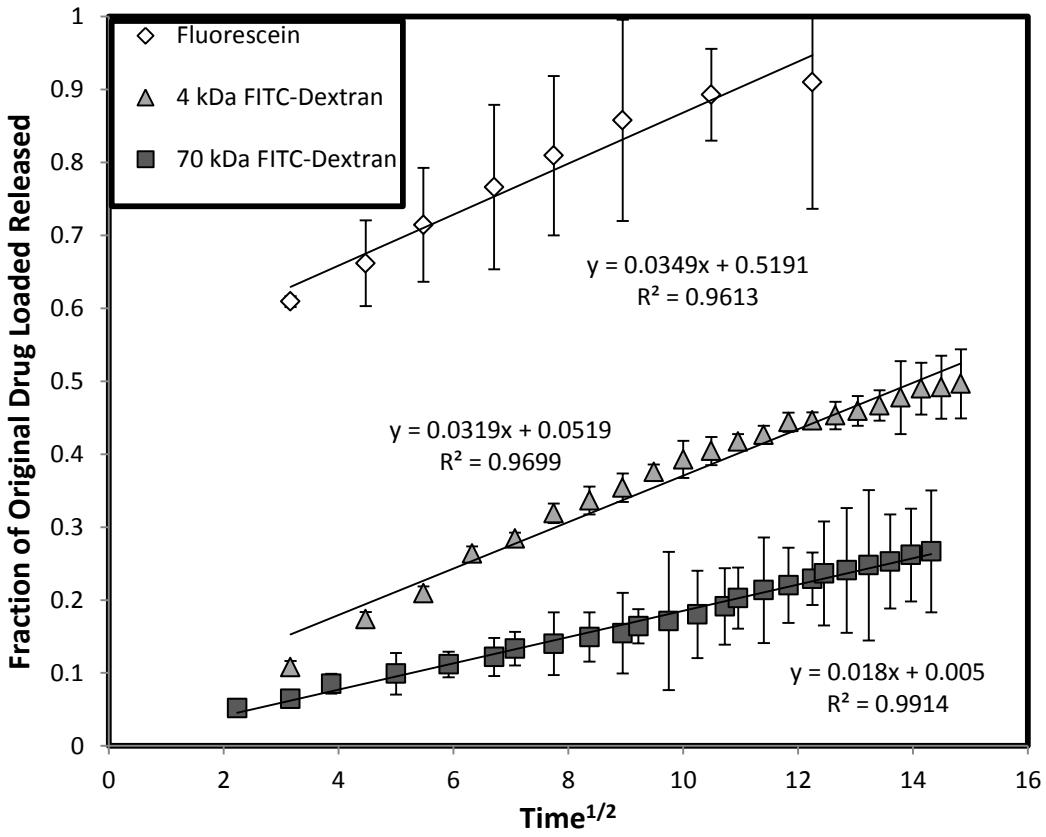

Figure C.9: $t^{1/2}$ kinetics of release of fluorescein, and 4 and 70 kDa FITC-Dextran from composites. Linearity of concentration vs $t^{1/2}$ supports diffusion-based release for all three model drugs.

Fick's Second Law Modelling:

The solution to Fick's 2nd Law used is approximated as (Zarzycki, Modrzejewska, and Nawrotek 2010):

$$\%\,\boldsymbol{Release} = \frac{\boldsymbol{M_t}}{\boldsymbol{M_o}}\,\boldsymbol{x}\,\mathbf{100\%} = \left[\mathbf{1} - \frac{\mathbf{6}}{\boldsymbol{\pi^2}}\sum_{\boldsymbol{n=1}}^{\mathbf{100}}\frac{\mathbf{1}}{\boldsymbol{n^2}}\mathbf{exp}\left(\frac{-\boldsymbol{D_A}\,\boldsymbol{n^2}\,\boldsymbol{\pi^2}\,\boldsymbol{t}}{\boldsymbol{r^2}}\right)\right]\boldsymbol{x}\,\mathbf{100\%} \quad \textbf{(C.1)}$$

assuming spherical composites where M_t is the mass released at time =t, M_o is the initial mass of drug available, n is a place holder, and r is the radius of the spherical hydrogel composite.

The baseline D_A for each composite was determined empirically from drug release data from the control composites (that were never exposed to the magnetic pulse). Equation C.1 was used to determine expected release from the composites for a given D_A. Excel Goal Seek was used to determine D_A by minimizing the sum of square differences between the model prediction and the experimental data for the first 4 hours of testing.

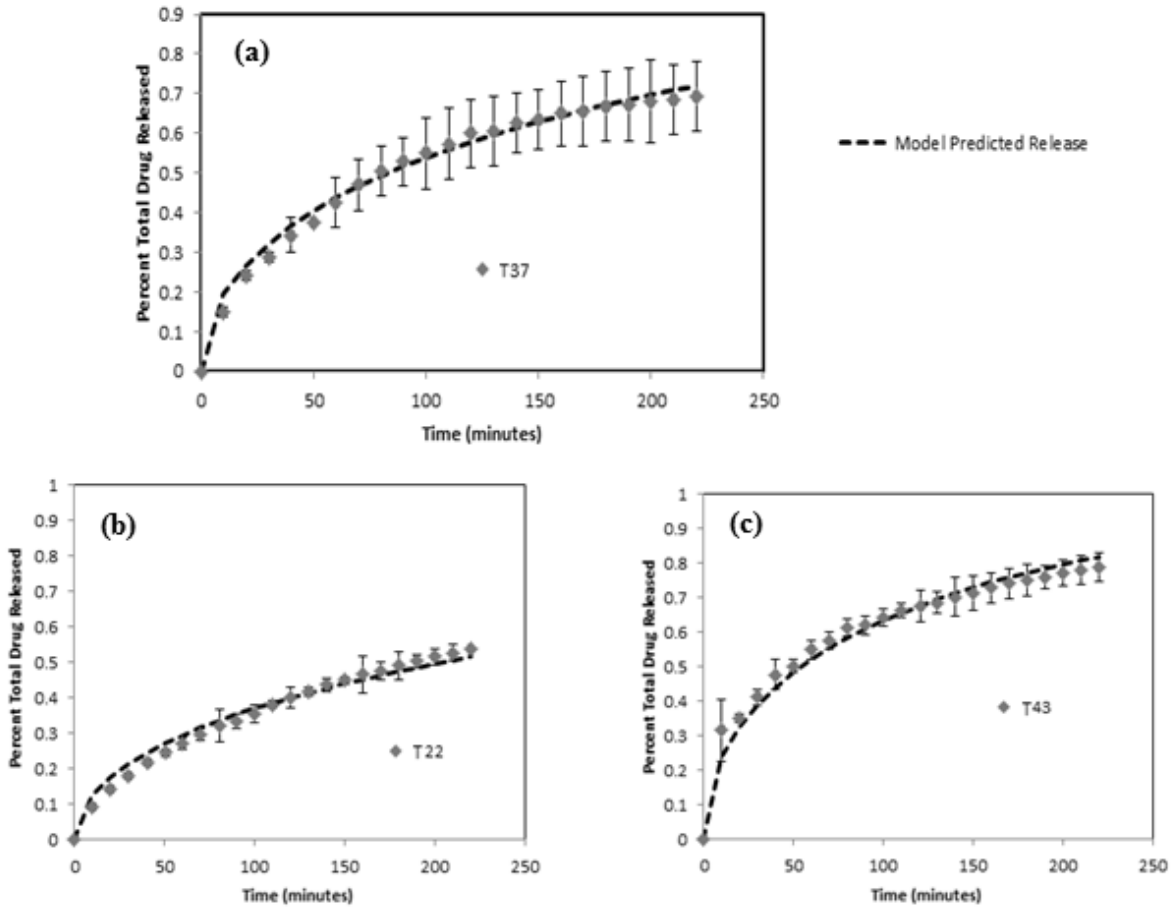

Figure C.10: Comparison between experimental results and model results for composites (a) incubated at 37°C (min sum of squares 0.013) $D_A = 5.51 \times 10^{-11}$ m^2/s (b) incubated at 22°C (min sum of squares difference = 0.009) $D_A = 2.25 \times 10^{-11}$ m^2/s, (b) incubated at 43°C (min sum of squares difference 0.016) $D_A = 8.44 \times 10^{-11}$ m^2/s.

v) Mechanical Degradation of pNIPAM-hydrazide-SPION Composites Based on Microgel Content and Exposure to an AMF.

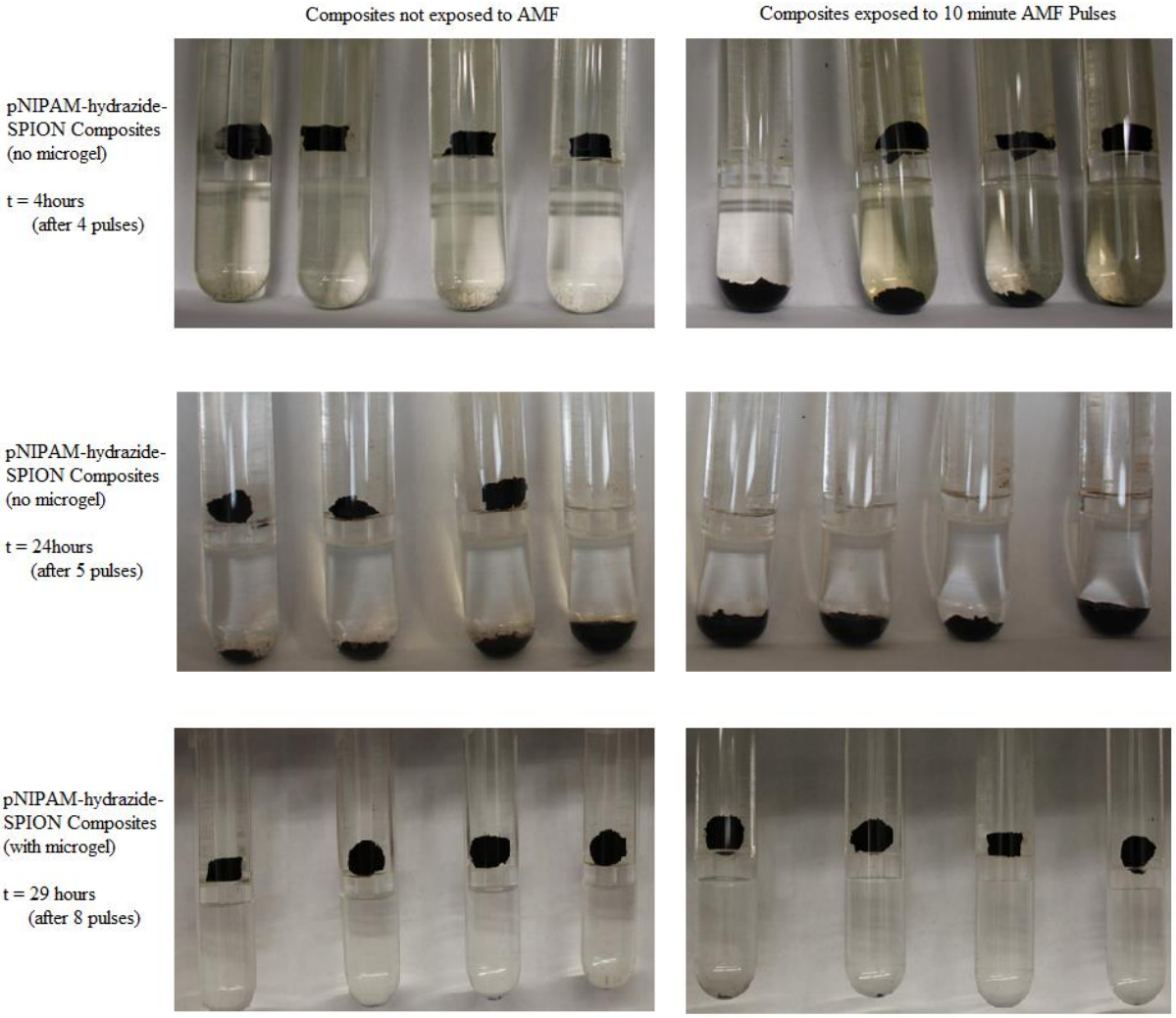

Figure C.11: Mechanical degradation of pNIPAM-hydrazide-SPION composites with and without microgel with application of AMF (n=4 replicates per sample pictured).